FACULDADE DE ENGENHARIA DA UNIVERSIDADE DO PORTO

Application of Absorbent Materials for Mitigation of Reflections in Anechoic Chambers with Robotic Arm

David Ferreira Coelho Barbosa

Mestrado em Engenharia Eletrotécnica e de Computadores

Orientador: Prof. Luís Pessoa

October 28, 2025

Resumo

A crescente exigência por sistemas avançados de assistência à condução (ADAS) e o desenvolvimento de veículos autónomos têm impulsionado a integração de radares de alta frequência nos automóveis, nomeadamente na faixa dos 76–81 GHz. Para garantir a fiabilidade destes sensores, os testes laboratoriais em câmaras anecoicas são essenciais. Contudo, a introdução de braços robóticos para posicionamento dinâmico dos sensores dentro da câmara levanta novos desafios, relacionados com reflexões eletromagnéticas indesejadas devido à presença de estruturas metálicas.

Esta dissertação investiga a aplicação de materiais absorventes de radiofrequência para mitigar essas reflexões, avaliando a sua adequação para futura integração em braços robóticos e para a otimização do ambiente anecoico. Foram considerados diversos absorvedores comerciais, incluindo estruturas à base de ferrite e espumas RAM. Entre estes, três materiais flexíveis: Eccosorb™ HR-25, Eccosorb™ HR-10 e Rezorb™ S foram selecionados para caracterização experimental devido à sua adaptabilidade a superfícies curvas de braços robóticos. Outros dois candidatos, o Conical RAM (Soliani EMC) e o PP-RAM (EMC Electronics), foram também analisados, embora a sua geometria ou disponibilidade tenham impedido a realização de testes neste trabalho. Uma chapa metálica foi utilizada como referência de reflexão máxima.

As medições foram realizadas em espaço livre, utilizando um analisador vetorial de redes (VNA), extensores de frequência e antenas corneta a operar na gama dos 76–81 GHz, em configurações monostática e bistática, para analisar os parâmetros de reflexão e transmissão (S_{11} e S_{21}).

Os resultados mostram que o HR-25 apresentou a refletividade mais baixa entre todas as amostras testadas, revelando um desempenho consistente perante variações angulares. O Rezorb™ S evidenciou a menor transmitância, demonstrando adequação em cenários que exigem elevada atenuação. O HR-10 revelou melhorias progressivas na configuração bistática com o aumento do ângulo de incidência, indicando um comportamento angular vantajoso. Estes resultados confirmam o potencial da aplicação localizada de absorventes em estruturas metálicas de braços robóticos para reduzir reflexões espúrias durante ensaios com radares automóveis.

Como trabalho futuro, propõe-se o revestimento direto de componentes do braço robótico com absorvedores e a expansão do estudo para outras geometrias, texturas, distâncias e condições angulares, de forma a validar a consistência dos resultados e melhorar a sua aplicação em cenários práticos de teste.

Abstract

The increasing demand for Advanced Driver Assistance Systems (ADAS) and the development of autonomous vehicles have driven the integration of high-frequency radars in automobiles, particularly within the 76–81 GHz band. To ensure the reliability of these sensors, laboratory testing in anechoic chambers is essential. However, the introduction of robotic arms for dynamic sensor positioning inside the chamber introduces new challenges, namely unwanted electromagnetic reflections caused by metallic structures.

This dissertation investigates the application of radiofrequency absorbing materials to mitigate such reflections, aiming to assess their suitability for future integration on robotic arms and for optimizing anechoic environments. Several commercial absorbers were considered, including ferrite-based structures and RAM foam sheets. Among these, three flexible materials: Eccosorb™ HR-25, Eccosorb™ HR-10, and Rezorb™ S were selected for experimental characterization due to their adaptability to curved robotic surfaces. Two additional candidates were also analyzed, Conical RAM (Soliani EMC) and PP-RAM (EMC Electronics), although their geometry or availability prevented their experimental testing in this work. A metallic plate was used as a reference for maximum reflection.

Measurements were conducted in free space using a Vector Network Analyzer (VNA), frequency extenders and horn antennas operating in the 76–81 GHz band, evaluating both monostatic and bistatic configurations to analyze reflection and transmission parameters (S_{11} and S_{21}).

Results show that HR-25 exhibited the lowest reflectivity among all tested samples, performing consistently well under angular variations. Rezorb™ S presented the lowest transmittance, confirming its suitability for applications requiring high attenuation. HR-10 showed progressive improvements in the bistatic configuration as the incidence angle increased, indicating advantageous angular behavior. These findings confirm the potential of applying localized absorber patches to metallic robotic structures to reduce spurious reflections during automotive radar testing.

Future work includes directly coating robotic arm components with absorbers and expanding the material study to additional geometries, textures and angular conditions to validate result consistency and improve generalization to practical testing scenarios.

UN Sustainable Development Goals

The United Nations Sustainable Development Goals (SDGs) are a global framework for achieving a better and more sustainable future for all. They include 17 goals that aim to respond to the world's most pressing challenges, including poverty, inequality, climate change, environmental degradation, peace and justice.

This dissertation contributes directly to the following SDGs:

SDG 9 Building resilient infrastructure, promoting inclusive and sustainable industrialization and fostering innovation.

SDG 11 Making cities and communities more inclusive, safe, resilient and sustainable.

SDG	Target	Contribution	Performance Indicators and Metrics
9	9.4	Improved radar validation infrastructure by optimizing anechoic chamber conditions and reducing electromagnetic reflections.	Reduction of unwanted reflections; Number of validated configurations
	9.5	Support for experimental research into advanced materials and radar technology in the automotive sector.	Number of materials characterized; Reproducibility of test results
11	11.6	Contribution to safer autonomous driving technologies by improving the reliability of automotive radar laboratory tests.	Reduction of test errors; Applicability to safer transportation systems

Acknowledgments

I would like to express my sincere gratitude to all the people and organizations who have contributed to the completion of this dissertation.

Firstly, I would like to thank my family for their unconditional support, patience and constant encouragement throughout my academic career. Their presence was essential in the most challenging moments.

I would like to thank the company *Controlar - Innovating Industry* for the opportunity to join their Research, Development and Innovation (RDI) team, where I was able to grow both technically and personally. Special thanks to the entire RDI team for the collaborative and motivating working environment. I would particularly like to highlight the engineers João Queirós and Rui Torres, for their close monitoring, technical guidance and constant availability throughout the project.

I also gratefully acknowledge the support of my internship colleague, Ruben Sil, who proved to be not only a great friend, but also a valuable help in the development of this work.

I would also like to express my deepest gratitude to Professor Luís Pessoa, for his scientific supervision, continuous availability and constructive suggestions, which made a decisive contribution to the development of the dissertation.

It is also my wish to thank Mohamed Ghatas, whose collaboration was fundamental in setting up the experimental setups at INESC TEC, always showing great dedication and a spirit of mutual help.

I am sincerely grateful to all.

David Barbosa

Contents

List of Figures

List of Tables

List of acronyms

ACC	Adaptive Cruise Control
ADAS	Advanced Driver Assistance Systems
AEB	Autonomous Emergency Braking
BSD	Blind Spot Detection
DUT	Device Under Test
FMCW	Frequency-Modulated Continuous Wave
HPBW	Half-Power Beamwidth
IF	Intermediate Frequency
IFFT	Inverse Fast Fourier Transform
LKA	Lane Keeping Assist
LO	Local Oscillator
MIMO	Multiple Input Multiple Output
RADAR	Radio Detection and Ranging
RAM	Radar Absorbing Material(s)
RCTA	Rear Cross Traffic Alert
RCS	Radar Cross Section
RF	Radiofrequency
RX	Receiver
SAR	Synthetic Aperture Radar
SDG	Sustainable Development Goals
SNR	Signal-to-Noise Ratio
SOLT	Short-Open-Load-Thru
TDR	Time Domain Reflectometry
TI	Texas Instruments
TRL	Thru-Reflect-Line
TX	Transmitter
ToF	Time of Flight
VNA	Vector Network Analyzer
WR10	Standard Waveguide for 75–110 GHz

Chapter 1

Introduction

1.1 Contextualisation

The growing digitalisation of the automotive sector has led to a profound transformation in the active safety systems of vehicles, with car radars being a central element in driving assistance systems (Advanced Driver Assistance Systems – ADAS). These sensors typically operate in the 77 GHz, enabling precise obstacle detection, traffic monitoring and distance control in adverse environmental conditions [1].

According to the World Health Organisation, road accidents continue to be one of the leading causes of death in young people between the ages of 5 and 29, with around 1.19 million fatalities worldwide every year [2]. This scenario has driven regulators and manufacturers to adopt increasingly rigorous and reliable technologies to mitigate the risk of collisions, accelerate the transition to autonomous vehicles and increase the safety of intelligent mobility systems.

In this context, rigorous validation of automotive radars is a critical step. This is usually conducted in controlled environments such as anechoic chambers, which simulate free space conditions by minimising reflections and external interference [3]. The evolution of testing methodologies has led to the introduction of automated robotic systems which, in addition to moving targets, are used to position the radar sensors themselves with high precision and repeatability. However, the introduction of mobile metal structures inside the chamber represents a new technical challenge: the electromagnetic reflections generated by these structures jeopardise the homogeneity of the field and reduce the reliability of the measurements [4].

In this emerging scenario, it is essential to develop strategies to mitigate these unwanted reflections, including the study of radar absorbing materials (RAM) applicable to mobile surfaces with complex geometry, such as robotic arms. Research in this area aims to improve the quality of laboratory tests and guarantee the compliance of sensors with the functional safety requirements imposed by the automotive industry.

1.2 Motivation

The integration of automotive radars into assisted and autonomous driving systems imposes high requirements for precision, robustness and reliability. To meet these requirements, it is necessary to rigorously validate the sensor's behaviour in various scenarios, both static and dynamic. The use of anechoic chambers offers an ideal environment for this type of testing, but the introduction of metal robotic arms to position the sensors introduces significant disturbances in the electromagnetic field – especially in the radar's direct radiation zone.

In the case of this dissertation, the study was conducted in collaboration with the company *Controlar Innovating Industry*, whose anechoic chamber is equipped with robotic systems for radar positioning. The unwanted reflections caused by its robotic structures, constituted the main motivation for the research work developed in this thesis.

These parasitic reflections can compromise the measurement of distance, angle and speed, directly affecting the evaluation of the sensor's performance. It is therefore imperative to mitigate these effects through functional solutions that are compatible with the robotic structure.

The application of radio frequency (RF) absorbing materials to the surface of robotic arms is one of the most promising solutions. However, this application requires the careful selection of materials with high attenuation in the range of 77 GHz, compatibility with curved surfaces and mechanical flexibility. In addition, the lack of specific standards for characterising absorbers applied to mobile systems highlights the need for in-depth research in this area.

This dissertation seeks to answer the following scientific questions:

- What are the physical mechanisms that govern the absorption of electromagnetic waves in the car radar range?
- What materials are best suited to minimise reflections caused by robotic arms in anechoic chambers?
- How can the performance of these absorbers be characterised experimentally?

The aim of this approach is to contribute to the improvement of testing methods applied to the automotive industry, promoting more reliable, rapid and representative tests, which are fundamental to the safe and efficient development of autonomous driving systems.

1.3 Dissertation objectives

The main aim of this dissertation is to evaluate and characterise radiofrequency absorbing materials for application in anechoic chambers, with a focus on minimising unwanted reflections caused by the introduction of metallic elements, such as robotic arms, and optimising the internal coating of the chamber. To achieve this general objective, the following specific objectives were defined:

- To study the physical principles of electromagnetic wave absorption and the interaction of absorbers with radar waves in the 77 GHz range.

- Identify and select RF absorbing materials with suitable characteristics for coating metal surfaces and optimising the anechoic environment.
- Implement experimental methods for characterising absorbers, including measurements with Vector Network Analysers (VNA) and tests in a controlled environment.
- Evaluate the effectiveness of absorbers in minimising RF reflections within the anechoic chamber.
- To propose solutions for improving the performance of laboratory tests on automotive radars, guaranteeing more reliable and representative measurements.

1.4 Organisation of the dissertation

This dissertation is structured in five chapters, as described below:

- **Chapter 1 - Introduction**: Presents the contextualisation of the problem, the motivation for the study, the research objectives, and the organisation of the dissertation.
- **Chapter 2 - Theoretical Foundations**: Explores the fundamental concepts related to automotive radars, electromagnetic wave propagation, RF absorption, and experimental methodologies for characterising absorbers.
- **Chapter 3 - Experimental Methodology**: Describes the methods used in the selection, preparation, and measurement of absorbers, including the experimental setups with the Vector Network Analyzer (VNA).
- **Chapter 4 - Experimental Results**: Presents the data obtained from the measurements (S-parameters) and describes the behaviour of the materials tested under different frequency and angle conditions.
- **Chapter 5 - Conclusion and Future Work**: Summarises the main conclusions of the study and proposes directions for future research in the field of absorbers and automotive radar testing.

The aim of this structure is to provide a comprehensive overview about the problem of unwanted reflections in anechoic chambers and to explore effective solutions for their mitigation, thus contributing to the improvement of laboratory testing of automotive radars.

Chapter 2

Theoretical Foundations

2.1 Introduction to speed chambers

Automotive radars operate in the radio frequency (RF) range, more specifically within the microwave sub-band, which covers approximately 300 MHz to 300 GHz. Modern radars used in vehicles typically operate between 24 GHz and 81 GHz, with 77 GHz and 81 GHz being the most common frequencies for advanced applications. These frequencies are chosen due to the physical relationship between frequency and wavelength: higher frequencies correspond to shorter wavelengths, which improves range resolution and the ability to detect smaller objects. A shorter wavelength allows the radar to distinguish targets that are closer together and to better resolve fine structural details. In addition, operation in this millimeter-wave band provides a favorable trade-off between resolution and propagation: it reduces susceptibility to interference from lower-frequency communication systems and minimizes the impact of multipath effects, while still allowing acceptable atmospheric penetration for automotive applications. [3].

The growing demand for greater road safety and traffic efficiency has led to the widespread adoption of car radars, making them indispensable sensors in modern vehicles. Their ability to operate in adverse conditions, such as rain, fog or low light, gives them a significant advantage over other sensors, such as chambers and ultrasounds [5].

2.1.1 History and evolution of radars

The concept of RADAR (Radio Detection and Ranging) came at the beginning of the 20th century, when scientists began to explore the propagation and reflection of electromagnetic waves in order to detect objects at a distance. The first experimental demonstration was carried out in 1904 by the German engineer Christian Hülsmeyer, who patented a device called the *Telemobiloskop*. This rudimentary system used radio waves to detect the presence of ships and is considered a precursor to modern radar [6].

Despite this initial breakthrough, radar only began to be developed systematically from the 1930s onwards, driven by military interests. During the Second World War (1939-1945), several nations invested heavily in the research and development of radars to detect enemy aircraft. One of the most important advances took place in the UK, with the creation of the *Chain Home*, a system of coastal radar stations that played a crucial role in British defense during the Battle of Britain.

Concurrently, the United States, Germany and the Soviet Union also developed their own versions of military radars. A significant milestone was the invention of the cavity magnetron, a device that enabled the generation of high-power microwave signals, making it possible to create compact and highly efficient radars [7].

After the end of the war, radars began to be applied in civilian contexts, including air traffic control, meteorology and maritime navigation. In the 1950s and 1960s, advances in transistors and electronic circuits led to the miniaturization of radar systems, making them more accessible and versatile [8].

2.1.1.1 Development of automotive radars

The use of radar in the automotive industry began to be explored in the 1970s, initially in military and experimental applications. One of the first studies was carried out by General Motors Research Laboratories, which investigated the feasibility of radar systems for collision avoidance [9]. However, the technological limitations at the time, such as the high cost and complexity of the circuits, prevented the practical implementation of the technology in commercial vehicles.

From the 1990s onwards, with advances in electronics and a cost reduction of semiconductors, radars began to be integrated into commercial vehicles. The first automotive radar systems were intended for adaptive cruise control (ACC), allowing automatic adjustment of the distance to the vehicle ahead [10].

With the start of the 21st century, the adoption of automotive radar grew exponentially, driven by the development of ADAS systems. Semiconductor manufacturers such as Texas Instruments, Bosch and Infineon began producing highly integrated radar chips, making it possible to use the technology on a large scale.

Today, automotive radars typically operate in the 24 GHz and 77-81 GHz bands and are used in a variety of applications.

2.1.2 Radar applications in the automotive industry

Radars play a key role in the active safety of modern vehicles. Their main applications include (figure 2.1):

- **Adaptive cruise control (ACC)**: Automatically adjusts the vehicle's speed to maintain a safe distance from the vehicle ahead.
- **Autonomous Emergency Braking (AEB)**: It detects obstacles and applies the brakes if the driver doesn't react in time.
- **Blind Spot Detection (BSD)**: Alerts the driver to the presence of vehicles in blind spots.
- **Lane Keep Assist**: Helps the vehicle to stay in the correct lane.

- **Assisted Parking**: Facilitates parking maneuvers by detecting obstacles near the vehicle.

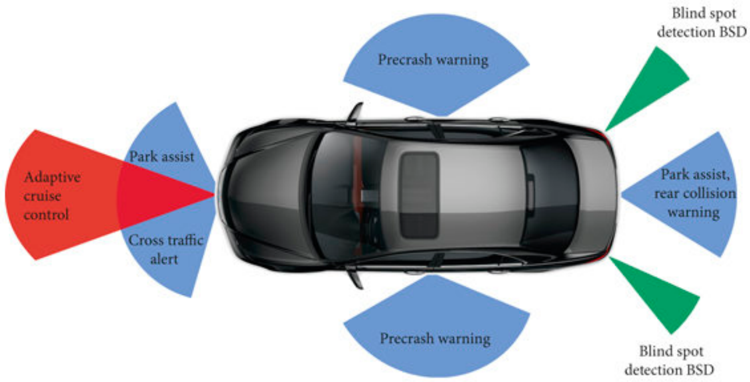

Figure 2.1: Automotive radar applications [11].

The use of radars in these systems allows for greater precision in detecting obstacles and vehicles.

2.2 Classification of automotive radars

Automotive radars can be classified based on different criteria, including detection range, operating frequency range, operating principle and specific application within automotive systems. Correctly distinguishing between these categories is essential to understanding the performance of each type of radar and its suitability for different detection scenarios.

2.2.1 Classification by detection range

The most common classification of car radars is based on their detection range, which defines the type of application for which they are used.

2.2.1.1 Short range radar (SRR)

Short range radars typically operate in the 24 GHz or 77 GHz ranges, and are designed to monitor areas close to the vehicle, in a range of 0.2 m to 30 m.

Main applications:

- Parking assist.
- Blind spot monitoring (BSD).
- Rear Cross Traffic Alert (RCTA).
- Pedestrian and cyclist detection at low speeds.

2.2.1.2 Medium-range radar (MRR)

Medium-range radars typically operate in the 76 GHz to 77 GHz range, covering distances between 30 m and 80 m. They are essential for monitoring traffic in adjacent lanes and helping to prevent collisions.

Main applications:

- Lane Change Assist (LCA).
- Side approach vehicle monitoring.
- Medium distance obstacle detection.

2.2.1.3 Long-range radar (LRR)

Long-range radars operate predominantly in the 76 GHz to 81 GHz range, covering distances greater than 80 m, and can reach up to 250 m in ideal conditions.

Main applications:

- Adaptive Cruise Control (ACC).
- Automatic Emergency Braking (AEB).
- Highway driving assistance.

2.2.2 Classification by frequency range

Speed chambers operate in specific frequency bands, which vary according to international regulations and technical requirements.

2.2.2.1 24 GHz radars

The 24 GHz radars were widely used in short-range applications, but are progressively being replaced by the 77 GHz radars.

Advantages:

- Relatively low cost.
- Good penetration through adverse atmospheric conditions.

Disadvantages:

- Lower spatial resolution.
- Frequency range subject to more restrictive regulations.

2.2.2.2 77 GHz radars

The 77 GHz radars have become the industry standard for automotive applications due to their higher resolution and spectral efficiency.

Advantages:

- Improved spatial resolution and accuracy in object detection.
- Less interference between radars from different vehicles.

2.2.2.3 81 GHz radars

The 81 GHz radars represent the next generation of automotive sensors, offering up to 4 GHz of bandwidth compared to the 1 GHz typically available at 77 GHz. This fourfold increase enables a significantly higher distance resolution, representing a substantial improvement over 77 GHz radars and legacy 24 GHz systems.

Advantages:

- Superior angular resolution for better detection of multiple targets.
- Better performance in dense urban environments.

2.2.3 Relevance of testing and experimental validation

The experimental validation of automotive radars is essential to guarantee their reliability before they are deployed in commercial vehicles. To do this, laboratory tests are carried out in anechoic chambers, where the radars can be analyzed without external interference and under controlled conditions.

The main challenges faced in laboratory testing include:

- **Radar calibration**: Ensures that sensors provide accurate distance and speed measurements of detected objects.
- **Moving target simulation**: Allows you to test the radar's ability to identify moving vehicles and obstacles.
- **Mitigation of unwanted reflections**: The introduction of metallic structures, such as robotic arms used to move targets, can generate reflections that compromise the accuracy of measurements [4].

Research into new radiofrequency (RF) absorbers has been essential to minimize the effects of unwanted reflections and improve the quality of laboratory tests. The development of more efficient and compact anechoic chambers has also been a focus of the industry, with the aim of optimizing experimental tests and reducing the associated costs [12].

2.3 Radar operating principles

Radar systems are fundamental for the perception of the environment in modern vehicles, enabling obstacle detection, distance measurement and velocity estimation. Their operation relies on the emission of electromagnetic waves and the analysis of their reflections from surrounding objects. The accuracy of these measurements depends mainly on the radar's operating frequency and available bandwidth.

2.3.1 Basic structure of an automotive radar

The architecture of a modern automotive radar can be divided into the following main blocks (figure 2.2) [13]:

- **Transmitter and transmitting antenna:** generate and radiate the RF signal into free space;
- **Target object:** reflects part of the incident energy back to the radar;
- **Receiving antenna and receiver:** capture and down-convert the reflected signal;
- **Signal processor:** extracts information such as distance, velocity and angle of arrival, applying digital processing techniques such as the Fourier transform.

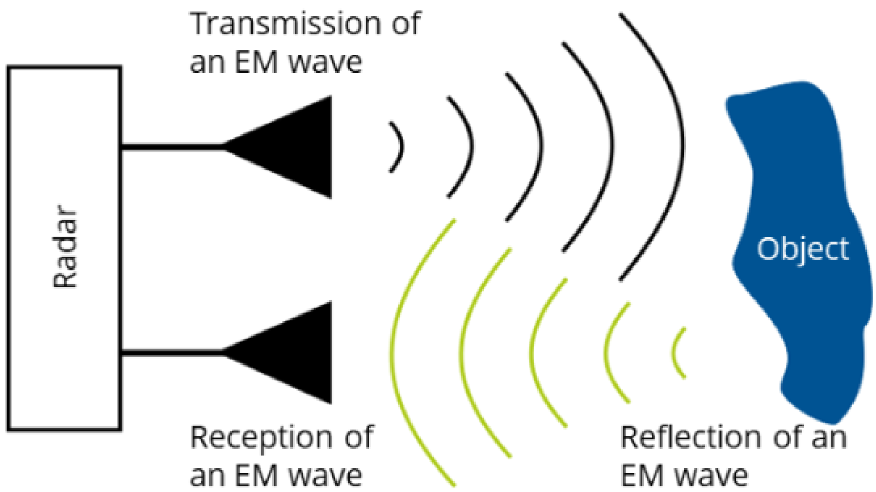

Figure 2.2: Operation principle of an automotive radar [14].

2.3.2 Distance measurement

The distance to a target is obtained from the round-trip time of the transmitted wave. In practice, automotive radars use modulation techniques such as FMCW (Frequency-Modulated Continuous Wave) to achieve centimeter-level resolution [10]. The achievable resolution is directly related to the system bandwidth, with wider bandwidths allowing finer separation between closely spaced objects.

2.3.3 Relative speed measurement (Doppler effect)

The relative velocity of a target is determined through the Doppler effect (figure 2.3), which produces a frequency shift proportional to the radial velocity between the radar and the object [8, 15]. A positive shift indicates that the object is approaching, while a negative shift indicates it is moving away. Higher operating frequencies, such as 77–81 GHz, increase sensitivity to small velocity variations, enabling detection of both fast vehicles and slow-moving pedestrians. This capability supports applications such as Adaptive Cruise Control (ACC), Autonomous Emergency Braking (AEB), and pedestrian monitoring [13, 16].

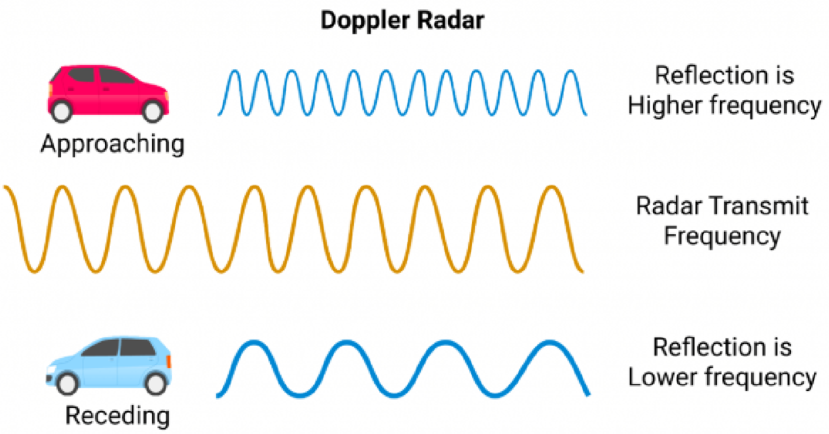

Figure 2.3: Representation of the Doppler effect in an automotive radar [17].

2.3.4 Radio frequency (RF) and intermediate frequency (IF)

The transmitted and received signals initially operate at RF. Before digital processing, they are down-converted to an Intermediate Frequency (IF) using a frequency mixer. This conversion simplifies filtering, amplification and analog-to-digital conversion, making the extraction of distance and velocity information more efficient. IF processing also improves noise rejection and robustness to interference, which are critical in automotive environments.

2.4 Radar Range Equation and Reflection Principles

The reflected signal power measured by a radar can be theoretically estimated using the Radar Range Equation (RRE), which relates the transmitted power to the power received after reflection from a target. In a monostatic configuration, where the same antenna is used for transmission and reception, the received power P_r is given by [8, 13]:

$$P_r = \frac{P_t G^2 \lambda^2 \sigma}{(4\pi)^3 R^4 L} \tag{2.1}$$

where:

- P_t is the transmitted power;
- G is the antenna gain;
- λ is the wavelength of operation;
- σ is the Radar Cross Section (RCS) of the target;
- R is the distance between the radar and the target;
- L represents losses in the propagation path.

The Radar Cross Section quantifies how detectable an object is by radar and depends on its geometry, material properties, and orientation. In the frequency range of interest (76–81 GHz), metallic structures exhibit high RCS values due to their high reflectivity, making them dominant sources of undesired reflections inside an anechoic chamber.

This equation highlights that even small metallic features located near the radar can produce measurable reflections, especially at short distances, where P_r decreases with R^{-4}. This effect is critical when positioning robotic arms inside the chamber, as their conductive surfaces can interfere with measurements if not properly covered with radiofrequency absorbing materials.

In this context, the S-parameter S_{11} experimentally quantifies the reflected wave amplitude from a material or structure under test. A lower $|S_{11}|$ (or a more negative value in $20\log_{10}|S_{11}|$) indicates that less power is being reflected back to the radar, which is consistent with the theoretical expectations of reduced RCS due to the application of absorbers.

Therefore, the Radar Range Equation provides the theoretical basis that justifies the evaluation of reflection reduction in this work, supporting the validity of the experimental methodology and the importance of absorber performance at millimeter-wave frequencies.

2.5 Fundamentals of Electromagnetic Waves

The propagation of electromagnetic waves in materials is governed by intrinsic physical parameters that determine how the wave interacts with the medium. The most relevant properties for radar applications are:

- **Permittivity** (ε) – characterises the ability of a material to store electric energy in an electric field.
- **Permeability** (μ) – represents the material's ability to support the formation of magnetic fields.
- **Impedance** (Z) – defined as $Z = \sqrt{\mu/\varepsilon}$, relates the electric and magnetic field amplitudes of the wave and governs transmission and reflection at material interfaces.
- **Conductivity** (σ) – describes the ease with which free charges move in the material, leading to conduction losses.

- **Loss tangent** (tan δ) – quantifies dielectric losses, defined as $\tan\delta = \varepsilon''/\varepsilon'$, where ε' and ε'' are the real and imaginary parts of permittivity.

- **Reflection parameter** (Γ) – determines the fraction of the incident wave reflected at an interface, given by

$$\Gamma = \frac{Z_2 - Z_1}{Z_2 + Z_1} \tag{2.2}$$

where Z_1 and Z_2 are the impedances of the two media [3, 18].

These parameters are essential to understand the behaviour of absorbing materials in the radar frequency range. Their combined effect determines how much of the incident energy is transmitted, reflected or absorbed when an electromagnetic wave encounters a surface.

2.6 Influence of the medium on radar wave propagation

Automotive radars operate in dynamic environments and are subject to a variety of adverse conditions that can affect the propagation of electromagnetic waves. The attenuation, dispersion and reflection of radar signals vary depending on the presence of rain, fog, snow, dust and moving objects. These factors can compromise the accuracy of measurements and reduce the performance of obstacle detection and driving assistance systems.

2.6.1 Impact of rain, snow and fog

The presence of water particles suspended in the atmosphere, such as rain droplets and snow crystals, can cause attenuation and dispersion of electromagnetic waves, reducing the intensity of the signal received and making it difficult to detect distant objects. This effect is more pronounced at higher frequencies, such as the 77 GHz band used by automotive radars.

Signal attenuation due to rain can be described by the empirical equation:

$$L_r = \gamma_r \cdot d \tag{2.3}$$

where:

- L_r is the attenuation in dB;
- γ_r is the attenuation parameter due to rain (dB/km), which depends on the precipitation rate;
- d is the distance traveled by the signal (km).

Studies indicate that in moderate rainfall (10 mm/h), attenuation at 77 GHz can reach approximately 2 dB/km, while in heavy rainfall (50 mm/h), attenuation can exceed 10 dB/km [19].

Fog can also affect the propagation of radar waves, especially when associated with sub-zero temperatures, where the formation of ice on radar surfaces can reduce their efficiency [3].

2.6.2 Reflections on wet surfaces

When roads are wet due to rain or melting snow, the road surface can act as a mirror for radar waves, resulting in multipath interference. This effect can cause inaccurate distance and speed measurements, especially at low radar beam elevations. To mitigate this problem, modern radars use multipath echo suppression algorithms, based on the arrival time of the signals and their Doppler spectrum [5].

2.6.3 Effect of dust and suspended particles

Environments with a high concentration of dust, such as dirt roads or industrial zones, can also interfere with the propagation of radar waves. Although attenuation at 77 GHz frequencies is lower compared to absorption by rain, the scattering caused by suspended particles can affect the radar's signal-to-noise ratio [20].

2.6.4 Mitigation of adverse effects

To reduce the impact of adverse environmental conditions on car radars, some strategies are adopted:

- Use of adaptive algorithms to compensate for signal attenuation in the presence of rain or fog.
- Advanced Doppler filtering to distinguish real targets from multi-path reflections.
- Sensory redundancy, combining radars with chambers and LiDAR sensors to improve the reliability of measurements in extreme conditions.
- Heating of the radar lens, preventing the formation of ice that could block signal propagation.

These approaches ensure more robust performance from automotive radars, enabling them to operate in a variety of challenging weather scenarios.

2.7 Test conditions and Fraunhofer distance

Laboratory tests on automotive radars require the creation of conditions that ensure the reliability and reproducibility of measurements. One of the fundamental aspects for guaranteeing the validity of the tests is the definition of the measurement zone within the electromagnetic field radiated by the radar antenna. This zone must correspond to the so-called far field, the boundary of which is defined by the Fraunhofer distance.

2.7.1 Concept of near field and far field

The electromagnetic radiation emitted by an antenna can be divided into three regions, as illustrated in figure 2.4 [21–23]:

- **Near reactive field region**: very close to the antenna, where stored electric and magnetic field components predominate. Measurements in this region do not represent the antenna's actual radiation pattern.
- **Near radiating field (or Fresnel) region**: intermediate region where radiated fields begin to dominate, but are still affected by the geometry of the source and interference between direct and reflected waves.
- **Far-field (or Fraunhofer) region**: at a sufficient distance from the antenna where the wavefronts can be considered flat and the radiation pattern becomes independent of the distance from the transmitter.

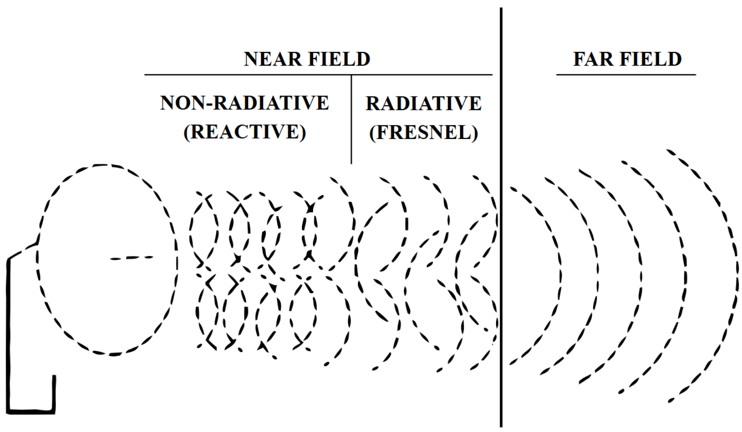

Figure 2.4: Representation of the near-field and far-field regions [24].

The correct definition of the Fraunhofer region is essential to ensure that the test targets are in a zone where the radar beam has stable and predictable characteristics.

2.7.2 Definition and calculation of the Fraunhofer distance

The boundary between the near field and the far field is given by the Fraunhofer distance, which depends on the maximum size of the antenna (D) and the wavelength (λ) of the radiation. The equation that defines this distance is:

$$R_F = \frac{2D^2}{\lambda} \tag{2.4}$$

where:

- R_F is the minimum distance to consider far field (in meters);

- D is the largest dimension of the antenna aperture (in meters);
- λ is the radiation wavelength ($\lambda = \frac{c}{f}$, with c the speed of light and f the operating frequency).

For example, for an antenna with an aperture of $D = 5$ cm operating at $f = 77$ GHz, we have:

$$\lambda = \frac{3 \times 10^8}{77 \times 10^9} \approx 3.9 \text{ mm}$$
$$R_F = \frac{2 \cdot (0.05)^2}{3.9 \times 10^{-3}} \approx 1.28 \text{ m}$$

Thus, any target placed less than 1.28 m from the antenna would be outside the far field, making the measurement less representative of the radar's actual behavior [25].

2.7.3 Importance of the Fraunhofer distance in radar tests

The definition of the Fraunhofer distance has direct implications for the design of laboratory tests with radars:

- This ensures that the antenna's angular pattern is stable and not distorted by proximity effects.
- Avoids interference due to the superposition of multiple wavefronts with different curvatures.
- Establishes minimum positioning for test targets and mobile structures such as robotic arms.

In the context of compact anechoic chambers, this is a major limitation, as the need to maintain a minimum distance can restrict the size of the chamber or the geometry of the tests. For this reason, many systems employ simulation or beam focusing techniques to reduce the spatial requirements [26].

2.7.4 Practical applications and impact on experimental tests

Knowledge and application of the Fraunhofer distance are indispensable at various stages of the automotive radar development and validation process:

- **Radar calibration**: ensure that the targets used for calibration are correctly positioned in the far field.
- **Anechoic chamber design**: optimize the internal space so that most of the signal trajectories develop in the Fraunhofer regime.
- **Electromagnetic simulations**: define appropriate boundary conditions and distances in the numerical models.

- **Reflection analysis**: identify whether reflections from internal chamber structures occur in the near or far field, with implications for the type of absorber required.

Consideration of the Fraunhofer distance is therefore essential to guarantee reliable and representative measurements in the prototyping, testing and certification phases of automotive radars.

2.8 Alternative models for calculating the Fraunhofer distance

The classic expression for the Fraunhofer distance (equation 2.13 in subchapter 2.6.2) assumes that the radiated beam can approximate a plane wavefront when the difference in path between the antenna's end rays does not introduce a significant phase error. However, this model is conservative and does not cover all practical scenarios, especially in the case of compact antennas or measurements carried out in restricted environments [27, 28].

2.8.1 Phase error criterion

A more precise formulation is based on the phase error introduced by the curvature of the wave front. Considering that a phase error of less than $\Delta\phi = \frac{\pi}{8}$ rad (22.5°) is acceptable, the Fraunhofer distance can be redefined as:

$$R_\phi = \frac{D^2}{8\lambda \sin^2(\Delta\phi/2)} \tag{2.5}$$

For $\Delta\phi = \frac{\pi}{8}$, this expression reduces approximately to:

$$R_\phi \approx \frac{D^2}{\lambda} \tag{2.6}$$

which represents a shorter distance than the classic formula, and is therefore more suitable for optimizing space in anechoic chambers [29].

2.8.2 Angle criteria

Another alternative criteria is based on the angular width θ of the antenna's main beam. It is possible to estimate the start of the far field by considering the point where the variation of the field with distance no longer influences the angular pattern. For antennas with a D aperture, this typically occurs when:

$$R_\theta \geq \frac{0.6D^2}{\lambda} \tag{2.7}$$

This model is often used in simulations and practical measurements, offering an intermediate estimate between the Fresnel zone and the classic Fraunhofer zone [30].

2.8.3 Directivity-based criteria

A third approach is based on the directivity D_0 of the antenna, relating the start of the far field to the directional gain. In this case, the minimum distance can be approximated by:

$$R_D = \frac{D_0 \lambda}{\pi} \tag{2.8}$$

This criterion is useful for highly directional antennas, where directivity directly influences the curvature of the wavefront [27].

2.8.4 Comparative discussion

The alternative formulas described above demonstrate that the Fraunhofer distance is not a rigid boundary, but rather a convention depending on the precision criterion adopted. For applications such as characterizing absorbers or testing automotive radar in restricted environments, these approaches allow for greater flexibility without compromising the validity of the results [31].

2.9 Definition and characteristics of anechoic chambers

Anechoic chambers are specialized test environments designed to replicate ideal wave propagation conditions, virtually eliminating any reflections and external interference. The term "anechoic" derives from the Greek *an-* (without) and echo, denoting a space "without echoes". These chambers are used in both the acoustic and electromagnetic domains, and are particularly relevant for testing radio frequency (RF) devices such as antennas, radar sensors and wireless communication systems [32].

In the electromagnetic context, anechoic chambers function as free-field environments, simulating ideal open space conditions, without disturbances caused by reflective surfaces or signals from outside. This behavior is achieved by completely coating the internal surfaces with absorbers that reduce the energy of the incident waves to residual levels. These materials, usually arranged in the form of foam pyramids impregnated with conductive compounds, are designed to have high absorption efficiency in a certain frequency range [33].

These chambers are a critical infrastructure for the precise characterization of radiation parameters, such as directivity, gain and angular pattern of antennas, as well as for the functional validation of sensors in controlled environments. Their use cuts across sectors such as the automotive, aerospace, defense and telecommunications industries, and they are also essential in academic and laboratory contexts.

2.9.1 Physical structure and configuration

A typical anechoic chamber consists of a large room lined internally with absorbers arranged in patterns that maximize the absorption of incident radiation. The structure is usually composed of:

- **Absorbent coating**: pyramids or blocks made of foam impregnated with conductive materials (such as ferrite or carbon), optimized to absorb radiation in specific frequency ranges [34].
- **Base and test platform**: flat surfaces, usually non-conductive, which support the devices under test and the measuring equipment.
- **Electromagnetic shielding**: exterior walls built with conductive materials (e.g. aluminum or steel) to prevent electromagnetic radiation from entering and leaving, ensuring an environment isolated from external disturbances.
- **Adapted lighting and ventilation**: systems designed not to interfere with the internal electromagnetic environment.

The geometry of the chamber is carefully designed to avoid resonances and stationary wave modes. The size of the chamber depends on the frequency range to be tested, with higher frequencies (such as 77 GHz) allowing for more compact structures due to the shorter wavelength.

2.9.2 Performance parameters

The effectiveness of an anechoic chamber is measured by various technical parameters, including:

- **Reflection level (Reflectivity)**: expressed in dB, this represents the amount of energy reflected by the internal surfaces. Typical values for high-performance chambers are around $-60\,\text{dB}$ to $-40\,\text{dB}$ for microwave bands.
- **Free-space attenuation**: defines how well the chamber simulates propagation in free space, without interference or multipath.
- **Field uniformity**: ensures that the electromagnetic field is homogeneous in the test area, allowing for consistent and reproducible measurements.

These characteristics make anechoic chambers indispensable for calibrating and validating automotive radar systems, particularly when assessing sensitivity, detection accuracy and resistance to interference.

2.9.3 Interior coating of anechoic chambers

The internal coating of anechoic chambers is one of the most critical elements for their performance, since its main function is to absorb the energy of incident electromagnetic waves, preventing them from being reflected back into the test area. This coating is generally made up of RF absorbers, whose structure and composition are carefully designed to provide high attenuation in a specific frequency range.

The absorbers currently used in the company's anechoic chamber, which motivated this study, are polyurethane foams impregnated with conductive particles such as graphite, ferrite or carbon, molded into pyramidal or conical geometries. In environments that require a high absorption density in a limited area, flat-plate ferrite absorbers are used, which are highly effective in the lower frequency ranges, complementing the absorption of foams in the higher ranges.

As mentioned earlier, although short-range radars have traditionally operated in the 24 GHz range, modern systems tend to be consolidated in the 76 GHz to 81 GHz range, covering short-, medium- and long-range applications with different antenna configurations and fields of view. In this range, absorption is more challenging due to the short wavelength, requiring materials with high permittivity and magnetic permeability. The thickness of the absorber also influences performance, and for higher frequencies, thicknesses of just a few centimetres can be enough to guarantee attenuations of over 40 dB [35].

Durability, resistance to adverse environmental conditions and dimensional stability are other important criteria when selecting the coating, especially in chambers where thermal cycles or humidity occur. In addition, the composition of the materials must be compatible with fire safety regulations and not emit volatile compounds that could affect the sensors under test.

Recently, advanced absorbers have been investigated, such as broadband electromagnetic absorbers, which promise greater efficiency over a wide range of frequencies, with less volume and weight. These innovations are particularly relevant for reducing the dimensions of the chamber while still respecting the Fraunhofer distance [36].

The internal coating of the anechoic chamber, as seen in figure 2.5 is essential not only to ensure an electromagnetically neutral environment, but also to enable accurate, reliable and repeatable tests, especially at the most commonly used frequencies in the automotive industry.

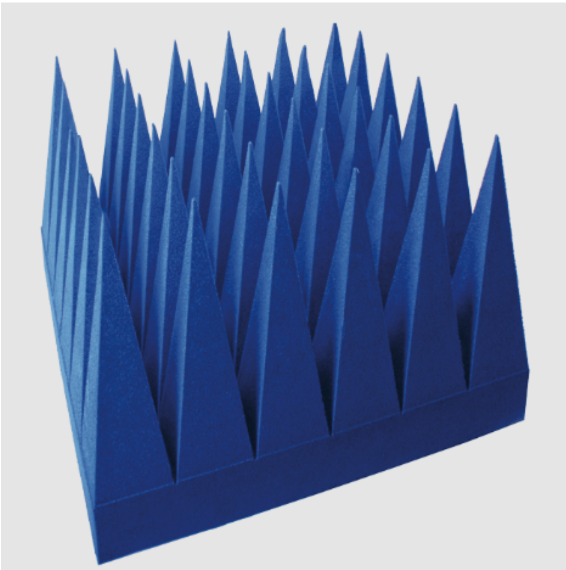

Figure 2.5: Polyurethane absorber typically used in anechoic chambers [37].

2.9.4 Absorption efficiency in the 77 GHz bands

The absorption efficiency of the materials must be evaluated for the specific operating range. In the case of automotive radars, which typically operate at 77 GHz, materials should be tested for their ability to achieve reflection levels below -40 dB. Tests carried out with vector network analyzers (VNA) make it possible to measure the reflection (S_{11}) and transmission (S_{21}) parameters, determining the effectiveness of the absorber [33].

The distribution and orientation of the absorbers also influences performance, and it is essential to avoid parallel surfaces that could give rise to resonance modes.

2.9.5 Absorbent materials used in coating

The absorbers used in the company's anechoic chamber are based on polyurethane foam impregnated with a conductive compound. The pyramidal geometry of these absorbers is designed to maximize absorption by gradually reducing the impedance from the free air to the conductive base (Figure 2.6). This impedance gradient minimizes wave reflection, allowing the electromagnetic energy to be dissipated in the structure of the material [32, 38].

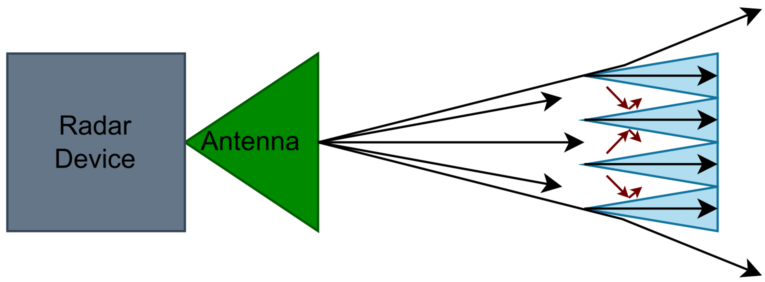

Figure 2.6: Examples of how pyramidal absorbers can reduce the number of reflected waves.

2.9.6 Justification for the selection of the tested absorbers

Although the absorbers considered in this work are commercially available solutions, the manufacturer datasheets do not provide sufficient information for the specific use case of automotive radar validation. In particular, performance data in the 76–81 GHz band is often limited or extrapolated, and the angular dependence of reflectivity and transmittance is typically not included.

Furthermore, the datasheets generally refer to normal incidence conditions, which do not represent the multi-angle exposure experienced in realistic anechoic chamber setups, especially when absorbers are applied to curved and metallic structures such as robotic arms.

For these reasons, experimental characterization is required to obtain reliable data under application-driven conditions. The three selected materials were chosen based on their mechanical flexibility, ease of integration in complex geometries, and their suitability for mitigating undesired reflections within the anechoic chamber. The measurements carried out in this work aim to fill the existing information gap and assess the materials' effectiveness for use in proximity to millimeter-wave sensors.

2.10 Advantages and challenges of anechoic chambers

Anechoic chambers offer several advantages in radar testing:

- Controlled environment isolated from external interference.
- High test repeatability, essential for sensor calibration.
- Flexibility for testing different scenarios with moving targets.

However, these structures also present significant challenges:

- High construction and maintenance costs.
- High space requirements, especially for far-field tests.
- Interference caused by internal auxiliary equipment.

These limitations motivate research into solutions to optimize the performance of chambers and reduce their physical and operational requirements.

2.11 Current method for testing automotive radars

As already mentioned, the experimental validation of automotive radars in a laboratory environment is carried out in anechoic chambers, which ensure a controlled environment free from external interference.

The typical system includes the radar under test (DUT Device Under Test) fixed on a stable support inside the anechoic chamber. In front of it, a target generator is placed which simulates radar echoes, making it possible to virtually adjust the distance, angle and relative speed of objects. One of the most commonly used pieces of equipment for this purpose is the Rohde & Schwarz AREG100A echo generator, which operates in the 76 GHz to 81 GHz range and allows multiple targets to be emulated simultaneously [39].

This system can be complemented with automatic positioning platforms that offer pan and tilt movements to the radar, adjusting its field of view. The distance between the DUT and the signal emitter (target antenna) can be varied linearly, which is important for testing in both monostatic and bistatic configurations.

In addition to active generators, semi-active target simulators are also used in production environments. These systems, such as those from Keysight and National Instruments, are designed for quick tests, with fixed parameters, which guarantee compliance with minimum specifications before integration into vehicles.

The main advantage of these methods lies in the reproducibility of the test conditions, making it possible to compare the performance of different sensors under the same conditions. However, the challenge of simulating dynamic scenarios remains, particularly with moving targets, which has encouraged the adoption of robotic arms or other automated movement systems inside the chamber.

2.12 Integration of robotic arms for radar positioning

The evolution of automotive radar testing methodologies has led to the incorporation of robotic arms into anechoic chambers, not only for moving targets, but above all for the precise placement of the radar sensor itself in the test environment. This solution makes it possible to reproduce multiple scenarios of real operation, through controlled and repeatable positioning of the radar at different angles and distances [40].

The use of robotic arms guarantees high flexibility and precision, essential aspects for measurements involving angular characterization of the emitted radiation, evaluation of directivity and analysis of the radar's response to different geometric configurations [41]. However, this approach also entails relevant technical challenges that must be duly considered.

2.12.1 Problems associated with the presence of metal structures

The main obstacle to integrating conventional robotic arms into anechoic chambers is their metal construction. The presence of conductive surfaces inside the chamber leads to unwanted reflections, affecting signal propagation and introducing multipath effects. These disturbances compromise the accuracy of the measurements, interfering with the estimation of the distance, angle and speed of the targets.

The problem is made all the more relevant by the fact that the radar is installed on the arm itself, i.e. in the immediate vicinity of its radiation zone. In this context, the interaction between the metal structure and the electromagnetic field requires careful analysis in order to minimize the disruptive influence of the physical presence of the positioning system.

2.12.2 Reflection mitigation with absorbers

An effective strategy for mitigating unwanted effects is to apply RF absorbers to the surface of the robotic arm. These materials are specifically designed to absorb the incident electromagnetic waves and minimize the reflected energy, helping to preserve ideal test conditions in the anechoic chamber.

For this application, the flexibility of the absorber material is an essential requirement, since the RAM must adapt to the complex geometry of the arm, enveloping it continuously and effectively. The ability to conform not only allows for integral coverage of the structure, but also ensures that absorption takes place in direct proximity to the emitting source, significantly reducing its electromagnetic signature.

In addition to flexibility, it is also necessary to ensure that the materials used maintain good performance in the 77 GHz range, are lightweight, mechanically stable and do not compromise the operability of the robotic system [33].

2.13 Physical principles of electromagnetic wave absorption and absorbers

2.13.1 Physical foundations of electromagnetic absorption

The interaction of electromagnetic waves with matter results in phenomena such as reflection, transmission and absorption. Absorption occurs when the wave's energy is converted into other forms of energy, usually thermal, within the material. This process is fundamental to the functioning of materials that absorb electromagnetic radiation.

The dielectric and magnetic properties of materials are very relevant to electromagnetic absorption. The complex electric permittivity ($\varepsilon = \varepsilon' - j\varepsilon''$) and the complex magnetic permeability ($\mu = \mu' - j\mu''$) describe how the material responds to electric and magnetic fields, respectively. The imaginary parts (ε'' and μ'') are associated with dielectric and magnetic losses, indicating the material's ability to dissipate energy from incident waves [42].

The impedance match between the absorbing material and the incident medium is a determining factor in reducing reflection at the interface, ensuring a smooth transition of the electromagnetic wave and improving absorption efficiency. When the impedance of the material is adjusted to match that of the incident medium, reflection is reduced, allowing more energy to be transmitted and subsequently absorbed within the material.

2.13.2 Classification of absorbers

Absorbent materials used in radio frequency (RF) applications, such as in anechoic chambers and structures near antennas or radar sensors, can be classified according to their physical mechanism for absorbing electromagnetic energy. The main types include dielectric absorbers, magnetic absorbers and hybrid absorbers or RAM foams. Each category has distinct properties that influence its suitability for different frequency ranges, application geometries and performance requirements.

- **Dielectric absorbers:** These are made up of materials with high electrical permittivity (ε) and significant dielectric losses. Absorption occurs due to the dissipation of energy in the polarization process of the material when subjected to alternating electric fields. They are generally used in high-frequency applications (typically above 10 GHz) and have good thermal and dimensional stability. Common examples include foams impregnated with carbon or graphite.
- **Magnetic absorbers:** These materials have high magnetic permeability (μ) and absorb energy through losses associated with alternating magnetization. They are mainly effective in the lower frequency ranges (VHF, UHF and even X-band) and are often made of ferrites or materials based on metal oxides. They have a high density and are heavier and more rigid, which limits their application in mobile structures.
- **RAM Foams (Radar absorbing materials):** These represent a hybrid class of materials that combine dielectric and magnetic properties, optimized for efficient absorption over a wide range of frequencies. They are made from polyurethane or silicone foams, impregnated with conductive (such as carbon) or magnetic (such as ferrite) fillers. They stand out for their high flexibility, lightness and ease of forming on uneven surfaces, making them ideal for application on robotic arms or mobile metal structures.

Table 2.1: Comparison of the main types of RF absorbers

Characteristics	**Dielectric**	**Magnetic**	**RAM Foam (Hybrid)**
Absorption mechanism	Dielectric losses	Magnetic losses	Dielectric and magnetic losses
Optimal frequency range	High (> 10 GHz)	Medium-low (1-10 GHz)	Low bandwidth (1-100 GHz)
Flexibility	Moderate	Low	High
Density	Medium	High	Low
Typical application	Fixed coating	Structural layers	Mobile surface coverage
Performance on metal	Requires optimization	Good	Excellent

2.13.3 High frequency absorber selection criteria

When selecting absorbers for applications at high frequencies, such as 77 GHz, several factors must be considered:

- **Electrical vs. physical thickness**: The thickness of the material must be sufficient to guarantee effective absorption, taking into account the relationship between the physical thickness and the wavelength of the incident radiation.
- **Thermal and mechanical stability**: The material must maintain its absorber properties under temperature variations and adverse mechanical conditions.
- **Compatibility with complex surfaces**: Flexibility and formability are important for applications on uneven or mobile surfaces, ensuring uniform coverage and consistent performance.

Understanding these principles and the proper classification of absorbers are fundamental to the development and effective application of technologies that require control of electromagnetic radiation.

2.14 Characterization of absorbers with a Vector Network Analyzer (VNA)

The rigorous characterization of the electromagnetic properties of absorbers is a fundamental requirement for the advancement of microwave and radiofrequency applications, namely in anechoic chambers and radar systems used in the automotive industry. The Vector Network Analyzer (VNA) is one of the main tools in this context, allowing detailed measurement of the scattering parameters (S-parameters) of materials over a wide range of frequencies.

2.14.1 VNA operating principles

The VNA is a measuring instrument that tests the electrical behavior of high-frequency components, consisting of an RF source and several test receivers. This is specially designed to measure the transmission characteristics of RF components, i.e. their transmission and reflection values (also called scattering parameters or S-parameters) as a function of frequency. The S-parameters have both a magnitude and a phase component and characterize the device under test. If the network analyzer is capable of analyzing not only the magnitude, but also the phases, it is called a vector network analyzer. It is only since the creation of vector network analyzers that devices that can only measure magnitudes have been called scalar network analyzers, to better distinguish them [43].

2.14.2 Measuring S-parameters

Scattering parameters, or S-parameters, are widely used to describe the electromagnetic behavior of linear systems in the frequency domain. In the context of characterizing absorbers in a free-space configuration, the most relevant parameters are S_{11} and S_{21}, corresponding respectively to the reflection and transmission of the electromagnetic signal.

2.14.2.1 Relevant parameters

- S_{11} – Reflection coefficient at the input port, representing the ratio between the amplitude of the reflected wave and the amplitude of the incident wave. The corresponding reflected power is given by $|S_{11}|^2$. This measurement is particularly sensitive to alignment, impedance matching, and parasitic reflections. In practice, accurate measurement of S_{11} in free-space configurations with a single antenna (typically a horn) can be challenging, especially at millimeter-wave frequencies, due to the low magnitude of the reflected signal and its susceptibility to noise and multi-path interference.

- S_{21} – Transmission coefficient between the transmitting antenna (port 1) and the receiving antenna (port 2), representing the ratio between the transmitted and incident wave amplitudes. The corresponding transmitted power is given by $|S_{21}|^2$. This parameter is generally more reliable in free-space configurations, as it is based on the directly received signal rather than the detection of low-amplitude reflections superimposed on the incident wave.

Figure 2.7 illustrates the both configurations:

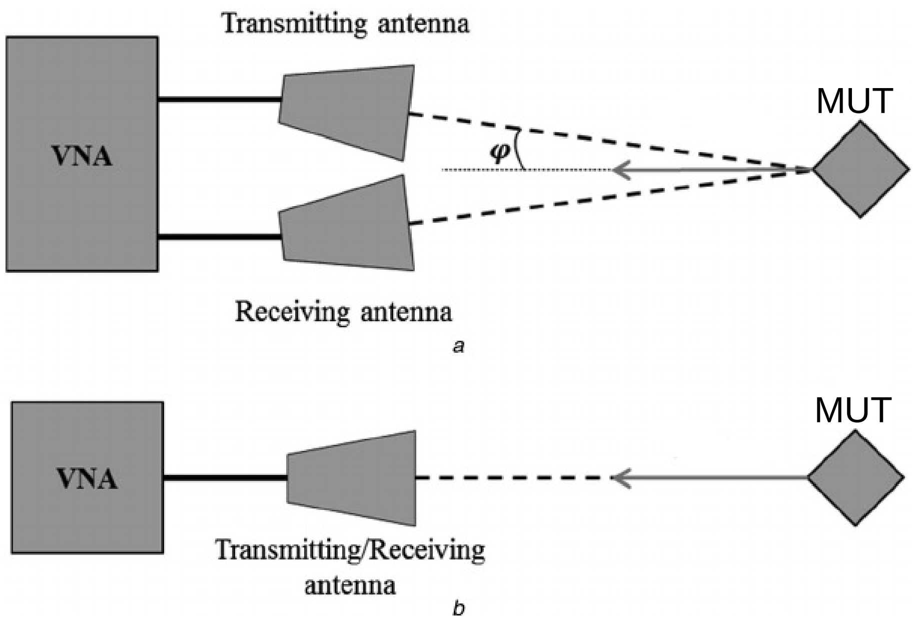

Figure 2.7: Typical measurement setups for characterizing materials using a VNA: (top) bistatic configuration, (bottom) monostatic configuration. In both cases, the material under test (MUT) is placed between the antennas, and the reflection (S_{11}) and transmission (S_{21}) parameters can be evaluated Adapted from [44].

2.14.2.2 Determining absorption

The total absorption (A) of a material, assuming there are no additional losses in the system (e.g. from lateral radiation or leakage), can be estimated from the S parameters using the following equation:

$$A = 1 - |S_{11}|^2 - |S_{21}|^2 \tag{2.9}$$

This relationship expresses the conservation of energy: part of the energy is reflected ($|S_{11}|^2$), another part is transmitted ($|S_{21}|^2$), and the rest is absorbed by the material.

2.14.2.3 Experimental considerations

In real measurements with vector network analyzers (VNAs), several factors can affect the measurement accuracy of the S parameters, especially S_{11}:

- The antenna must be correctly calibrated and positioned in a far-field area so that the beam is sufficiently flat.
- The reflected signal can be of very low intensity, making it difficult to distinguish it from system noise.
- Multiple reflections between the material and the antenna, or with nearby structures, can introduce interference that distorts the measured value.
- The alignment of the material and its distance from the antenna directly influence the coherence of the measured reflections.

For these reasons, the S_{21} parameter is often preferred when comparing the effectiveness of absorbers, especially when two antennas (horns) are aligned, one for emission and one for reception, with the absorber material placed between them.

2.14.2.4 Use in angular characterization

In the case of variable angle measurements, the angular dependence of the S parameters can provide additional information on the directional performance of the material. Variations of S_{21} as a function of the angle of incidence make it possible to evaluate the effectiveness of the absorber under different orientations of the electromagnetic beam, which is particularly relevant for applications such as the coating of robotic arms or panels exposed to multiaxial radiation[45][46].

2.14.3 Frequency and time domain measurements

Although vector network analyzers (VNA) typically operate in the frequency domain, it is possible to convert the data obtained to the time domain using the Inverse Fourier Transform (IFT).

This approach is particularly useful for characterizing absorbers and in situations where multiple reflections or discontinuities along a transmission line are to be identified.

The transformation makes it possible to obtain a temporal representation of the parameters $S(f)$, converting them into a function $s(t)$, which provides information on the instant at which the reflections occur. This conversion is mathematically described by:

$$s(t) = \int_{-\infty}^{\infty} S(f)\, e^{j2\pi ft}\, df \tag{2.10}$$

In practice, as VNA data is discrete and limited to a finite range of frequencies, this operation is implemented using an Inverse Discrete Fourier Transform (IDFT), usually calculated using an Inverse Fast Fourier Transform (IFFT) algorithm.

Applying this technique makes it possible to obtain a temporal profile of the reflection or transmission, which is particularly useful for identifying multiple discontinuities or analyzing composite materials.

2.14.3.1 Frequency domain

Analysis in the frequency domain makes it possible to measure the electromagnetic response of the system for each frequency of interest. This approach is essential for identifying resonances, transparency bands and areas of strong attenuation in materials. In the context of absorbers, it provides direct information on the S_{11} and S_{21} parameters as a function of frequency, making it possible to assess their effectiveness over the entire operating band.

However, when there are multiple discontinuities or internal structures, such as resonant layers or cavities, it is difficult to isolate the contributions of each of the reflections using spectral analysis alone. In these cases, the time domain is used.

2.14.3.2 Time domain reflectometry (TDR)

Time domain analysis, using the technique known as time domain reflectometry (TDR), is a complementary tool to the traditional spectral characterization carried out with vector network analyzers (VNA). This technique makes it possible to visualize the impulse response of the system, identifying the location of electromagnetic discontinuities and separating distinct contributions in the signal path.

TDR is based on applying an Inverse Fourier Transform (IFT) to the frequency data obtained by the VNA. As the measured signal is limited to a finite band and sampled at discrete frequencies, the practical implementation uses the Inverse Fast Fourier Transform (IFFT), allowing the time profile of the response $s(t)$ to be reconstructed from the parameters $S(f)$.

This approach is particularly useful when analyzing absorbers, as it makes it possible to distinguish the energy reflected at the air-material interface from that resulting from internal reflections, mechanical supports or foreign elements in the measurement field. It also makes it possible to check for:

- Imperfections in the coupling between the absorber and the supporting surface;
- Multiple reflections internal to the material;
- Parasitic reflections from the surrounding environment.

TDR also makes it possible to apply time gating techniques, which consist of selecting a specific time window - centered on the desired reflection - eliminating external contributions and significantly improving measurement accuracy.

2.14.3.3 Time resolution and limitations

The temporal resolution of the measurement is directly related to the total bandwidth of the frequency sweep (Δf), and is approximately given by:

$$\Delta t \approx \frac{1}{\Delta f} \tag{2.11}$$

Thus, in order to effectively distinguish reflections from nearby interfaces, it is necessary to scan a wide range of frequencies. On the other hand, the total length of the observable time window depends on the spacing between frequency points (δf), being greater the smaller this step is. This compromise means that the choice of acquisition parameters (start, end and number of points) must be carefully adjusted to the resolution and range requirements.

2.14.3.4 Time to distance conversion

To associate time peaks with physical positions, it is common to convert the time delay Δt into distance d using the relation:

$$d = \frac{c \cdot \Delta t}{2} \tag{2.12}$$

where c represents the speed of light in the medium of propagation (approximately 3×10^8 m/s in air). The factor $\frac{1}{2}$ reflects the round trip of the electromagnetic wave [8].

2.14.3.5 Single antenna test applications

A particularly relevant application of TDR is to carry out measurements with a single antenna operating in reflection (S11), making it possible to extract useful information without the need for a bistatic configuration. In this case, the antenna emits and receives the reflected signal, and analysis in the time domain makes it possible to isolate reflections from the target from parasitic reflections from the environment or the antenna structure, provided they are sufficiently separated in time [27, 47–50].

In summary, time domain reflectometry offers a spatial view of reflections and discontinuities in a measurement system, making it a valuable technique for improving the spatial selectivity of measurements and assessing the integrity of the materials tested, as illustrated in Figure 2.8:

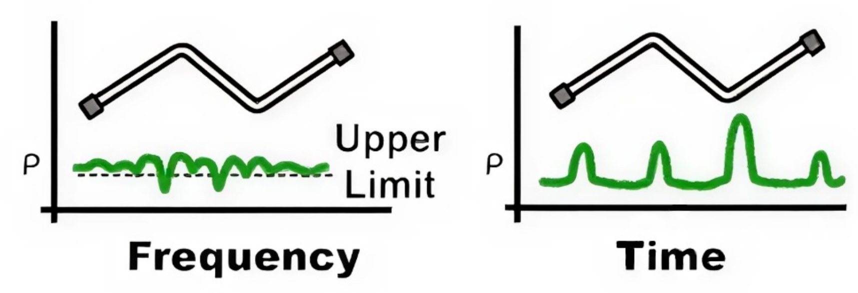

Figure 2.8: Comparison between the representation of a reflection in the frequency domain (left) and in the time domain (right). The conversion makes it possible to spatially separate the reflected contributions, making it easier to identify discontinuities [51].

2.14.3.6 Comparison and practical considerations

In practice, measurement in the time domain can be more sensitive to the presence of small discontinuities, while the frequency domain provides a more comprehensive view of the absorber's performance in the desired spectral range.

It should be noted that for time domain measurements to be effective, a sufficiently high bandwidth and a continuous frequency window are required. The temporal resolution depends directly on the acquired bandwidth, while the maximum depth of analysis is inversely proportional to the spectral resolution.

2.14.4 Experimental procedures for characterizing absorbers

The electromagnetic characterization of absorbers can be carried out using different experimental methods, depending on the frequency range, the type of material and the objectives of the test. The main procedures are presented below, with a particular focus on the 76 to 81 GHz band used in this work.

2.14.4.1 Waveguide measurement

Measuring absorbers using rectangular waveguides (Figure 2.9) is a classic and widely accepted technique for accurately characterizing electromagnetic parameters, especially in high frequency ranges. The method consists of inserting the sample to be tested between two metallic waveguide sections, which are connected directly to the VNA ports, forming a rigidly mounted test cell [52].

In this configuration, the sample must completely fill the cross-section of the guide, ensuring good mechanical and electrical continuity between the two metal sections. To do this, the sample surfaces need to be flat, parallel and carefully prepared to avoid air inclusions or discontinuities, which could alter the measurement result.

The electromagnetic wave then propagates in the dominant TE_{10} mode, which is the fundamental mode of propagation in rectangular waveguides. The designation *TE* (Transverse Electric) indicates that the electric field has no component along the direction of propagation (usually the z axis). The indices accompanying this notation define the number of electric field variations in the directions transverse to the propagation: the first index ($m = 1$) refers to the widest direction of the guide (usually the x axis) and indicates a single field variation in that direction, while the second index ($n = 0$) refers to the narrowest direction (y axis) and indicates no variations. Thus, the TE_{10} mode has a maximum electric field at the center of the cross-section, with a field node near the side walls, and no vertical variation.

This mode is the first to propagate above the guide's cut-off frequency and ensures that the energy propagates in a stable and predictable manner. Using the TE_{10} mode therefore makes it possible to measure the reflection (S_{11}) and transmission (S_{21}) parameters of the material with high precision, since interference from higher modes or complex fields is eliminated.

From these parameters, it is possible to estimate the complex dielectric constant (ε_r) and, in some cases, the magnetic permeability (μ_r) of the material, using methods such as the Nicolson-Ross-Weir (NRW) [53] or the Baker-Jarvis method [54].

Despite the advantages in terms of accuracy, this technique has significant practical limitations for the frequency range used in this work. In the case of the W band, the cross-section of a WR-10 guide is extremely small - just 2.54ṁm by 1.27ṁm - making sample preparation and insertion a complex task. This difficulty is compounded when measuring flexible materials, porous foams or structures with non-uniform geometry, such as conical or pyramidal absorbers.

In addition, the assembly process requires extreme care in aligning the guides, the use of compatible flanges and often the use of presses or clamping systems to ensure proper contact. These technical requirements, combined with the reduced representativeness of the sample (which may not reflect the behavior of the material on a full scale), justify the exclusion of this method in this study. Alternatively, free-space measurements were used, which are more suitable for characterizing bulky samples or those with complex geometry.

An important advantage of this method is that, unlike measurements with free-field antennas, the problem of the Fraunhofer zone does not arise. This zone, which determines the minimum distance needed to guarantee a flat wavefront, is irrelevant in the context of the waveguide, since the field is confined between the metal walls and propagates in a stable and controlled manner. Thus, the waveguide method eliminates the need for remote positioning and allows for more precise measurements even at high frequencies, where the Fraunhofer distance would be prohibitive.

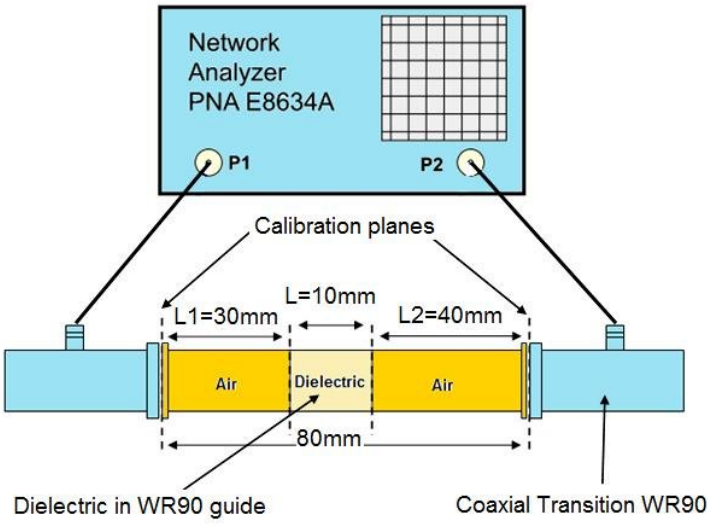

Figure 2.9: Example measurement setup with WR90 rectangular waveguide, using a vector network analyzer (VNA) with coaxial transitions. Adapted from [55].

2.14.4.2 Free space measurement with extenders and antennas

To take measurements in the desired frequency range, a system consisting of:

- **A vector network analyzer (VNA)**, which generates and analyzes the RF signals;
- **Frequency extenders (W-band)**, which convert the VNA signal to higher frequencies, typically between 75 and 110 GHz;
- **Directionally stable horn antennas**, attached to the extenders, which radiate and pick up the signal in free space.

This method, also known as free-space measurement (Figure 2.10), allows the absorbing material to be positioned between two antennas and the parameters S_{11} and S_{21} to be measured under realistic conditions. To ensure that the test takes place in the far field, it is necessary to maintain a sufficient distance between the antennas and the sample, usually greater than the Fraunhofer distance.

The main advantage of this approach is the possibility of testing larger samples with representative thickness and curvature, as well as taking angular measurements by varying the angle of incidence. The use of extenders and horns makes the system adaptable to different bands and with high directivity, which contributes to a more reliable and repeatable measurement.

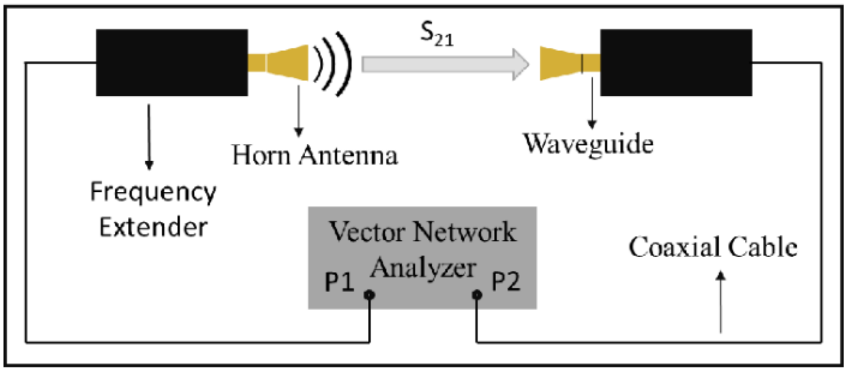

Figure 2.10: Free-space measurement scheme with vector network analyzer (VNA), frequency extenders and horn antennas. The sample is placed between the antennas, allowing the S_{11} and S_{21} parameters to be measured. Adapted from [56].

2.14.4.3 Other approaches

In addition to these methods, there are other more specific techniques that can be applied in different contexts:

- **Reverberation chambers**, used for statistical measurements of the average absorption of surfaces, not very suitable for directional measurements;
- **Coaxial measurements**, limited to frequencies much lower than the W band, generally used up to a few GHz;
- **Holographic analysis or radar imaging**, applied in advanced spatial characterization studies or in structural fault detection.

2.14.5 Operating principle of frequency extenders

Conventional vector network analyzers (VNA) are limited in their operating range, generally up to 50 GHz. To take measurements at higher frequencies, such as the W band (75-110 GHz), it is necessary to use additional modules called frequency extenders. These devices make it possible to extend the measurement capacity of VNAs to millimeter and sub-terahertz ranges.

The typical operation of frequency extenders is based on heterodyne mixing. In this process, radio frequency (RF) and local oscillator (LO) signals from the VNA are fed into the extender and mixed internally by a non-linear mixer (Figure 2.11). The mixer produces sum and difference components of the input signal frequencies, from which the desired frequency is selected using band-pass filters. This technique allows both the generation of signals in the high band (transmission) and the down-conversion of the received signal to an intermediate frequency (IF), compatible with the input of the VNA [57, 58].

Alternatively, some extenders are based on direct frequency multiplication to generate signals in the desired range. In these cases, the RF or LO signal is multiplied by a fixed factor (e.g. $\times 6$ or

×9) using non-linear devices such as scanning diodes, without the need for traditional heterodyne mixing. This approach is simpler in architecture and can have advantages in terms of system stability and compactness, although it typically offers less tuning flexibility.

Integrating the extenders with the VNA requires careful configuration. The extenders are connected to the VNA via coaxial cables for RF, LO and IF, and require their own power supply. Correct calibration with suitable waveguide kits is essential to compensate for losses and lags. In addition, the VNA must be configured with the correct multiplication factors and, in many cases, requires additional software to support the external modules.

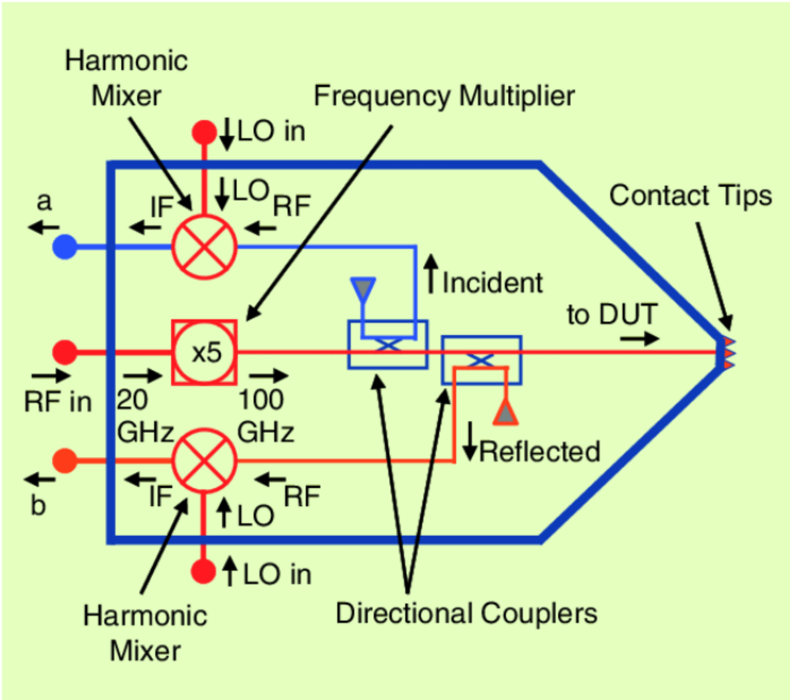

Figure 2.11: Internal schematic representation of a frequency extender for VNA with harmonic mixing and 5× multiplication. The RF signal is amplified and multiplied before being applied to the DUT, and the incident and reflected signals are converted to IF by harmonic mixers [59].

Figure 2.11 represents the internal functional diagram of a frequency extender used with vector network analyzers (VNA), typically in the W band (75-110 GHz). This type of extender allows vector measurements of S parameters by converting the RF and IF signals based on harmonic multiplication and non-linear mixing techniques.

The radio frequency signal (RF in) generated by the VNA enters the module and undergoes frequency multiplication, in this case by a factor of 5×, generating a 100 GHz signal from a 20 GHz signal. This process is carried out by an active multiplier (indicated by ×5), whose output is applied to the device under test (DUT) via internal transmission lines.

On the outward journey, the incident signal passes through a directional coupler, which diverts a fraction of the wave for internal analysis, allowing the transmitted power to be measured. Similarly, the signal reflected by the DUT is picked up by another directional coupler, both of which are redirected to the harmonic mixers.

These mixers combine the captured signals with a local oscillator signal (LO in), also coming from the VNA. The mixing process results in the generation of intermediate frequency (IF) signals, compatible with the VNA. The outputs of the mixers are connected to the `a` and `b` ports, which represent the detection of the incident and reflected wave components respectively. These signals are used to calculate the S_{11} and S_{21} parameters based on the VNA's internal algorithms.

This circuit thus integrates three essential functions: generation of high-frequency RF (via multiplication), detection of incident and reflected energy (via couplers), and down-conversion (via mixers). The architecture is symmetrical and allows bidirectional measurements, being representative of modern extenders such as those developed by Erevant [60].

2.14.6 Calibration techniques in VNA measurements

Calibration is a fundamental process for ensuring accuracy and repeatability in measurements with vector network analyzers (VNA), especially when characterizing absorbers in millimeter bands such as the W band (75-110 GHz). In laboratory configurations with frequency extenders and horn antennas, the systematic errors introduced by losses, reflections and discontinuities in the cables, connectors, waveguides and measurement devices themselves must be rigorously compensated [61, 62].

The calibration technique adopted in this work will be the SOLT (Short-Open-Load-Thru) method, which is based on the sequential measurement of four well-characterized reference standards: a short circuit, an open circuit, an adapted load and a direct connection between ports. This approach allows system errors to be modeled using a 12-term error matrix, including effects such as mismatch, decoupling between ports, losses and lags. Its main advantage lies in the commercial availability of calibration kits even for waveguide configurations, as well as the familiarity and robustness of its process.

Although the SOLT method is often used in coaxial systems, its application in waveguides is possible when appropriate standards are available for the cross-section considered (e.g. WR-10). Measurements are made directly at the interface of the extenders, and the antennas are only connected after calibration, ensuring that the effects of free propagation are treated separately.

Other relevant calibration techniques include:

- **TRL (Thru-Reflect-Line)**: uses a feed-through connector, a reflector (usually a short one) and a transmission line of known length. It is especially useful in waveguide configurations, where it is not trivial to define load or open circuit patterns. However, it requires greater dimensional precision and more careful planning, and is not the option adopted in this work.
- **LRM (Line-Reflect-Match)** and **LRR (Line-Reflect-Reflect)**: variations of TRL that offer additional flexibility, such as eliminating the need for a perfect load. They are useful for measuring free space or built-in structures, but require a controlled environment and specific standards.

- **ECal (Electronic calibration)**: electronic automatic calibration modules that integrate the standards internally and communicate directly with the VNA. They allow for fast and reliable calibration, but their high cost and lower suitability for the W-band frequency range limit their application in this context.

- **GRL (Gated-Reflect-Line)**: widely used in free-space measurements with antennas. It is based on the time-domain transformation to isolate unwanted reflections, and is advantageous when you want to calibrate without physically moving the components. Although this is a viable option, it will not be implemented in this study [63].

The choice of the SOLT method, despite the limitations associated with waveguide operation, is justified by its robustness, the availability of kits compatible with the WR-10 section, and the clarity of the execution process. The correct definition of the cutoff frequency, losses, and physical parameters of the waveguide in the VNA is essential to ensure calibration quality. During the procedure, the frequency extenders must remain connected to the VNA and thermally stabilized to minimize variations introduced by environmental fluctuations. Figure 2.12 shows a basic scheme of the SOLT method:

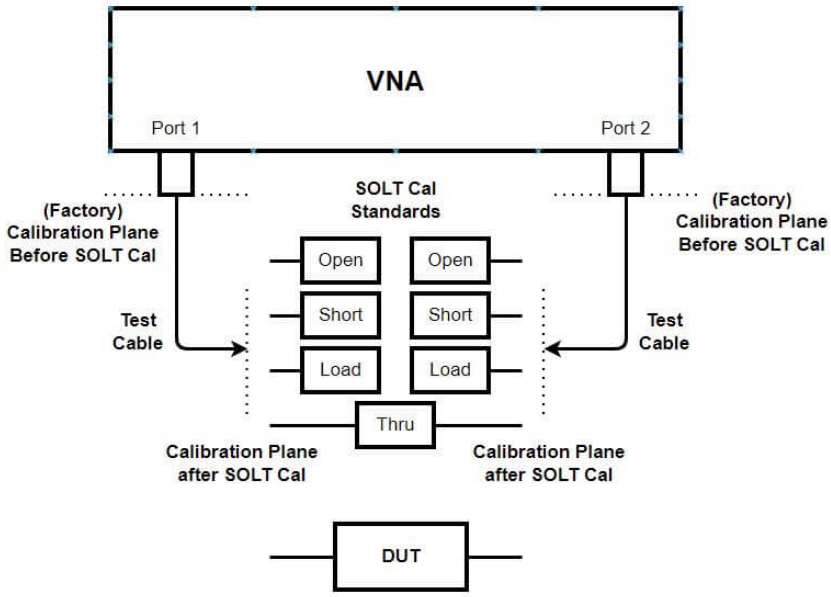

Figure 2.12: Schematic example of SOLT calibration configuration of a complete system [64].

2.14.7 Applications in the characterization of absorbers

The characterization of absorbers with VNA is widely used in various applications, including:

- **Development of materials for electromagnetic shielding**: Evaluation of the effectiveness of new composites in attenuating unwanted signals.

- **Design of anechoic chambers**: Selection of materials that minimize internal reflections, ensuring a controlled environment for testing RF equipment.
- **Automotive industry**: Analysis of materials used in bumpers and radomes to ensure radar transparency and interference minimization [65].

2.14.8 Challenges and considerations

Despite the versatility of VNA, the characterization of absorbers presents challenges, such as:

- **Sample preparation**: Ensuring that the samples have suitable dimensions and characteristics for the chosen measurement method.
- **Influence of environmental factors**: Control variables such as temperature and humidity, which can affect the electromagnetic properties of materials.
- **Interpretation of data**: Analyze the results considering the limitations of the method and possible sources of error.

Understanding these challenges is essential for obtaining reliable results and for advancing the development of efficient absorbers.

Chapter 3

Experimental methodology

3.1 Overview of the experimental approach

Given the characteristics of the materials under test (flexible, porous, or with variable geometry), free-space measurement with horn antennas and W-band extenders was considered the most appropriate. This configuration ensures practical representativeness of the tests, while maintaining compatibility with the available VNA system and offering versatility for future angular and time-domain analyses.

The aim of the adopted methodology is the electromagnetic characterization of absorbers in the 76 GHz to 81 GHz band, simulating the operating conditions of automotive radars. To this end, measurements of the scattering parameters (S-parameters) were carried out with a focus on analyzing the reflection coefficient (S_{11}) and the transmittivity (S_{21}) of the materials.

Two main approaches were followed:

- S_{11} **measurements with an antenna**: were used to determine the intensity of the wave reflected by each material. The time gating technique was used to isolate the desired reflection in the time domain and eliminate external contributions.
- S_{21} **measurements with two antennas**: allowed the response of the materials to be analyzed under different incidence angles (0°, 15°, 30° and 45°), assessing their influence on the attenuation of the transmitted signal.

3.2 Candidate materials for laboratory testing

For the experimental phase, various absorbers were selected in order to assess their effectiveness in attenuating millimeter waves, as well as their practical suitability for coating a robotic arm. The selection took into account not only the electromagnetic properties of the materials, but also their flexibility and ability to adapt to curved and articulated surfaces, essential characteristics for the intended application.

Each material will be analyzed in terms of its response to the signal emitted by the radar, taking into account absorption, ease of application and mechanical resistance in real contexts of use. The following subsections describe the materials tested, highlighting the most relevant properties in the context of this work.

3.2.1 ReZorb™ S

ReZorb™ S is a silicon-based millimeter wave absorber designed to provide high electromagnetic attenuation over a wide range of frequencies, with particular effectiveness between 60 and 90 GHz. This material stands out for its ability to reduce reflections to almost -35 dB, as a result of the combination of its dielectric formulation and textured surface which contributes to a more effective impedance match with the surrounding environment. The absence of magnetic components does not compromise its performance, which remains stable even when subjected to significant temperature variations.

With a controlled thickness of around 4.7 mm, ReZorb™ S offers a compromise between absorption capacity and ease of handling. Its elastomeric structure gives it sufficient flexibility to be molded to complex geometries, such as those of an articulated robotic arm, without any significant loss of effectiveness. In addition, the material's mechanical strength and durability, combined with its compliance with environmental standards, reinforce its applicability in demanding industrial environments where long-term performance is critical [66].

3.2.2 Eccosorb™ HR – Laird performance materials

O Eccosorb™ HR is a broadband, lightweight and flexible microwave absorber made up of open-cell polyurethane foam loaded with carbon, forming a conductivity gradient throughout the thickness of the material. This structural configuration promotes effective absorption of electromagnetic energy, essentially due to dielectric losses associated with its cellular structure. The material is available in sheets of 610 mm by 610 mm, with typical thicknesses of 10 mm (HR-10) and 25 mm (HR-25), and a density of around 45 kg/m^3.

Its performance varies depending on the thickness: the HR-10 model has reflection losses of more than -20 dB between 12 and 70 GHz, while the HR-25 extends this effectiveness to lower frequencies, maintaining reflection losses of more than -20 dB between 5 and 27 GHz. Although not weatherproof, Eccosorb HR is particularly effective indoors, and is also suitable for installation in curved or irregular structures due to its flexibility and ease of cutting.

Thermal stability up to 90°C and low density make Eccosorb HR a versatile solution for integration into test structures and mobile components, justifying its inclusion in this comparative study [67].

3.2.3 Conical RAM 95.00344-00 – Soliani EMC

Soliani EMC's Conical Radar Absorbent Material (RAM), reference number 95.00344-00, is a broadband electromagnetic absorber made of charged nitrile rubber. It has a conical geometry and a thickness of 6 mm, with a tolerance of ± 1 mm, and is supplied in sheets with approximate dimensions of 150 mm by 300 mm. Its design aims to reduce unwanted reflections of millimeter waves, and it is particularly suitable for applications related to automotive radars (ADAS systems), intelligent trains and other advanced sensing systems.

It is a lightweight material (around 190ġ per sheet), weather resistant and suitable for operation in harsh environments, maintaining mechanical integrity and electromagnetic performance over a wide range of temperatures, from -50°C to 80°C. The conical surface allows the incident energy to be dispersed efficiently, contributing to effective attenuation of reflections at multiple angles of incidence.

In terms of performance, this material covers the frequency range between 40 and 110 GHz, with reflection losses of at least -12ḋB at 40 GHz and -15ḋB between 77 and 110 GHz, for near-normal incidence. These characteristics make it particularly relevant for laboratory tests with sensors at 77 GHz, such as those considered in this dissertation, offering a good compromise between reduced thickness, lightness and efficiency in free-space absorption [68].

3.2.4 PP-RAM - EMC Electronics absorber

PP-RAM is a high-performance electromagnetic absorber developed by EMC Elektronik, based on low-density polypropylene foam. It is lightweight, robust and compatible with a wide range of frequencies. It is suitable for technical applications in laboratories as well as for concealment and camouflage scenarios in military environments. Its structure is optimized to reduce side lobes, improve the front-to-back ratio of antennas and mitigate unwanted interference close to the emitting source.

This absorber has a particularly wide operating range, from 30 MHz to 120 GHz, covering practically all the bands of interest for civilian and military applications. Typical reflection losses are between 35 and 50ḋB, varying according to thickness and frequency, indicating an extremely high absorption capacity, compatible with the most demanding levels of attenuation in free space.

In addition to its electromagnetic characteristics, PP-RAM also stands out for its mechanical resistance and environmental stability. It is prepared to operate in harsh environments, with temperatures between -50°C and +90°C on a continuous basis, and up to -100°C or +120°C in short-term conditions. It also has a B2 flame resistance rating (GB8624-1997), with an oxygen index of more than 29%, and operates stably under relative humidity of 55% ± 15%. These properties make PP-RAM especially suitable for critical applications where electromagnetic performance must coexist with safety requirements, longevity and resistance to the environment.

The high electromagnetic performance, combined with its lightness, wide frequency range and mechanical versatility, justifies its inclusion as a leading candidate in this comparative study.[69].

3.3 Material evaluation criteria

The selection of the absorbers to be tested is based not only on their ability to attenuate millimeter waves, but also on their practical viability for application in mobile components, such as a robotic arm. The evaluation will therefore be conducted along two main lines: electromagnetic performance and physical suitability for the application.

Table 3.1: Comparison of absorbers analyzed

Material	**Thickness**	**Freq. (GHz)**	**Reflection loss (77 GHz)**	**Flexible**
ReZorb S	4.7 mm	60–90	$\approx$ -30 dB	Yes
Eccosorb HR-10	10 mm	5–90	$\approx$ -28 dB	Yes
Eccosorb HR-15	15 mm	5–90	$\approx$ -27 dB	Yes
Eccosorb HR-25	25 mm	5–90	$\approx$ -25 dB	Yes
Soliani RAM	6 mm	40–110	$\approx$ -15 dB	No
EMC Pyramidal	96–700 mm	10–100	$\leq$ -45 dB	No

From the electromagnetic point of view, the central criterion will be the reduction in the reflected signal, measured by the intensity of the echo detected by the radar in the presence of each material. This reduction will be quantified in dB by comparing the power of the reflected signal with and without the absorber material. The Signal-to-Noise Ratio (SNR) metric will also be analyzed, since effective materials should not only reduce the reflected signal, but also maintain a consistent response without introducing significant noise.

In addition to intensity, the stability of absorption under different conditions will be considered, namely variations in angle of incidence and distance. The ability of the material to maintain a uniform performance in these situations will be essential for its practical use. In addition, the influence of the thickness and texture of the material on the overall response will be observed, in order to understand how these characteristics affect its effectiveness in the radar's operating range.

On a physical level, the flexibility of the materials will be assessed qualitatively, considering how easy they are to apply to curved surfaces and joints, without compromising their mechanical integrity. Materials that resist deformation well while maintaining their absorber properties will be considered more suitable. Thermal resistance and expected durability will also be taken into account, especially in industrial contexts.

The combination of these criteria will allow for a comprehensive analysis aimed at identifying solutions that combine good performance in attenuating millimeter waves with practical characteristics suitable for coating robotic systems.

3.4 Equipment used

To carry out the experimental measurements, we used a set of equipment capable of operating in the frequency range between 67 GHz and 115 GHz, compatible with the band of interest (76-81 GHz). The equipment used is described below:

- **Vector Network Analyzer (VNA)**: Keysight PNA N5224B, responsible for generating and measuring high-frequency signals. It operates in the 10 MHz to 43.5 GHz range without frequency extenders.

- **Frequency extenders**: two VNAX WR10+ modules for operation in the 67 GHz to 115 GHz range, connected to the VNA via dedicated cables (IF, LO and RF).

- **Directional horn antennas**: two SAR-2507-10-S2 model antennas, with WR10 connector and high gain, suitable for near-field measurements and car radar simulation.
- **Calibration kit**: set of SOLT (Short, Open, Load, Thru) standards, used to calibrate the measurement system in the waveguide plane.
- **Alignment system**: Bosch GLL 3-80 line laser, used to ensure correct alignment of extenders, antennas and materials during measurements.
- **Supports and physical structure**: includes adjustable tripods for the extenders, stable supports for the tested materials, and background absorbers to minimize unwanted reflections.
- **Materials tested**: various types of absorbers, as well as metallic and dielectric surfaces (such as wood), placed under the same conditions for comparison purposes.

This set of equipment ensured precise, stable measurements compatible with the requirements of electromagnetic characterization in the desired band, while guaranteeing repeatability and control of the experimental variables.

3.4.1 Vector Network Analyzer – Keysight PNA N5224B

The Keysight PNA N5224B is a four-port vector network analyzer designed for high-precision microwave and radio frequency measurements. Its native operating range is from 10 MHz to 43.5 GHz, with the possibility of expansion to the terahertz range via external modules. The presence of four physical ports allows complex measurements to be made on multifunctional devices such as amplifiers, filters, antennas or multiple input multiple output (MIMO) networks, with full support for bidirectional measurements and mapping of all S parameters.

The N5224B has high-performance internal receivers, with a noise trace of less than 0.002 dB (rms) and a dynamic range of more than 120 dB, depending on the frequency and configuration. It integrates advanced features such as time domain analysis (Time Domain Reflectometry), inverse Fourier transforms for visualizing reflection events, and time gating support for isolating signals in time or distance. The calibration system is compatible with SOLT, TRL and LRM methods, among others, with support for automatic, manual or remote calibration.

In terms of connectivity, the equipment includes dedicated ports for LO, IF and RF connections, necessary for operation with external frequency extenders, as well as multiple interfaces for remote control and acquisition (LAN, USB, GPIB). It also has an internal processor with support for SCPI scripting, integration with MATLAB and LabVIEW, and graphical display in various formats (Smith diagram, magnitude and phase, parameters in dB or time).

Its high-resolution touch screen and intuitive interface make it easy to configure and analyze measurements, and it is possible to perform operations such as frequency sweeps, band segmentation, dynamic compression, and power measurements with vector correction. These capabilities make the N5224B a versatile tool both for device development and characterization and for production environments and automated testing [70].

3.4.2 Frequency extenders - VNAX WR10+

In order to extend the VNA's capacity to the desired frequency band, a pair of Virginia Diodes millimeter band extenders, model VNAX WR10+, was used (Figure 3.1). These devices can take vector measurements between 67 GHz and 115 GHz, fully covering the operating band of this kind of radars (76-81 GHz), the target of this study.

The WR10 band has a typical dynamic range of 120 dB, with a guaranteed minimum value of 110 dB, which ensures highly sensitive measurements. The typical output power on the test port is 18 dBm, and the maximum estimated input power (without causing damage) is 30 dBm for the TxRx and TxRef ports. Stability is also remarkable, with a typical variation in magnitude of less than ±0.10 dB and a phase variation of less than ±1.5°, which contributes to the reliability of measurements over time.

These extenders operate with dedicated connections for RF, LO (Local Oscillator) and IF (Intermediate Frequency) signals, with the typical input power level for LO and RF signals being approximately +6 to +10 dBm, as indicated on the device connectors. This type of architecture allows signals to be generated, converted and amplified outside the main VNA, extending its frequency range in an external and controlled manner.

The connection to the VNA is made using specific cables for the IF, RF and LO bands, and it is necessary to ensure that the lengths and losses are compatible with the system's requirements. The use of the extenders also requires the activation of the frequency offset mode in the VNA, which allows the correct processing of signals in bands higher than the instrument's native band.

These devices were made available by INESC TEC, the research institute with which this work was carried out. These extenders were chosen not only because of their compatibility with the Keysight PNA N5224B VNA, but also because they allow high-frequency measurements to be made without the need for more expensive dedicated equipment. At the Controlar Innovating Industry company, where the internship was carried out, instruments capable of operating in these frequency ranges were not available, justifying the collaboration with INESC TEC for this purpose [71].

Figure 3.1: Keysight N5224B vector network analyzer together with WR10 frequency extenders.

3.4.3 SOLT calibration kit

To guarantee the accuracy of the measurements with the vector network analyzer in conjunction with the millimeter band extenders, a calibration kit based on the SOLT (Short, Open, Load, Thru) method was used (Figure 3.2), as recommended by Virginia Diodes for configurations with VNAX modules. The calibration kit used is compatible with WR10-type waveguides and includes high-precision mechanical standards that make it possible to calibrate the systematic errors associated with vector measurement, such as losses, impedance mismatches and couplings.

Calibration was carried out directly on the flanges of the VNAX WR10+ extenders, using the four basic standards:

- **Short**: conductive end that fully reflects the signal with inverted phase.
- **Open**: open end that fully reflects the signal without phase inversion.
- **Load**: absorbent termination that minimizes reflection.
- **Thru**: direct connection between the two measurement ports for transmission reference.

These standards were connected sequentially to the extender ports using alignment screws suitable for WR10, according to the manufacturer's instructions. The calibration was carried out in the VNA's 2-port mode, with the frequency offset option active to compensate for the internal multiplication of the signals. This calibration made it possible to remove the effects of imperfections in the cables, adapters and flanges, establishing a reliable reference for the *S*-parameter measurements in the materials analyzed.

The procedure was essential to ensure that the measurements taken reflected only the characteristics of the materials under test, without contamination due to imperfections in the measurement system [72].

Figure 3.2: SOLT calibration kit used to calibrate the measuring system in the plane of the WR10 extender connectors.

3.4.4 SAR-2507-10-S2 antennas

The antennas used during the tests were model SAR-2507-10-S2 (Figure 3.3). These antennas are of the pyramidal horn type and operate in the 75 GHz to 110 GHz frequency band, thus covering the entire operating range of the VNAX WR10+ extenders.

The antenna has a nominal gain of 25 dBi, with typical values between 23.5 dBi and 26 dBi, minimizing lateral interference. The polarization of the signal is linear.

The antenna's input port is a WR-10 waveguide with a UG-387/U-M flange, compatible with the extenders used. In terms of construction, the antenna is made of brass with a gold-plated finish, providing good conductivity and resistance to corrosion. The approximate dimensions of the antenna are 6.86 cm (length) × 2.77 cm (width) × 2.26 cm (height), with a weight of approximately 36.9 grams.

This antenna was chosen because of its high radiation efficiency, directivity and good impedance matching over the entire operating band. The typical return is over 23 dB, ensuring low reflection at the input port.

These characteristics make the antenna suitable for both reflection measurements (S_{11}) and direct transmissions (S_{21}), in conjunction with the use of absorbent or reflective materials placed on the beam propagation line [73].

Figure 3.3: SAR-2507-10-S2 antenna used in the measurements.

3.4.5 Bosch GLL 3-80 alignment laser

The alignment of the experimental components, namely the antennas and the materials under test, was facilitated by the use of a Bosch GLL 3-80 line laser (Figure 3.4). This equipment allows the projection of three 360º laser lines - one horizontal and two vertical - making simultaneous leveling and alignment in multiple planes possible. It operates with a class 2 laser, with a wavelength between 630 and 650 nm and a power of less than 1 mW, making it visible and safe for use in a laboratory environment.

The automatic leveling accuracy is approximately $0.2\,\mathrm{mm\,m^{-1}}$, and it can automatically correct inclinations up to 4° in around four seconds. Under normal conditions, the maximum projection range is around 30 m, which can be extended up to 120 m with a dedicated laser receiver (not used in this work). It is powered by four AA batteries, providing an autonomy of around four hours in continuous projection mode of the three lines.

This equipment was chosen due to its high stability and optical precision, characteristics that are particularly relevant for the rigorous assembly of the measurement system, where small angular variations can significantly affect the reflection results [74].

Figure 3.4: Line laser used for measurements.

3.5 System calibration

3.5.1 Preparing the system for calibration

Before the actual calibration, it was necessary to correctly establish the connections between the Keysight N5224B vector network analyzer and the WR10+ frequency extenders. The connection between the devices consists of three main cables: RF, IF and LO, which connect the extenders' connectors to the corresponding ports on the VNA. The order of connection and the identification of each cable were strictly followed based on the diagram provided in the VNAX manual. This procedure was essential to ensure the correct operation of the extenders and to prevent damage to the sensitive circuits.

To ensure reliable contact and avoid unwanted losses, all the connectors were carefully tightened using suitable tools. A screwdriver and a fixed wrench were used to ensure consistent torque and prevent any looseness in the connections.

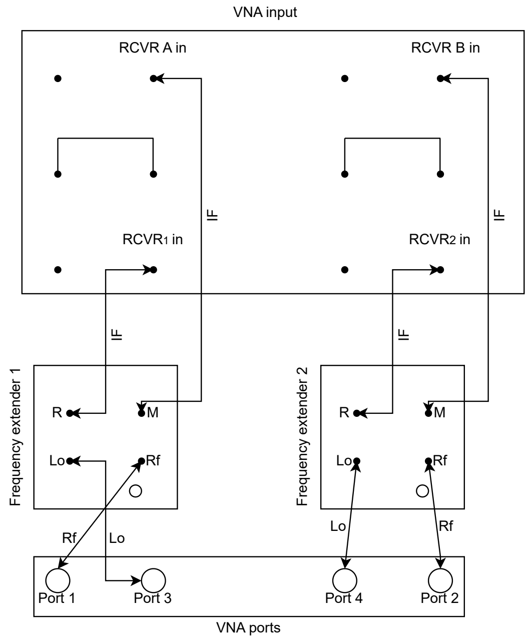

Diagram of the connections between the VNA and the extensors.

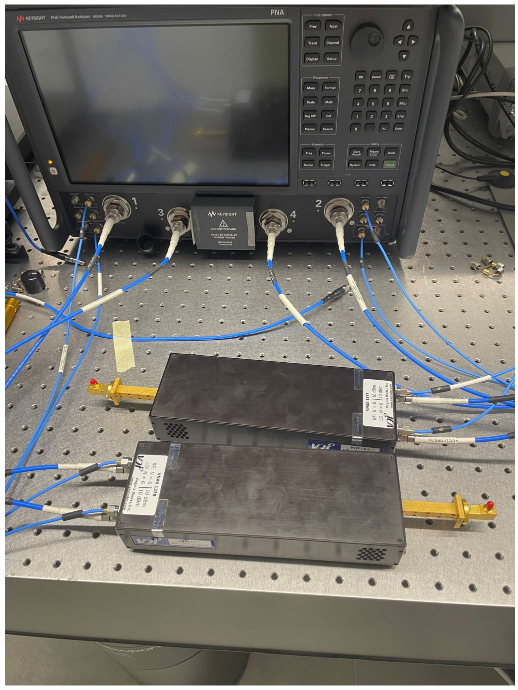

Connection made in the laboratory.

Figure 3.5: Connections between the VNA and the frequency extenders.

After the physical connections were made (Figure 3.5), the necessary adjustments were made to the VNA software to adapt the measurement parameters to the characteristics of the WR10+ extenders. This procedure was based on the VDI extender manual, which defines the ideal power values for the RF and LO signals, as well as the permitted frequency range. The adjustments essentially consisted of defining the operating frequency range (from 67 GHz to 115 GHz), selecting the appropriate LO source and configuring the measurement mode to reflect operation with external extenders.

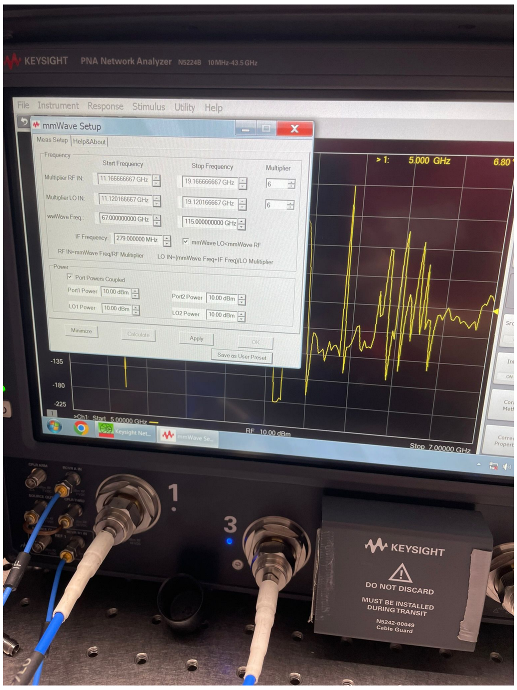

Figure 3.6: Configuring the VNA for operation with WR10+ extenders.

With the connections established and the parameters duly adjusted, the system was then calibrated using the SOLT method (Short, Open, Load, Thru). The procedure followed the standards in the kit supplied with the extenders, as described in the next section.

3.5.2 SOLT calibration process

Calibration was carried out directly on the vector network analyzer, using the VDI standards kit mentioned above. During the procedure, the VNA software recognized the Short, Load and Thru patterns, while the Open pattern, which is common in the SOLT method, was absent due to the physical limitations of the waveguide implementation. This behavior is to be expected and is in line with the kit manufacturer's recommendations, which define the three available standards as sufficient for correcting systematic errors in this frequency range.

After selecting the calibration method and the corresponding kit, the standards were connected sequentially, with the system recording each step. Figure 3.7 shows photographs of the three standards used, while Figure 3.8 shows the VNA interface after calibration, with the standards correctly applied.

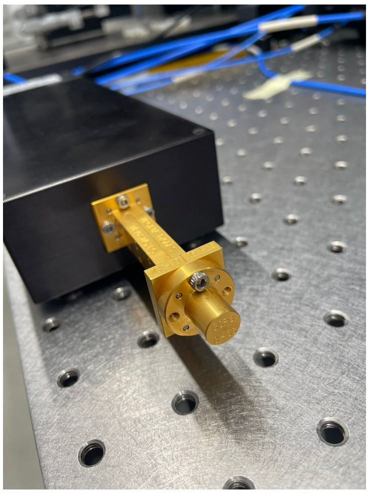

Short standard .

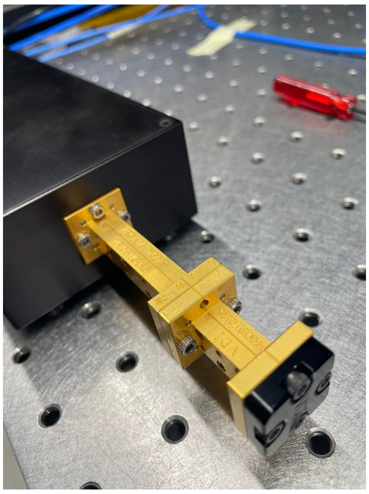

Load standard.

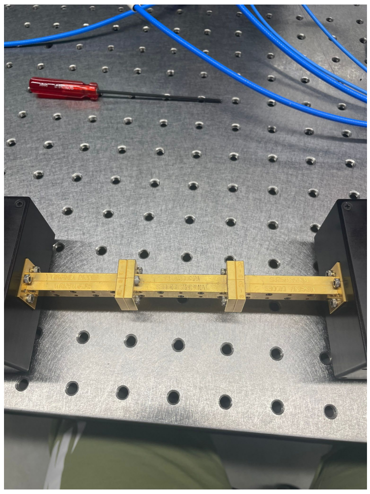

Thru standard.

Figure 3.7: Application of the three physical standards from the SOLT calibration kit.

Figure 3.8: VNA interface after calibration with the Short, Load and Thru standards.

3.5.3 Calibration check

Once the SOLT calibration process was complete, it was validated to ensure that the systematic errors had been effectively compensated for. This check consisted of observing the response of the S_{21} function with the Thru standards connected between the two frequency extenders.

Given that correct calibration must eliminate the main transmission and reflection errors, an ideal response would show an S_{21} value close to 0 dB over a wide frequency range. This value indicates that the signal transmitted between the two ports suffers minimal losses, which shows that the correction parameters have been correctly applied.

Figure 3.9 shows the vector network analyzer screen after calibration, with the two extenders connected via the Thru standard. As can be seen, the value of S_{21} is effectively close to 0 dB in the desired frequency range, which validates the success of the calibration.

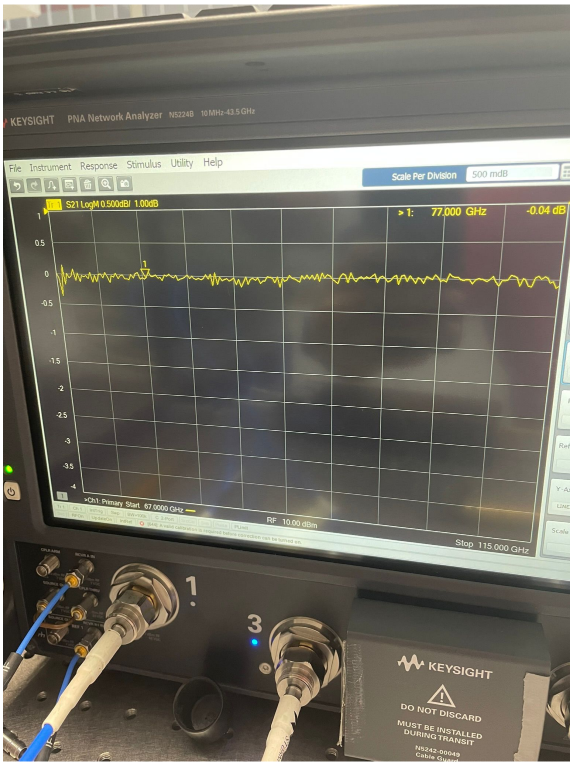

Figure 3.9: Verification of SOLT calibration by measuring S_{21} with the Thru standard.

It is important to note that any change in the layout of the extenders or cables, however slight, can introduce new discontinuities or parasitic reflections. For this reason, whenever the physical configuration of the system changes, it is necessary to repeat the calibration to ensure the reliability and repeatability of the measurements obtained.

3.6 Materials tested

During the experimental planning phase, the characterization of a wider range of absorbers was considered. However, due to logistical and budgetary constraints, some of these materials were not purchased. In particular, certain candidates had significantly high prices or delivery times that were incompatible with the internship schedule, making it impossible to use them in the context of this work.

Thus, four different materials were selected for characterization, based on their availability and practical relevance:

- Eccosorb™ HR 10.
- Eccosorb™ HR 25.
- Rezorb S™.
- A metal plate, used as the ideal reflective reference.

3.7 Measurements of S_{11} - reflection with a single antenna

For most of the internship period, a second antenna was not available for taking transmission measurements (S_{21}). In view of this limitation, a characterization methodology was devised based exclusively on reflection measurements (S_{11}), using a single antenna. This approach, although more limited, allows for an effective assessment of the electromagnetic absorption capacity of materials, provided it is complemented with appropriate techniques such as time gating.

3.7.1 Half-power beamwidth (HPBW)

To ensure that the antenna beam falls completely on the sample to be tested, it is essential to know the main beam width, or Half Power Beam Width (Figure 3.10), which represents the opening angle corresponding to an attenuation of 3 dB with respect to the maximum.

In these measurements, it is important to ensure that the antenna's beam hits the material completely. To do this, it is necessary to know the angular width of the main beam - the HPBW, which corresponds to the angle at which the radiation intensity decreases by 3 dB from the peak.

The SAR-2507-10-S2 antenna has an HPBW of 9° in the E (vertical) plane and 10° in the H (horizontal) plane [73], which results in an elliptical-shaped radiation pattern, slightly wider in the horizontal direction.

The affected area can be estimated geometrically from the equation (3.1) [75]:

$$D = 2 \cdot d \cdot \tan\left(\frac{\text{HPBW}}{2}\right) \tag{3.1}$$

Given a distance of $d = 0{,}20\,\text{m}$, the following beam diameters are obtained:

- E plane (9°):

$$D_E = 2 \cdot 0.20 \cdot \tan(4.5^\circ) \approx 3.14\,\text{cm}$$

- H plane (10°):

$$D_H = 2 \cdot 0.20 \cdot \tan(5^\circ) \approx 3.50\,\text{cm}$$

In this way, the beam is incident on an elliptical area with approximate dimensions of $3.1 \times 3.5\,\text{cm}^2$. As all the materials tested have dimensions significantly greater than these values, it is guaranteed that all the incident energy interacts exclusively with the sample, without interference from supports or edges. This controlled geometry is also crucial for the effective application of time gating, allowing direct reflection to be isolated with high temporal precision.

In addition, this distance allows this technique to be applied effectively, since it translates into a round trip time for the electromagnetic wave of approximately 1.33 ns, the value around which the time window for extracting the reflected signal was centered.

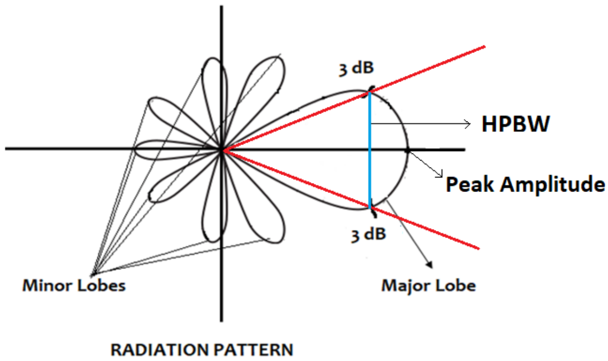

Figure 3.10: Schematic representation of the radiation pattern of an antenna, highlighting the main lobe, the secondary lobes and the half-power beamwidth (HPBW), corresponding to the zone where the power is up to 3dB below the peak [76].

3.7.2 Application of time gating

The time gating technique proved essential for isolating the contribution of the absorbing sample during S-parameter measurements, particularly to exclude interference from secondary reflections, mechanical supports or nearby objects. The central idea is to transform the data acquired in the frequency domain into the time domain using the Inverse Fourier Transform. This operation makes it possible to visualize the different echoes that make up the system's response, organized according to the time of flight of the electromagnetic signal.

After this transformation, it is possible to identify the main reflection associated with the sample and apply a time window centered on this response, excluding all other components that do not belong to the zone of interest.

3.7.2.1 Transform On and Gating On

In the vector network analyzer (VNA) used, the application of time gating is based on two complementary functionalities: Transform On and Gating On, which must be used in a coordinated manner to ensure correct isolation of the desired response.

Transform On: This option activates the transformation of data from the frequency domain to the time domain, allowing the impulsive response of the system to be visualized. With this visualization, it becomes possible to identify the time instant corresponding to the main reflection of the sample, distinguishing it from other reflections or interferences outside the zone of interest.

Gating On: After identifying the position of the peak of interest in the time domain, this option allows you to apply a time window (gate) with user-defined limits. The zone contained within this window will then be converted back to the frequency domain, excluding all external contributions to that region. In order for the effect of gating to be directly reflected in the frequency domain traces, Transform On must be deactivated, leaving only Gating On active.

The typical procedure consists of: 1. Activate Transform On to visualize the response in the time domain; 2. Adjust the position and width of the time window based on the peak of the main reflection; 3. Activate Gating On with the limits set; 4. Deactivate Transform On so that the trace in the frequency domain only shows the contribution contained within the applied window.

3.7.2.2 Choice of gate type: Band pass vs. Low pass

During the analysis, the Band Pass window option was selected instead of Low Pass. The choice of Band Pass mode allows the analysis to be restricted to a specific region of the time response, i.e. only the peak reflection of the sample, ignoring both the previous and subsequent echoes. Low Pass mode, on the other hand, would keep the entire response up to the window instant, which is not desirable in this context, as it would include unwanted contributions.

3.7.2.3 Configuring and interpreting the time window

Initially, a wide window was applied to observe the entire impulse response in time, allowing the position of the peak of interest to be clearly identified. After this identification, the window was fine-tuned, centered on the peak corresponding to the sample's reflection and reduced to a typical width of 500 ps. Figure 3.11 shows an example of the window configuration, centered on 1,566 ns.

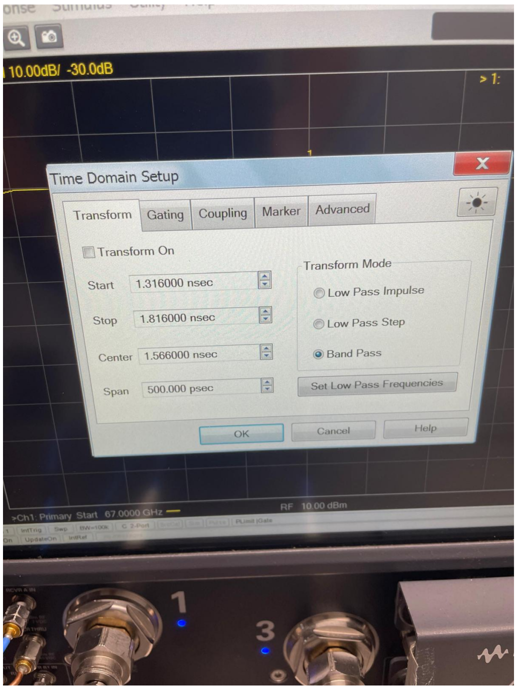

Figure 3.11: Configuration of the Transform window in the time domain. The analysis uses a window centered on 1,566 ns, with a span of 500 ps, in Band Pass mode.

3.7.2.4 Time-distance correspondence

The time observed in the center of the window is directly related to the distance between the antenna and the sample, bearing in mind that the signal travels this path twice (round trip). It is therefore possible to calculate the distance d corresponding to a given time t using the following expression [77]:

$$d = \frac{c \cdot t}{2} = \frac{3 \times 10^8 \cdot 1{,}566 \times 10^{-9}}{2} \approx 0{,}2349 \text{ m} = 23{,}5 \text{ cm} \tag{3.2}$$

Although this calculation is useful as confirmation, the VNA itself automatically performs this time-distance correspondence. Figure 3.12 illustrates the visualization of the reflection peak in the time domain, with a marker at 1,401 ns, which corresponds to a distance of approximately 210 mm (value shown directly on the equipment interface).

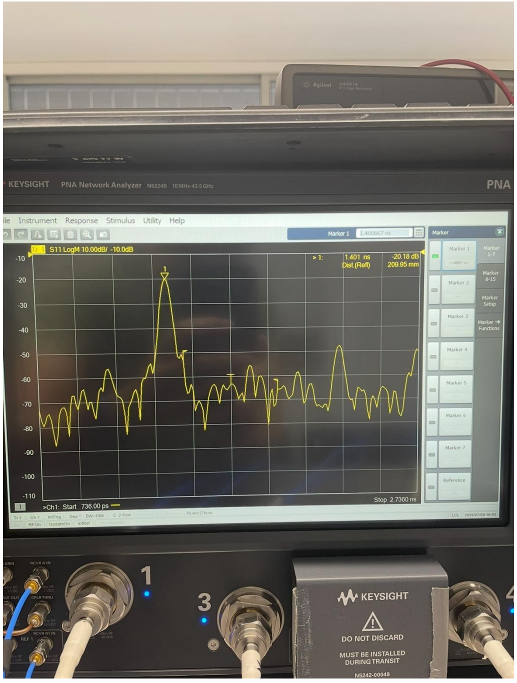

Figure 3.12: Visualization of the reflection peak in the time domain, with the corresponding distance calculated automatically by the VNA.

3.7.2.5 Validation with physical measurement

Figure 3.13 shows a ruler placed vertically between the surface of the sample and the transition point of the antenna waveguide, which was taken as the origin of the emission since the VNA calibration was performed in that exact reference plane. The reading is between 20 cm and 21 cm, thus validating the accuracy of the observed time values.

Figure 3.13: Checking that the physical distance between the sample and the antenna's radiation point is compatible with the measured time.

3.7.3 Choice of distance 20 cm

The choice of a distance of 20ċm between the antenna and the tested material was motivated by various technical and practical factors that make it ideal for this type of measurement. Although this distance is below the far-field zone of the SAR-2507-10-S2 antennas, whose Fraunhofer distance is greater than 40ċm, the use of time gating, as mentioned above, makes it possible to precisely isolate the signal reflected directly by the material, suppressing contributions from multiple unwanted reflections. In this context, the requirement to operate in the far-field becomes less relevant.

In addition, a distance of 20 cm represents an adequate compromise between ensuring a good signal-to-noise ratio and keeping the measurement system compact and stable. Longer distances would imply significant propagation losses in free space, especially in highly absorbers, which would compromise the quality of the measurement. On the other hand, very short distances (<10ċm) could introduce reactive field effects and parasitic reflections from the antenna itself or the support surface.

It should also be remembered that, at a distance of 20ċm, the antenna beam covers a circular area with a diameter of around 3.5ċm, which is consistent with the dimensions of the materials tested, ensuring that all the incident energy interacts only with the sample. In addition, this distance translates into a flight time of approximately 1,33 ns (round trip), which allows the effective application of the time gating technique, with a window centered on this value.

Thus, adopting a fixed distance of 20ċm proved to be efficient, consistent and compatible with the experimental requirements, ensuring the quality and repeatability of the measurements taken.

3.7.4 Configuration of the experimental set-up

The SAR-2507-10-S2 antenna was connected to port 1 of the VNA, with the other ports deactivated. The antenna was positioned at a distance of approximately 20 cm from the sample to be tested, with alignment guaranteed using a line laser (Bosch GLL 3-80).

Figure 3.14 shows the experimental assembly used for this type of test. The antenna is connected to the frequency extender and is positioned vertically on the support that holds the tested materials.

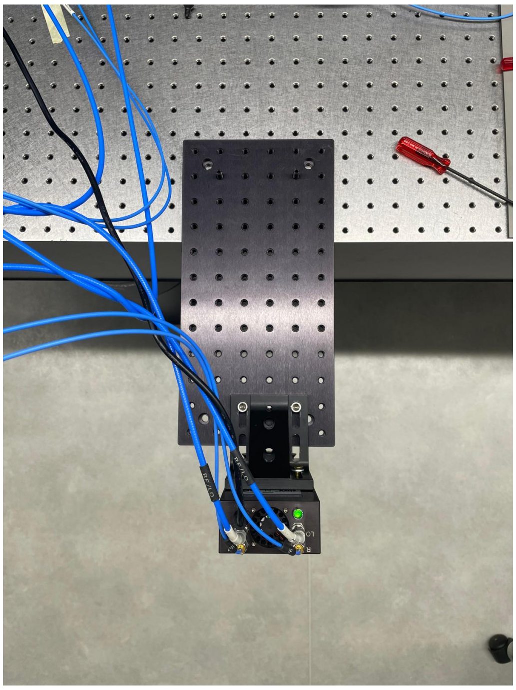

Top view of mounting the extender with the antenna.

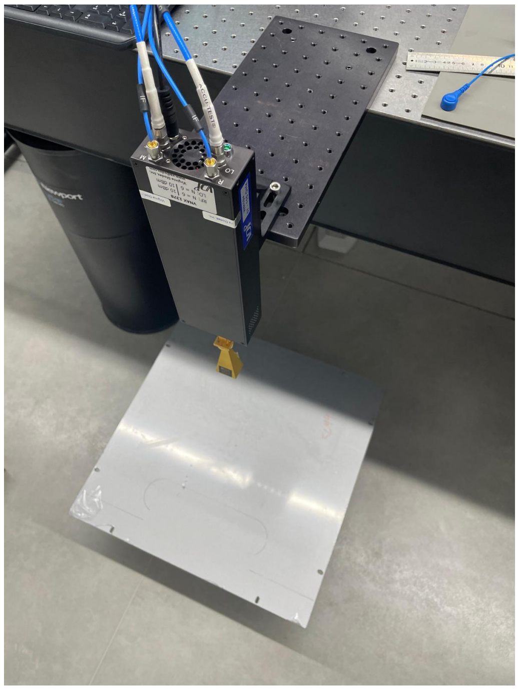

Side mounting of the S11 measurement configuration.

Figure 3.14: Setting up the system to measure the parameter S_{11} 20 cm from the sample.

3.7.5 Data export

The S_{11} data was saved in '.s2p' and '.csv' format and then analyzed in MATLAB using RF Toolbox, both in the frequency and time domain. The '.csv' format was used more in this first stage, as the '.s2p' format does not store measurements by time.

3.8 S_{21} Measurements - Reflection and transmission with two antennas

With the arrival of a second antenna, and in order to further characterize the electromagnetic behaviour of the materials tested, S_{21} measurements were carried out using one antenna as the transmitter and the other as the receiver. This approach made it possible to analyze both the transmission component, with the sample positioned between the antennas, and the reflection component, by varying the angle of incidence.

3.8.1 Fraunhofer distance

Unlike the S_{11} measurements, where only one antenna was used, as well as the measurement using time gating, characterization with two antennas requires greater care regarding the minimum distance between the transmitting antenna and the sample. This is because the antenna must operate in its far-field zone, where the radiation pattern is stable and predictable. This condition is guaranteed when the measurement distance exceeds Fraunhofer distance. Recalling his equation [25]:

$$R_f = \frac{2D^2}{\lambda} \tag{3.3}$$

where D is the largest dimension of the antenna aperture and λ the wavelength corresponding to the central frequency of the band.

In the case of the SAR-2507-10-S2 antennas, the largest dimension of the aperture is 27.7 mm [73], and the central frequency considered was $f_c = 79\,\text{GHz}$, which corresponds to a wavelength of:

$$\lambda = \frac{c}{f_c} = \frac{3\times10^8}{79\times10^9} \approx 3.80\,\text{mm}$$

Substituting in the Fraunhofer equation:

$$R_f = \frac{2\cdot(0.0277)^2}{0.0038} \approx 0.404\,\text{m} = 40.4\,\text{cm}$$

Thus, to ensure that the antennas operate in the far field, measurements were carried out at a distance of 40,4ċm or more, minimizing the impact of near-field interference and ensuring the validity of the measurement conditions for transmission and reflection analysis.

3.8.2 Configuration of the experimental set-up perpendicular to measure material transmission

A configuration with two antennas positioned symmetrically in relation to the material under test was used to measure the transmission of the materials. This approach makes it possible to assess the amount of energy passing through the material.

The experimental set-up consisted of placing the test sample between the two antennas, so that the incident beam was oriented perpendicular to the surface of the material. Both antennas were rigidly fixed to independent tripods and precisely aligned, ensuring that the main beam of each antenna was centered on the sample.

Figure 3.15 shows the configuration used. The sample was fixed vertically on a stable base, allowing direct alignment between the two antennas. The transmitting antenna (TX) was connected to port 1 of the vector network analyzer (VNA), while the receiving antenna (RX) was connected to port 2.

Assembly with the material ECCOSORB™ HR-10.

Assembly with the material ECCOSORB™ HR-25.

Figure 3.15: Experimental setup for measuring the S_{21} parameter, with the SAR-2507-10-S2 antennas arranged perpendicular to the sample.

The distance between the sample and each of the antennas was approximately 45ċm. This value was chosen because it was the largest possible with the equipment available, since the length of the IF and LO cables, which connect the extenders to the network analyzer, physically limited the distance between the antennas. Even so, this distance satisfies the far-field condition (Fraunhofer regime), ensuring that the wavefront incident on the material is approximately flat.

This configuration guarantees a reliable and direct measurement of the energy transmitted through the sample, and is particularly suitable for partially transparent materials or those with absorption properties to be quantified. Symmetrical mounting and sufficient distance between antennas and absorbers minimize parasitic reflections, ensuring the integrity of the data collected.

3.8.3 Configuration of the experimental set-up with angular variation for measuring reflection

In order to evaluate the performance of absorbers in situations closer to real applications, the parameter S_{21} was measured with reflection, varying the angle of incidence of the electromagnetic wave. The angles tested were 15°, 30° and 45°, representing oblique incidence situations.

In this configuration, the sample was placed in the center of the propagation line between the transmitting and receiving antennas. The material was fixed with adhesive tape to maintain the desired orientation during the different measurements.

The correct orientation of the antennas was validated with the aid of the line laser, allowing the emission beam to be visually aligned with the surface of the material, ensuring that the reflection was measured with geometric consistency between all the tests.

The distance between the emitting antenna and the center of the sample was always at least 40 centimeters and increased slightly as the angle of incidence increased. Figure 3.16 shows two representative configurations of the 15° and 45° mounts, respectively.

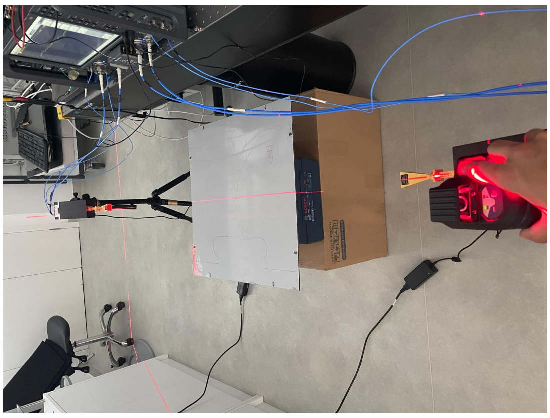

Reflection measurement set-up at 15°.

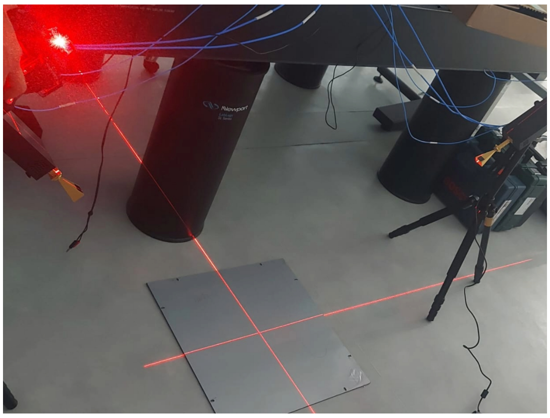

Reflection measurement set-up at 45°.

Figure 3.16: Experimental setup for measuring the parameter S_{21} with angular variation.

3.8.4 Antenna and sample alignment procedure

To ensure the accuracy of the measurements of the S_{21} parameter, a strict alignment of the antennas and absorbing samples was carried out. The main objective was to ensure that the antennas were perfectly aligned with each other and that the illuminated area was completely contained on the sample surface, even in angled configurations.

3.8.4.1 Alignment with laser level

Alignment between the transmitting and receiving antennas was carried out using a laser level that simultaneously projects horizontal and vertical lines (Figure 3.17 and Figure 3.18). The horizontal line was used to project a reference line onto the ground, allowing a straight guide line to be drawn between the two measurement points. This line served as the basis for positioning the tripods and ensuring that both axes of propagation were aligned.

The vertical laser line was used directly above the antennas to check that both were aligned in the same direction, since the line passed over the center of the antenna mouths. This reference was essential to ensure the angular and lateral alignment of the two elements.

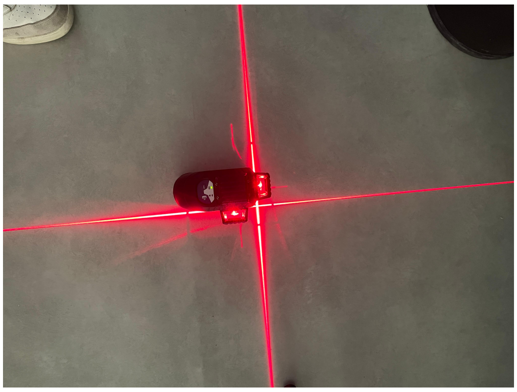

Figure 3.17: Projection of the laser beam onto the ground, used as a guide for alignment.

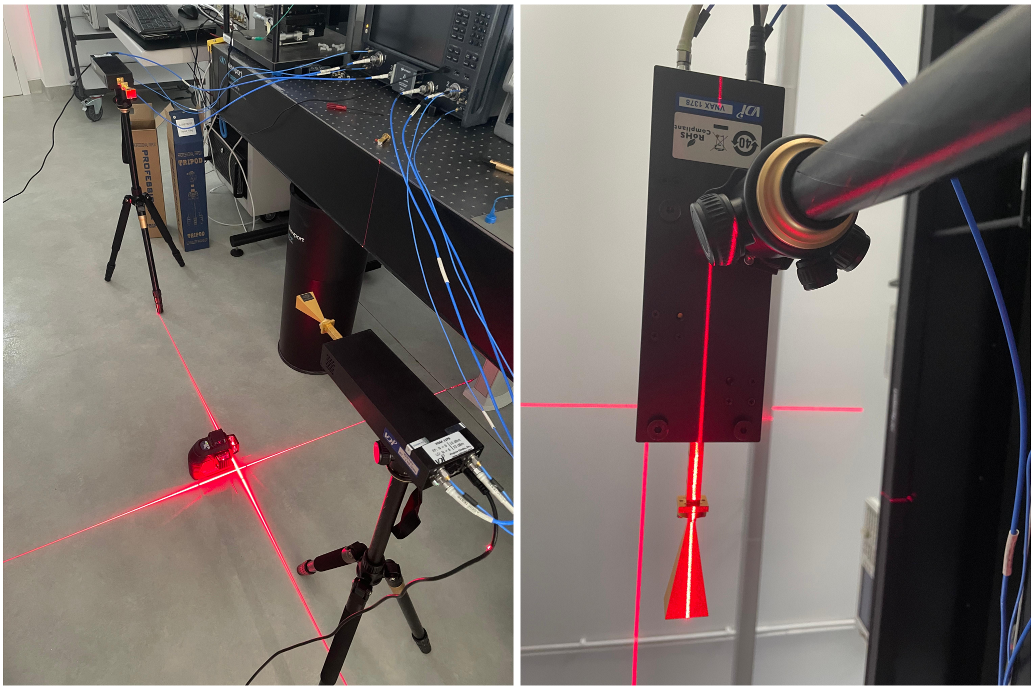

Figure 3.18: Alignment of the antennas and the sample based on the projected laser lines.

3.8.4.2 Defining the angle of incidence

The inclination of the transmitting and receiving antennas was adjusted symmetrically for each test configuration to form incidence angles of 15°, 30° and 45° with respect to the normal to the surface of the material. To ensure that the angles were correctly defined and replicable, a digital level application was used on a smartphone (Figure 3.19), placed over the extender of each VNA. This method allowed a direct and stable reading of the actual inclination of the antennas, making it easier to obtain precise and consistent configurations.

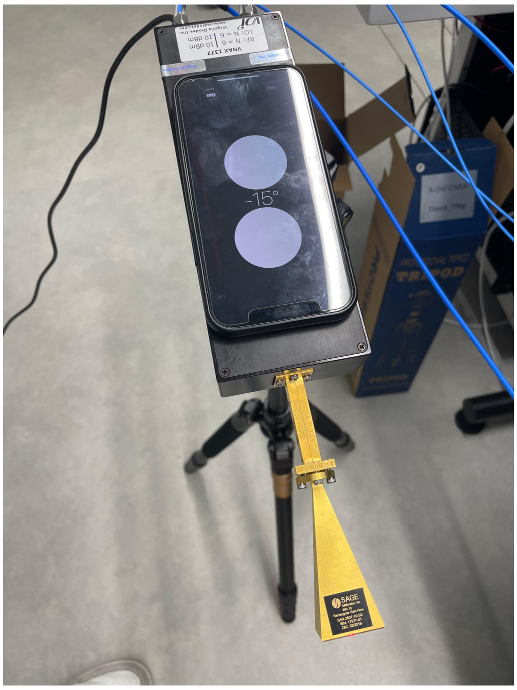

Figure 3.19: Reading the angle of inclination of the antenna using a mobile application.

3.8.4.3 Tripod leveling

The height of the antennas was adjusted based on the markings on the tripods (Figure 3.20), ensuring symmetry between the two sides. To do this, it was checked that all the tripod legs were extended in the same relative position, ensuring that the antennas were perfectly level with each other, which is essential to avoid asymmetries in the measurements.

Figure 3.20: Detail of the tripod leg adjustment for precise leveling of the antennas.

3.8.4.4 Sample alignment in perpendicular configuration

For the perpendicular incidence measurements (0°), it was necessary to ensure that the absorbing sample was correctly aligned in relation to the antennas and perpendicular to the ground. To do this, the laser level was once again used as a visual reference. The projection of the horizontal and vertical lines made it possible to check that the front plane of the sample was parallel to the front of the antennas and perpendicular to the direction of beam propagation (Figure 3.21).

This alignment was essential to ensure that the beam fell orthogonally on the center of the sample, minimizing lateral reflection effects and guaranteeing representative measurements.

Figure 3.21: Alignment of the absorbing sample in the perpendicular incidence configuration.

3.8.5 Limitations and challenges of the experimental setup

During the implementation phase of the configuration for measuring the S_{21} parameters, several practical challenges arose which affected the quality and repeatability of the results obtained. In theory, it would be ideal to ensure that transmission between the antennas took place in an environment completely free of obstructions, with precise alignment and total absorption of non-transmitted energy. However, physical constraints in the laboratory and the limitations of the equipment available meant that adaptations had to be made.

The main difficulty concerned the elevation of the absorber panel. In order to correctly align the central area of the absorber with the axis of the antennas, so as to ensure that the main beam falls completely on the sample, cardboard boxes had to be used as a support (Figure 3.22). This practical solution made it possible to correct the unevenness between the absorber tripod and the antenna tripods, but introduced a possible source of error. Although the boxes are made of dielectric material, their irregular geometry and exposed edges can slightly influence the incident or reflected electromagnetic field, creating variations in the results.

Another setback would be an increase in the angle of incidence. As the angle of incidence increased, especially in simulations that sought to explore situations close to 60°, new geometric challenges arose. The steep inclination of the antennas meant that the tripods came significantly closer together, reducing the useful space available for placing the absorbing sample. Under these conditions, it became impossible to position large materials without them physically interfering with the tripod legs. This spatial limitation would compromise the ideal measurement geometry and introduce potential parasitic reflections or shading, making it difficult to analyze the results.

It was therefore decided to restrict the tests to angles of incidence up to 45°, which is already a sufficiently demanding scenario for performance evaluation.

In an attempt to mitigate these factors, a second approach was considered: setting up the system with completely free space between the two antennas, positioning the absorbing sample in the center, suspended or supported only by the edges. This solution, illustrated in Figure 3.22, aimed to reduce interference and ensure the cleanest possible propagation. However, it quickly proved impractical. Aligning the antennas proved extremely difficult to do accurately - any small angular deviation caused significant losses in reception. Even with the aid of laser levels and careful geometric measurements, keeping the beam centered over the entire distance proved inconsistent, leading to unstable measurements with high variability.

We therefore opted to keep the assembly with the support boxes, prioritizing the stability and reproducibility of the measurements, even acknowledging the limitations that such a configuration introduces. In the future, the use of dedicated support structures, adjustable in height and made from absorbent or neutral dielectric materials, could significantly mitigate these unwanted effects.

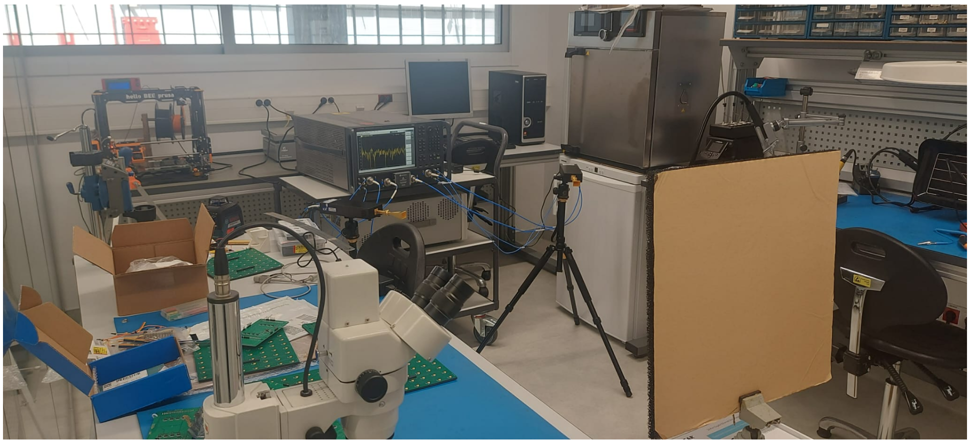

Figure 3.22: Alternative configuration attempted with antennas side by side and absorber suspended in free space.

To minimize the unwanted effects caused by the presence of the box (potential secondary reflections or disturbances in the incident beam), an intermediate solution was adopted: the placement of a base of absorbent material under the tested sample.

In all measurements with angular variation, an HR-25 panel with significant thickness was used as the base platform, in order to isolate the influence of the cardboard box on the results as much as possible. This strategy proved to be effective, guaranteeing a stable, electrically neutral surface that was more representative of the ideal test conditions. Figure 3.23 shows the final setup used for the tests with angular variation, with the HR-25 base under the material to be tested.

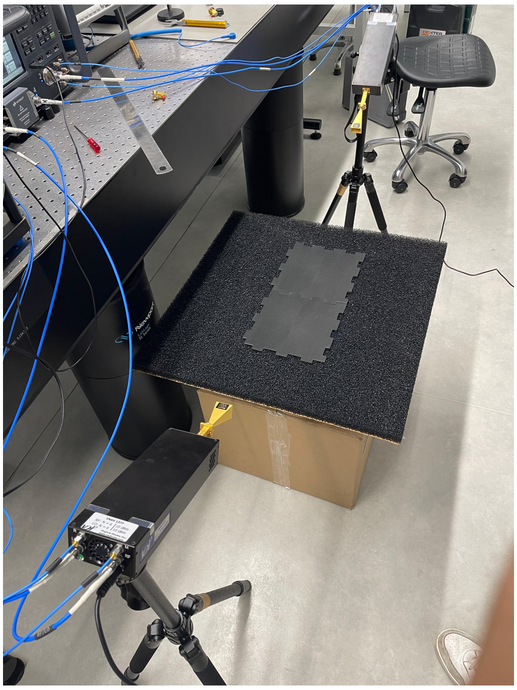

Figure 3.23: HR-25 base assembly for measuring Rezorb S at 30 degrees.

3.8.6 Influence of the angle of incidence on the area incident by the beam

Even for an incidence perpendicular to the surface of the material (0°), as in S_{21} and transmission measurements, the area incident by the main beam of a directional antenna is not perfectly circular. This slight ellipticity results from the fact that, as seen above, the Half Power Beam Width (HPBW) is different in the two main planes of the antenna: around 9° in the E plane and 10° in the H plane, as specified by the manufacturer [73].

When the antenna is tilted to perform measurements with oblique incidence - namely at 15°, 30° and 45° - the beam undergoes additional deformation. In particular, the projection of the beam onto the plane of the sample elongates in the direction of the tilt, resulting in an ellipse with a sharper major axis. This effect only occurs in the plane where the antenna is rotated.

In the measurements carried out, the antenna was tilted in plane E, which is defined as the plane that contains both the beam propagation direction and the electric field vector $\vec{E}$. As such, it is in this plane that the dilation of the beam projection occurs. Plane H, on the other hand, perpendicular to plane E and associated with the magnetic field vector $\vec{H}$, maintains its geometry unchanged, since it does not undergo any rotation [78]. In Figure 3.24 we can observe an example of both planes:

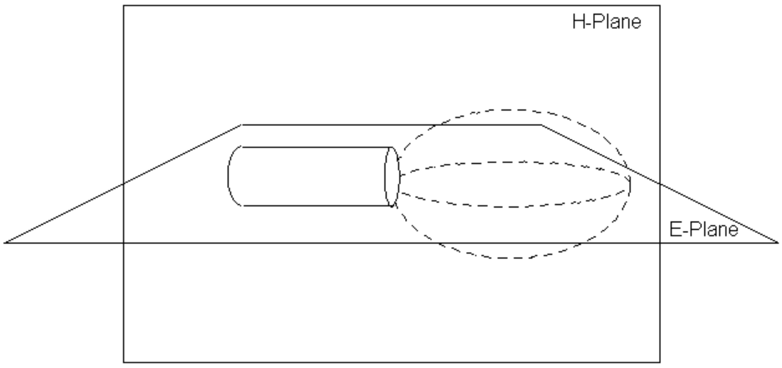

Figure 3.24: E-plane and H-plane of a horn antenna. The E-plane, containing the propagation direction and the electric field $\vec{E}$, is where the beam projection dilates when tilted, while the H-plane, associated with $\vec{H}$, remains unchanged [78].

This contrasts with the typical projection of, for example, a flashlight: when tilting a flashlight downwards, the beam of light can appear to expand globally. However, a waveguide antenna like the SAR-2507-10-S2 emits a highly directional beam with a well-defined conical shape.

This effect can be quantified by a geometric expansion factor of the projection, given by [75]:

$$D_{\text{proj}} = \frac{D}{\cos(\theta)} \tag{3.4}$$

To illustrate this phenomenon, consider the most demanding situation among the tests carried out: a measurement with the antenna at 1 m from the sample, inclined at 45°. In the cases of 30° and 15°, the antenna-material distance was reduced (and the materials elevated) in order to keep the point of incidence in the center of the sample, which naturally resulted in smaller incident areas.

Using the HPBW of 9° in the E plane, the diameter of the incident region, without inclination, at 1 m distance, is:

$$D_E = 2 \cdot d \cdot \tan\left(\frac{\text{HPBW}}{2}\right) = 2 \cdot 1.00 \cdot \tan(4.5^\circ) \approx 0.157\,\text{m} \tag{3.5}$$

With a slope of 45°, the projection of the major axis of the ellipse becomes:

$$D_{\text{proj,E}} = \frac{0.157}{\cos(45^\circ)} \approx \frac{0.157}{0.707} \approx 0.222\,\text{m} = 22.2\,\text{cm}$$

This value corresponds to the largest dimension of the area impacted on the surface of the material during the tests. For this reason, it was essential to ensure that all the samples used had a useful area greater than this value, in order to avoid energy being lost outside the sample, which would compromise the accuracy and reproducibility of the measurements.

Table 3.2: Minimum dimensions of the region hit by the beam in the E and H planes for different configurations

Distance (cm)	**Angle (°)**	D_E **(cm)**	D_H **(cm)**	$D_{\mathbf{proj,E}}$ **(cm)**	$D_{\mathbf{proj,H}}$ **(cm)**
20	0	3.14	3.50	3.14	3.50
45	0	7.07	7.88	7.07	7.88
50	15	7.85	8.75	8.12	8.75
75	30	11.77	13.13	13.58	13.13
100	45	15.71	17.50	22.22	17.50

3.8.7 Sample size and coverage of the affected area

The physical dimensions of the samples used were evaluated to ensure that the incident area by the beam was completely contained on the surface of the material in all test configurations. The Eccosorb HR-10 and HR-25 absorbers, supplied in sheets of $610 \times 610\,\mathrm{mm}^2$, far exceed the maximum dimensions of the beam projection, even in the most demanding scenario of incidence at 45° and distance of 1 m, where the projected incident area reached approximately 22.2 cm in the E plane (direction of enlargement).

However, the ReZorb S were supplied in individual blocks of only $200 \times 200\,\mathrm{mm}^2$, which would not be enough on its own to guarantee full coverage of the area affected in this scenario. To overcome this limitation, a modular arrangement was adopted using the only two samples available, positioned side by side to create a continuous surface with $400 \times 200\,\mathrm{mm}^2$.

This arrangement was carefully oriented to maximize the coverage of the elliptical projection of the beam: the blocks were arranged with the longer side (400 mm) parallel to the E plane, i.e. aligned with the direction of widening of the projection caused by the inclination of the antenna. This orientation ensures that the beam falls completely on the absorbing surface, even in the most geometrically demanding conditions.

It should also be noted that it was only possible to test two samples of each absorber, including two Rezorb S, which made it impossible to use more units to make up a larger surface. Thus, the arrangement described was the only viable configuration to guarantee the integrity of the measurements in the test at 45°, which ended up being extended to the tests for the other incidence angles in order to acquire more coherent measurements, as can be seen in Figure 3.23.

Chapter 4

Results

This chapter presents and analyzes the results obtained from the measurements of the parameters S_{11} and S_{21}, with the aim of evaluating the electromagnetic performance of the absorbers tested. As mentioned in the previous chapter, the measurements were carried out in both transmission configurations (antennas facing each other) and reflection configurations (sample tilted), for different angles of incidence.

The parameter S_{21} represents the ratio between the transmitted and incident wave amplitudes, and the corresponding transmitted power is given by $|S_{21}|^2$. Similarly, S_{11} defines the ratio between the reflected and incident wave amplitudes, while the reflected power fraction is expressed as $|S_{11}|^2$. Together, these parameters allow assessing the propagation, reflection, and attenuation behavior of each material when illuminated by millimeter waves in the 76–81 GHz range.

4.1 Objectives of the analysis of S_{11} and S_{21}

The electromagnetic characterization of the absorbers was based on the analysis of the parameters S_{11} and S_{21}, collected in different experimental configurations. Each of these parameters provides different information about the interaction of the millimeter wave with the material under test.

The parameter S_{11} corresponds to the reflection coefficient of the emitting antenna, and is measured in a configuration with only one antenna, oriented directly towards the sample placed at 0°. This arrangement makes it possible to quantify the energy reflected back to the source, reflecting the material's ability to absorb or reflect the incident radiation. Ideally, materials with good absorption performance have low $|S_{11}|$ values, indicating that most of the energy is dissipated internally in the material rather than being reflected.

In turn, the S_{21} parameter was measured with two antennas facing each other, in a configuration that makes it possible to study both direct transmission and reflection at oblique incidence. In the configuration with the sample perpendicular to the propagation line, S_{21} is the ratio of transmitted to incident wave amplitudes between ports 1 and 2. The squared magnitude, $|S_{21}|^2$, represents the fraction of transmitted power. In this context, a high attenuation of $|S_{21}|$ is indicative of good absorption throughout the thickness. In addition, S_{21} was measured with the sample tilted at 15°, 30° and 45°, in order to simulate more realistic angles of incidence. In these cases, the energy reflected in the direction of the receiving antenna makes it possible to infer the behavior of the material in the face of angular reflections.

The following results were obtained by recording the measurements on a USB stick in the VNA and then extracting them using Matlab + RF Toolbox.

4.2 Experimental results of S_{11}

For the analysis of material reflectivity, the decibel (dB) unit is used to express the magnitude of the reflection coefficient $|S_{11}|$, a common choice in microwave measurements because it allows a straightforward comparison of amplitudes over a wide dynamic range. The value displayed in dB is computed as $20\log_{10}|S_{11}|$. Although this representation refers to the ratio of wave amplitudes, it provides an indirect indication of reflected power, since the fraction of reflected power is given by $|S_{11}|^2$.

In this scale, a value of 0 dB corresponds to a fully reflective surface ($|S_{11}| = 1$), while more negative values indicate a reduction in the reflected amplitude. Therefore, a lower $|S_{11}|$ in dB is associated with reduced reflected power and, consequently, a higher absorption effectiveness of the sample.

The following figures show the results of S_{11} in the frequency domain for four different materials: a metallic reference (red), the absorbers HR-10 (blue) and HR-25 (green), and ReZorb S (purple). All the graphs are limited to the range between 75 GHz and 110 GHz, corresponding to the effective band of the antennas used. Although the VNA with the extenders allows measurements between 67 GHz and 115 GHz, it was decided to restrict the analysis to this safe range to ensure the reliability of the data presented.

Before analyzing the results in the frequency domain, we applied an inverse Fourier transform to the S_{11} data, obtaining its representation in the time domain. This approach allows us to observe the temporal location of the reflection peaks, which makes it easier to distinguish between the reflection coming directly from the sample and other unwanted echoes, such as those generated by antennas or connections. The following figures show the time signals corresponding to each material.

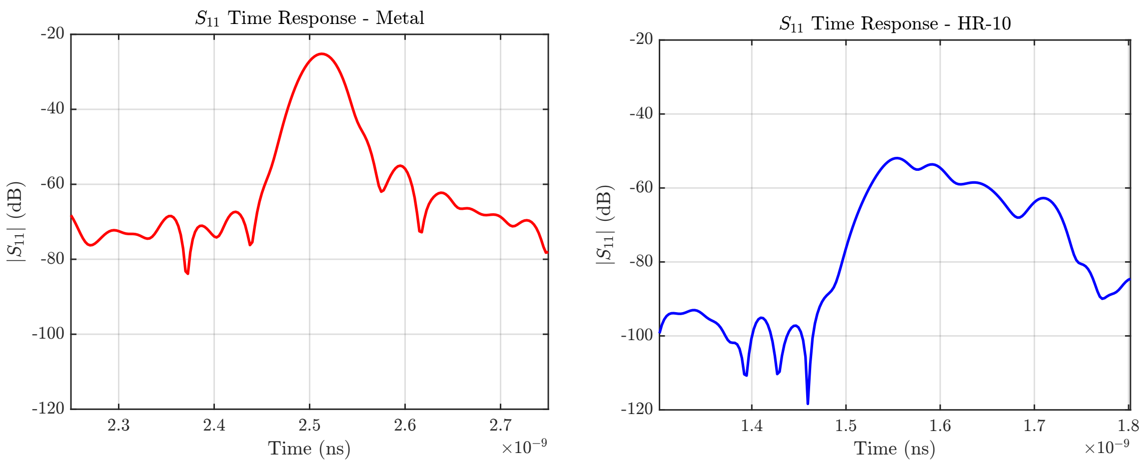

(a) Time response - Metal

(b) Time response - HR-10

Figure 4.1: Time signals obtained for metallic and HR-10 materials after inverse Fourier transformation.

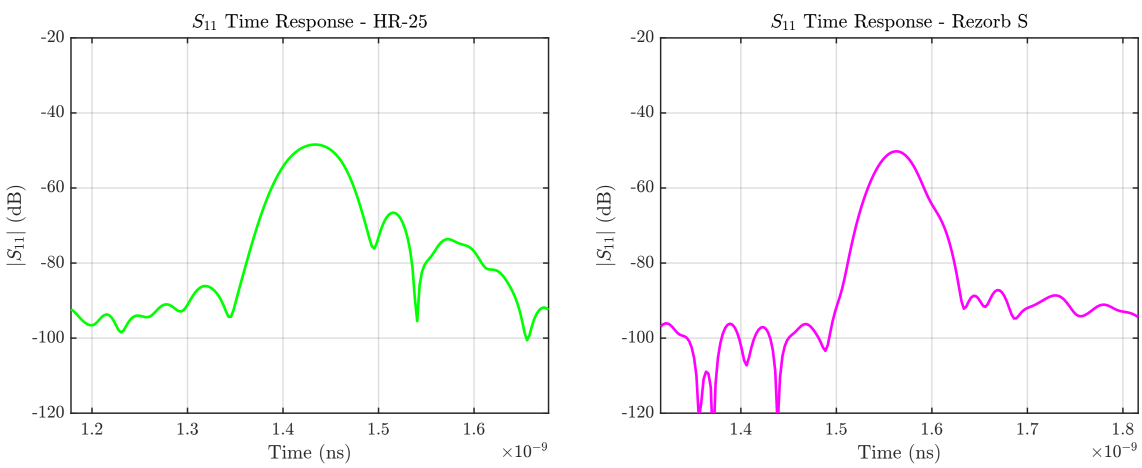

(c) Time response - HR-25

(d) Time response - ReZorb S

Figure 4.2: Time signals obtained for HR-25 and ReZorb S materials after inverse Fourier transformation.

From the time graphs (Figure 4.1 Figure 4.2), it can be seen that the reflection peak for the HR-10 material is not so well isolated from the other echoes, unlike the other materials analyzed. This overlap may be related to the physical properties of HR-10, namely its composition and thickness. Being a thinner absorber material, it may allow some partial transmission of the electromagnetic wave, resulting in multiple reflections close together in time. This characteristic makes it more difficult to clearly identify the exact moment of the main reflection.

It should also be noted that in some of the graphs shown, the line corresponding to the S_{11} time signal does not extend over the entire time interval shown. This behavior is due to the fact that the VNA's transform function was used in conjunction with gating, i.e. the inverse Fourier transform was applied to obtain the signal in the time domain, and at the same time a time window was defined to filter out components outside the interval of interest. When this gating window is shorter than the total duration of the transformed signal, the values outside the selected range are suppressed, resulting in no line at the ends of the graph. This approach makes it possible to isolate the main reflection of the material and eliminate multiple reflections, noise or unwanted contributions, making the analysis clearer and more reliable.

Next (Figure 4.3 Figure 4.4), the results in the frequency domain are presented for the same materials, allowing a more direct analysis of the spectral response of each sample over the operating band of the antennas used.

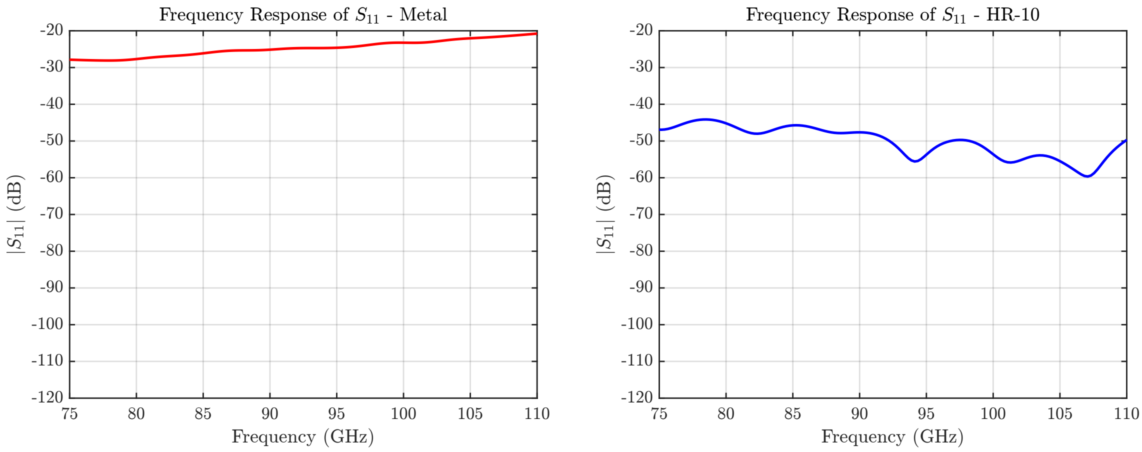

(a) Frequency response - Metal (b) Frequency response - HR-10

Figure 4.3: Frequency responses of S_{11} for metallic and HR-10 materials.

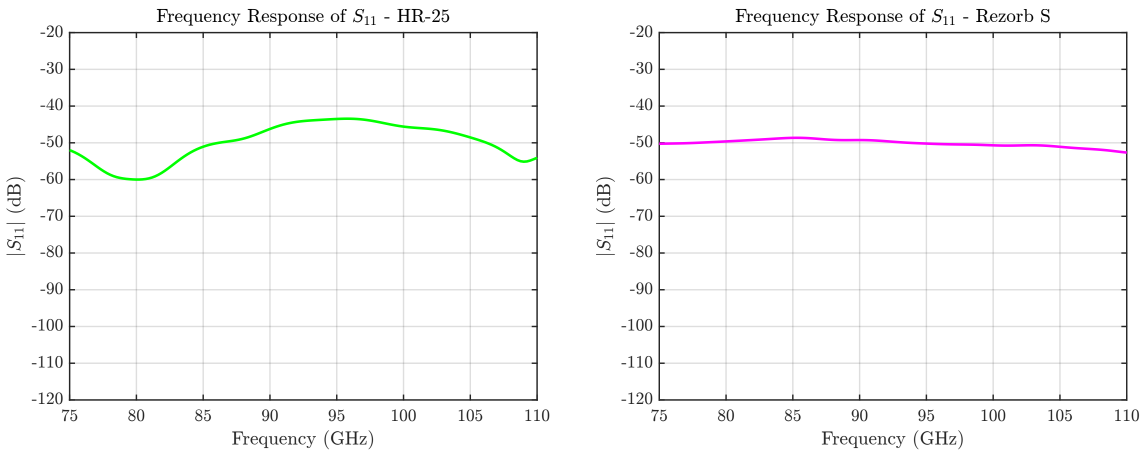

(c) Frequency response - HR-25 (d) Frequency response - ReZorb S

Figure 4.4: Frequency responses of S_{11} for HR-25 and ReZorb S materials.

For a clearer comparison between the different materials, the S_{11} graphs in the frequency domain were also plotted together, as illustrated in Figure 4.5.

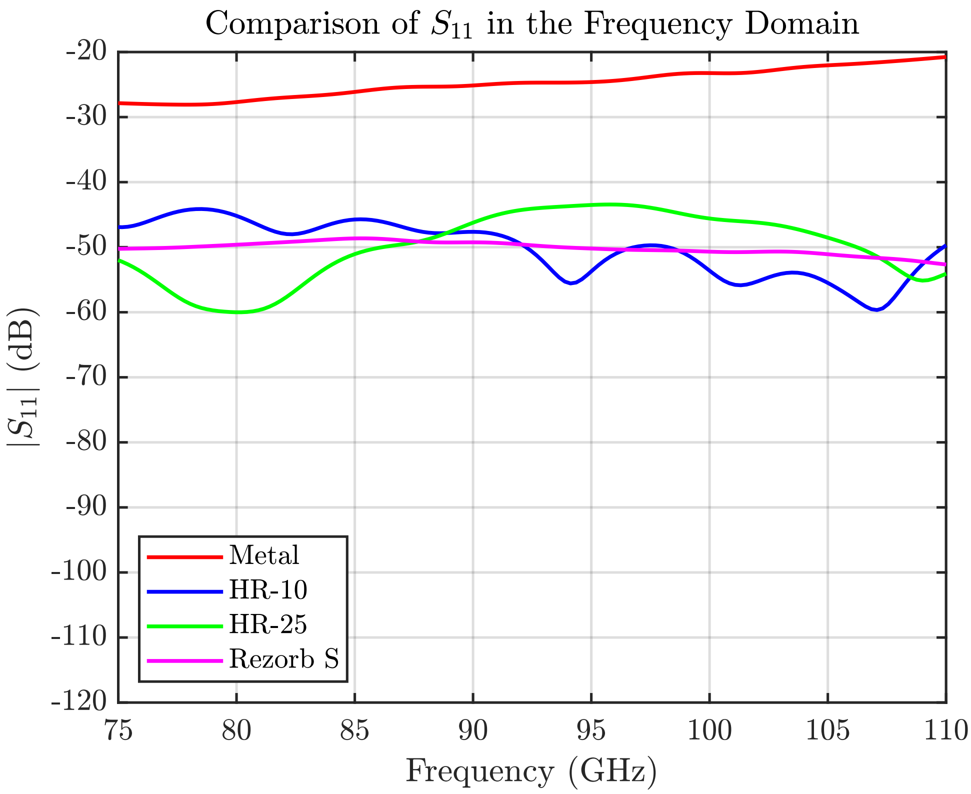

Figure 4.5: Comparison of the S_{11} parameter in the frequency domain for the different materials.

As expected, the metallic material shows higher values of $|S_{11}|$, between -30 dB and -20 dB, which reflects its highly reflective nature. This behavior is consistent with the fact that practically all the incident energy is reflected by the metal, with few losses.

On the other hand, absorbers exhibit significantly more negative S_{11} values, which indicates greater efficiency in absorbing the incident wave. In the 76 GHz to 81 GHz range, the band of greatest interest for practical application, the HR-25 material clearly stands out as the most effective, reaching values close to -60 dB. However, outside this range, its performance becomes more erratic, showing greater variations and, in some cases, worsening compared to the other materials.

ReZorb S proves to be the most stable throughout the entire band analyzed, with a consistent response around -50 dB, without significant oscillations. HR-10 shows the best results at higher frequencies, above 90 GHz, where it momentarily reaches -60 dB, but in the 76 GHz to 81 GHz range it proves to be the least effective of the three absorbers, with higher (less negative) reflection values.

This comparison highlights the different behaviors of the materials as a function of frequency, with HR-25 being the most promising for applications in the 76-81 GHz band, while HR-10 may be preferable for higher ranges. ReZorb S, on the other hand, offers an interesting compromise between performance and stability throughout the band.

4.3 Experimental results of S_{21} for transmittance

This section presents the S_{21} results obtained in the transmission regime, with the antennas positioned opposite each other and the samples placed between them. This configuration makes it possible to analyze the amount of electromagnetic signal passing through each material, acting as a direct measure of its transmittance.

More negative values of S_{21} indicate lower transmission and, consequently, greater attenuation capacity of the material. On the other hand, values close to 0 dB show high transparency of the incident signal. This analysis is particularly useful for evaluating the degree of effective absorption, in addition to the reflection analysis based on S_{11} and future analysis on S_{21} measurements with different incident angles.

Although the use of time gating in S_{21} measurements was not initially considered, a preliminary analysis of the data obtained without any TDR function revealed that the results were neither sufficiently stable nor reliable. The sharp fluctuations in the signal throughout the frequency band suggest interference caused by multiple reflections and discontinuities external to the sample, which compromises the assessment of the real transmittance of the materials.

As an example, Figure 4.6 shows the response obtained for the ReZorb S material without any time gating. The presence of rapid variations and significant noise in the trace is visible, making the physical interpretation of the data difficult. For this reason, it was decided to apply a TDR function with gating in the following measurements of S_{21}, in order to isolate the direct contribution of the sample and improve the quality of the measurements.

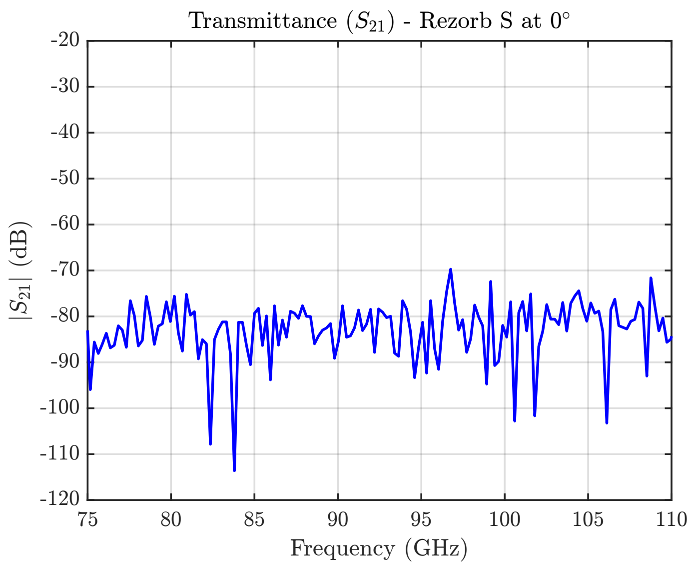

Figure 4.6: Transmittance $|S_{21}|$ of ReZorb S material without time gating. The visible oscillations and noise indicate the presence of unwanted reflections.

To gauge the basic behavior of the measurement system, a measurement was carried out without any sample between the antennas, i.e. with the antennas positioned face-to-face in perpendicular alignment. This test serves as an absolute reference for the maximum expected transmittance, allowing for a later relative comparison of the attenuation introduced by each material.

Figure 4.7 shows the result obtained in this configuration. As expected, the S_{21} values are close to 0 dB (full transmission reference), albeit with a slight attenuation along the band, which can be attributed to losses in the connectors, antennas and experimental environment. These values serve as a basis for interpreting the reductions observed in measurements with absorbers.

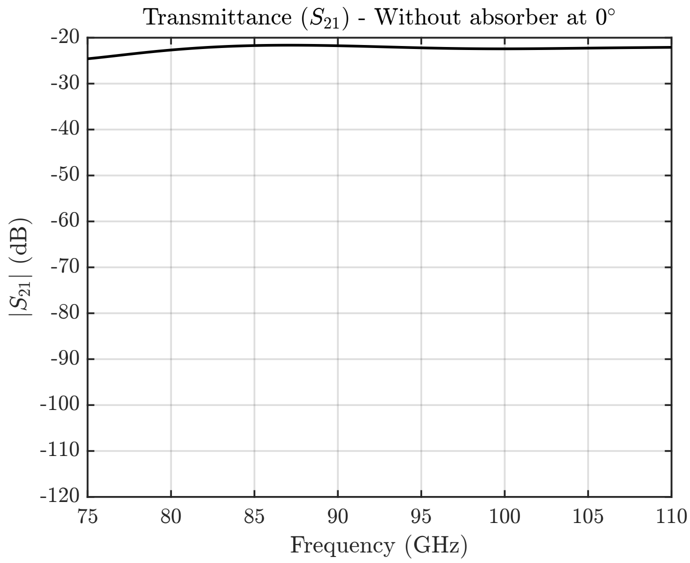

Figure 4.7: Transmittance S_{21} measured with the antennas aligned face to face, without any absorber between them.

Below are the results of the average of three independent measurements for each material, obtained with perpendicular alignment of the antennas. These measurements were carried out by changing the sample between each acquisition and reversing its orientation, in order to check the reproducibility of the system and ensure that there were no significant discrepancies associated with the position or placement of the sample.

Averaging the three tests reduces small experimental variations and measurement noise, providing a more reliable representation of the electromagnetic behavior of each material. The following graphs also show the individual curves for each measurement, to visually illustrate the consistency between the tests carried out.

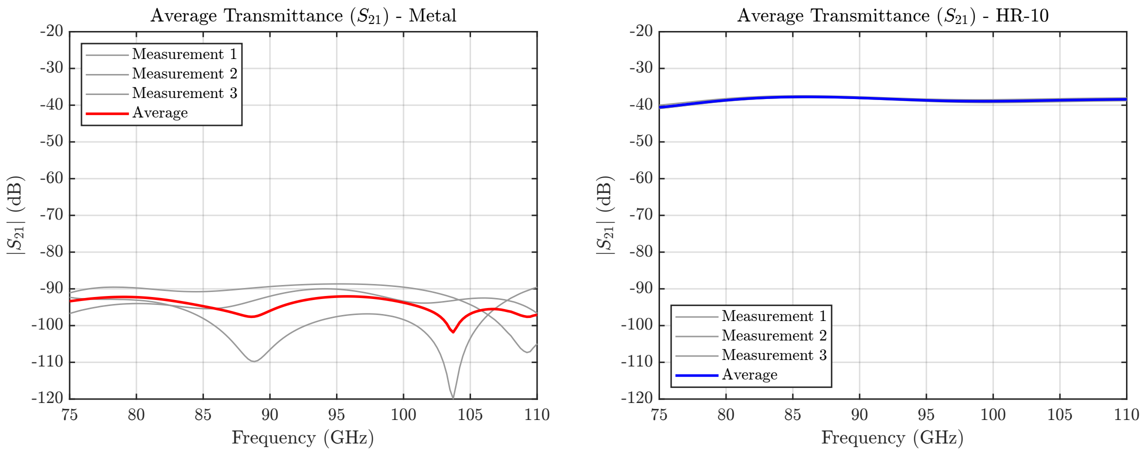

(a) Average transmittance - Metal

(b) Average transmittance - HR-10

Figure 4.8: Average transmittance $|S_{21}|$ of metal and HR-10 materials.

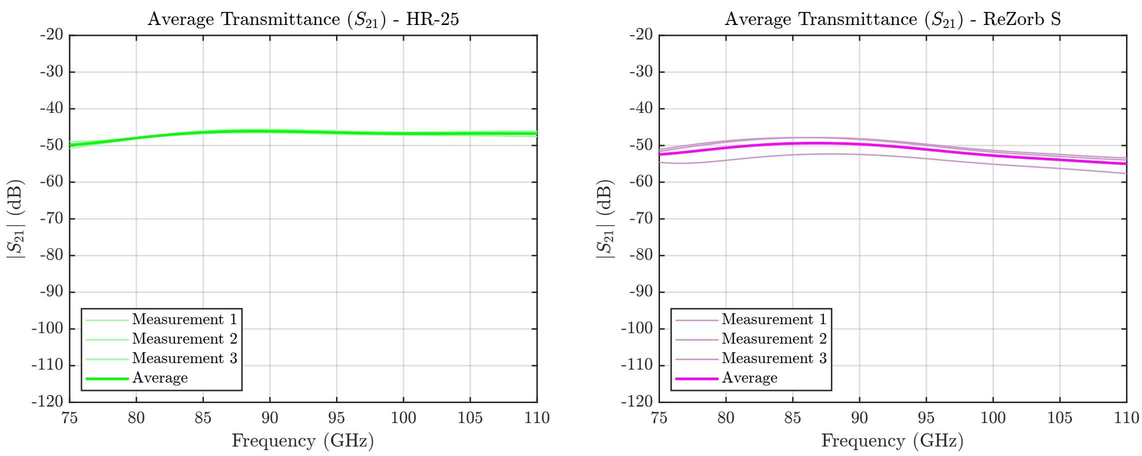

(c) Average transmittance - HR-25

(d) Average transmittance - ReZorb S

Figure 4.9: Average transmittance $|S_{21}|$ of the HR-25 and ReZorb S materials.

After analyzing each material individually (Figure 4.8 Figure 4.9), it is important to directly compare the average results obtained for the four absorbers tested. This joint comparison makes it possible to clearly observe the differences in transmittance between the materials over the entire frequency band considered, showing which are more effective at attenuating the incident signal and which maintain a more stable response. The following graph summarizes these differences, highlighting the relative performance of each sample in the perpendicular configuration.

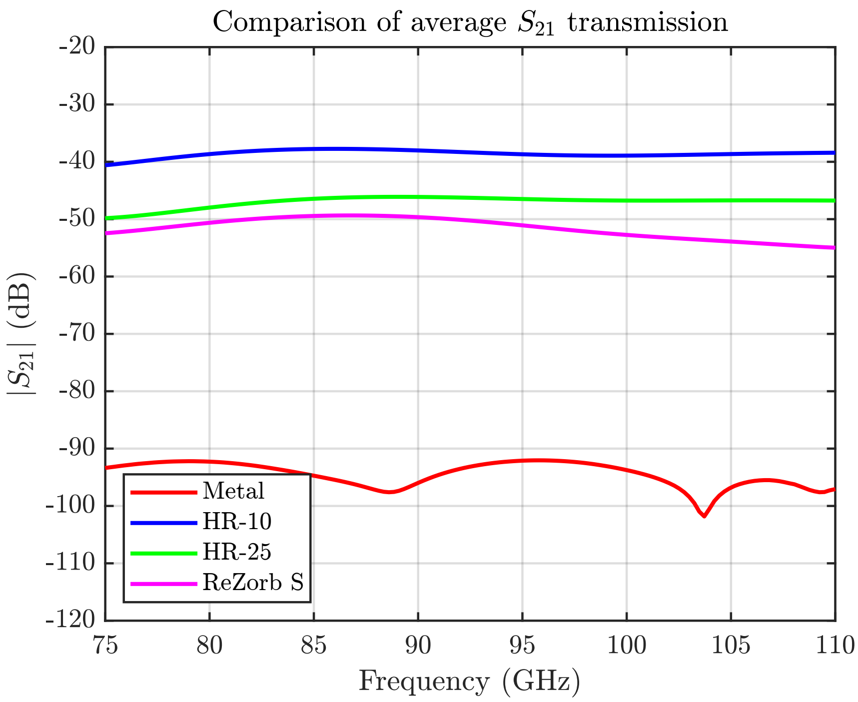

Figure 4.10: Comparison of the average transmittance $|S_{21}|$ between the four materials tested.

The behavior observed (Figure 4.10) corroborates the expected properties of each sample.

The metallic material shows the lowest S_{21} values, below -90 dB throughout the band, demonstrating its reference function as an almost perfect reflector, with practically no transmission of the incident signal.

On the other hand, the HR-10 material shows the highest transmittance among the absorbers, with values close to -35 dB, proving to be the least effective in terms of attenuating the electromagnetic signal. Even so, it maintains a relatively stable response throughout the band. The inferior performance of HR-10 as an absorber can be explained by its more translucent nature, which is visible in the experimental assembly of Figure 3.15, where it is possible to see partially through the material. This physical characteristic suggests a lower density or effective thickness, which contributes to the higher transmittance measured in this test.

HR-25 shows an intermediate behavior, with S_{21} values between -47 dB and -50 dB, and a slight negative variation with increasing frequency, indicating a moderate attenuation capacity, more effective than HR-10, but lower than ReZorb S.

ReZorb S stands out as the material with the best absorption performance among the three, not only in the critical 76-81 GHz band, but consistently throughout the entire range analyzed, with values consistently lower than -50 dB and a downward trend throughout the frequency, indicating high efficiency in absorbing the incident wave.

4.4 Experimental results of S_{21} with angular variation for reflection

The measurements were taken at three different angles of incidence: 15°, 30° and 45°, representing different oblique reflection conditions. In all cases, time gating was applied, as in the previous measurements, in order to eliminate unwanted reflections from outside the sample and guarantee the fidelity of the results.

For each combination of material and angle, three independent measurements were also carried out, with the sample repositioned between tests. The following figures (Figure 4.11 Figure 4.12) show the plot corresponding to the average of the three measurements, representing the real behavior of each sample more robustly.

4.4.1 Experimental results of S_{21} for reflection at 15°

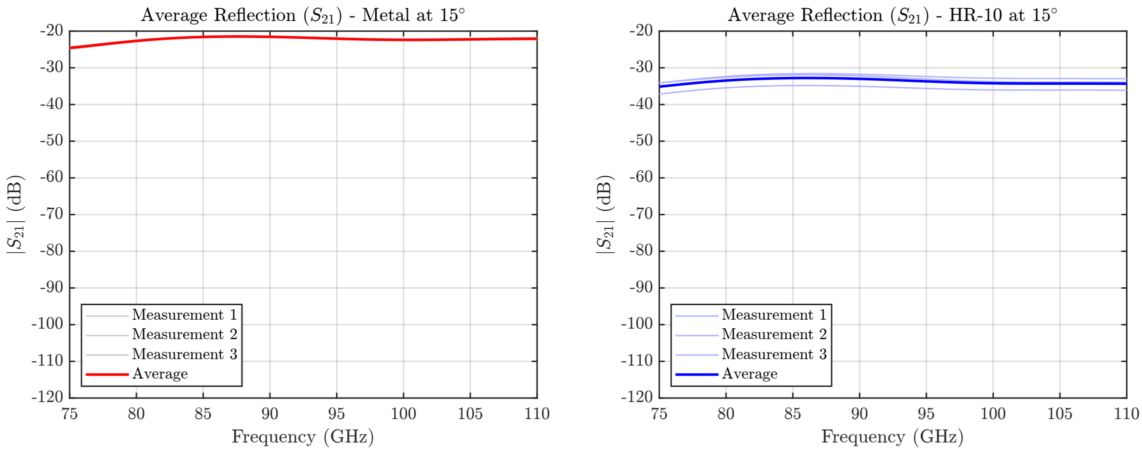

(a) Average reflection - Metal (15°)

(b) Average reflection - HR-10 (15°)

Figure 4.11: Average reflection $|S_{21}|$ of metallic materials and HR-10 at 15°.

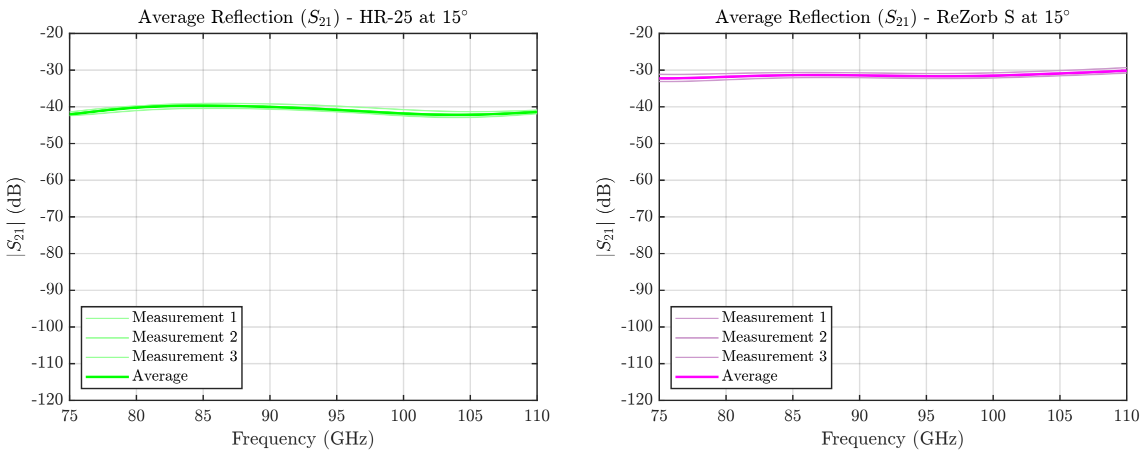

(c) Average reflection - HR-25 (15°)

(d) Average reflection - ReZorb S (15°)

Figure 4.12: Average reflection $|S_{21}|$ of HR-25 and ReZorb S materials at 15°.

Once again, a graph is shown below to make it easier to compare the measurements.

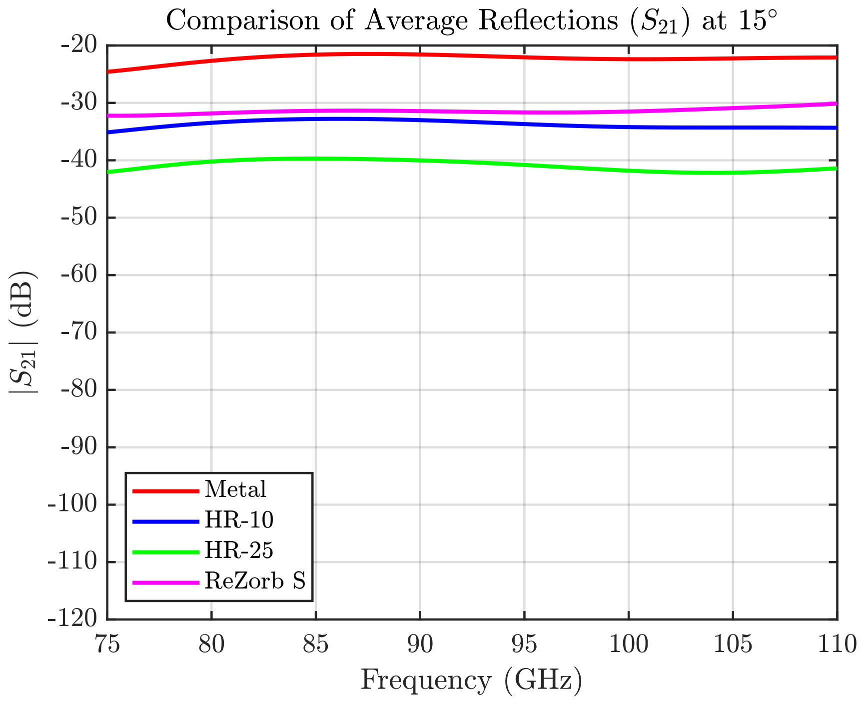

Figure 4.13: Comparison of the average reflection $|S_{21}|$ for the materials tested at 15° incidence.

Figure 4.13 allows a direct comparison between the four materials tested in terms of their ability to attenuate the reflection of the electromagnetic signal at an angle of incidence of 15°. As expected, the metallic material shows the highest values.

In the case of absorbers, ReZorb S and HR-10 showed very similar results across the band. Both maintain their average reflectance between -30 and -35 dB, indicating some absorption capacity, but not much. On the other hand, the HR-25 shows superior performance, with lower $|S_{21}|$ values, below -40 dB in various regions of the band, indicating better absorption efficiency at this angle.

Even so, it's important to note that none of the absorbers show exceptional performance at 15°. The low obliquity of the signal may hinder effective interaction with the internal structure of the materials, limiting their absorption potential.

4.4.2 Experimental results of S_{21} for reflection at 30°

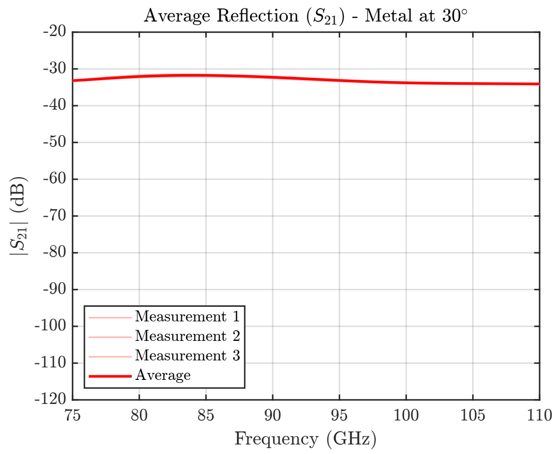

(a) Average reflection - Metal (30°)

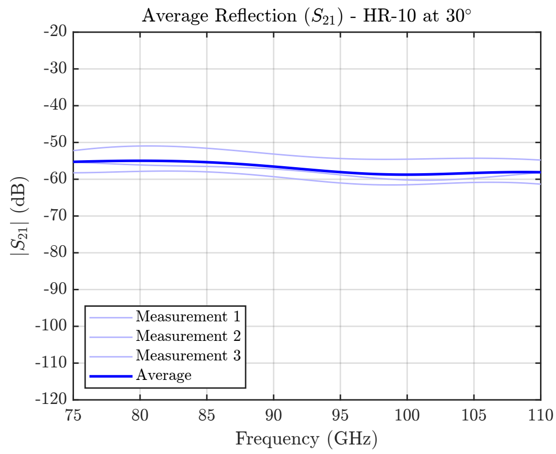

(b) Average reflection - HR-10 (30°)

Figure 4.14: Average reflection $|S_{21}|$ of metallic and HR-10 materials at 30°.

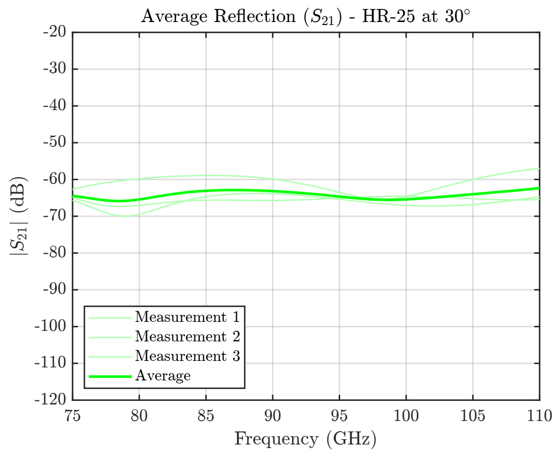

(c) Average reflection - HR-25 (30°)

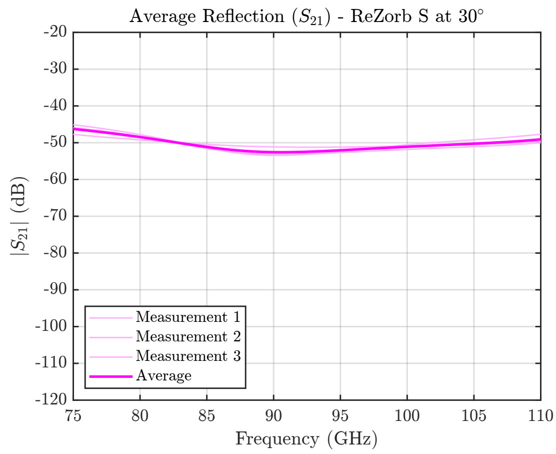

(d) Average reflection - ReZorb S (30°)

Figure 4.15: Average reflection $|S_{21}|$ of the HR-25 and ReZorb S materials at 30°.

There is a significant discrepancy between the three individual measurements in the case of HR-10 and HR-25 (Figure 4.14 Figure 4.15). This variation may be associated with the very nature of these materials, both composed of absorber foams whose internal structure is porous and compressible. Small differences in the positioning or inclination of the sample during the tests can substantially affect the way the electromagnetic waves interact with the material, especially at steeper oblique angles.

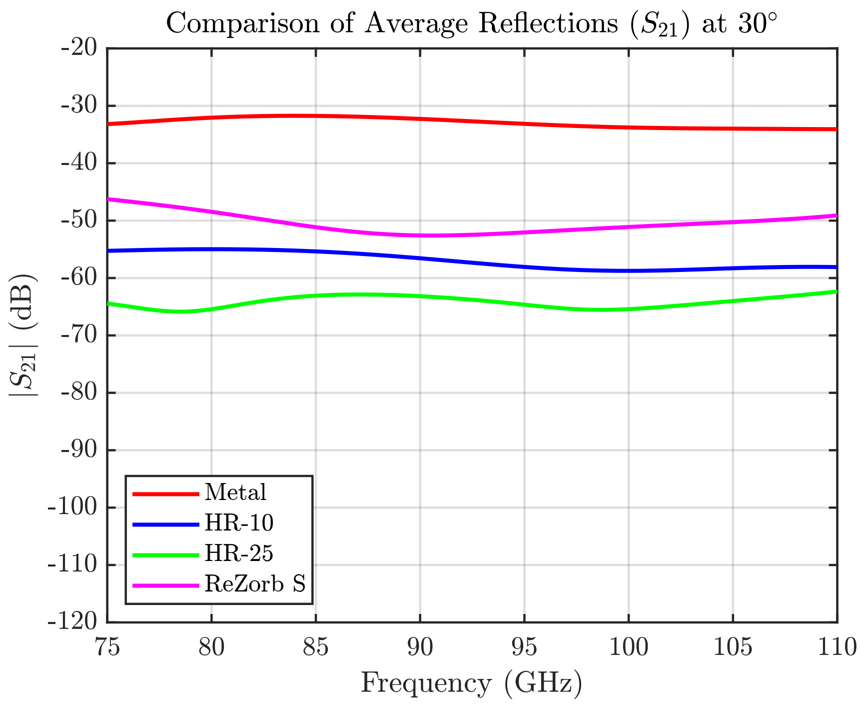

Figure 4.16: Comparison of the average reflection $|S_{21}|$ for the materials tested at 30° incidence.

Figure 4.16 shows a general improvement in the performance of the absorbers compared to the results obtained for 15°. There is a more pronounced attenuation of the reflected signal, with more negative $|S_{21}|$ values across the frequency band.

Among the absorbers tested, HR-25 again stands out as the best performing material, showing the lowest levels of average reflection across the entire frequency range. Its values below -60 dB in all areas of the band demonstrate a high absorption capacity in this angular range. Overall, the results for 30° are very satisfactory and confirm the increasing effectiveness of absorbers under more oblique incidence conditions.

It should also be noted that, in the case of the metal material, there are slightly higher losses compared to 15°, which can be explained by the fact that a metal that is not completely flat was used. This detail, which was only carefully identified after analyzing the results, may have contributed to small additional losses due to dispersion or imperfect reflections.

4.4.3 Experimental results of S_{21} for reflection at 45°

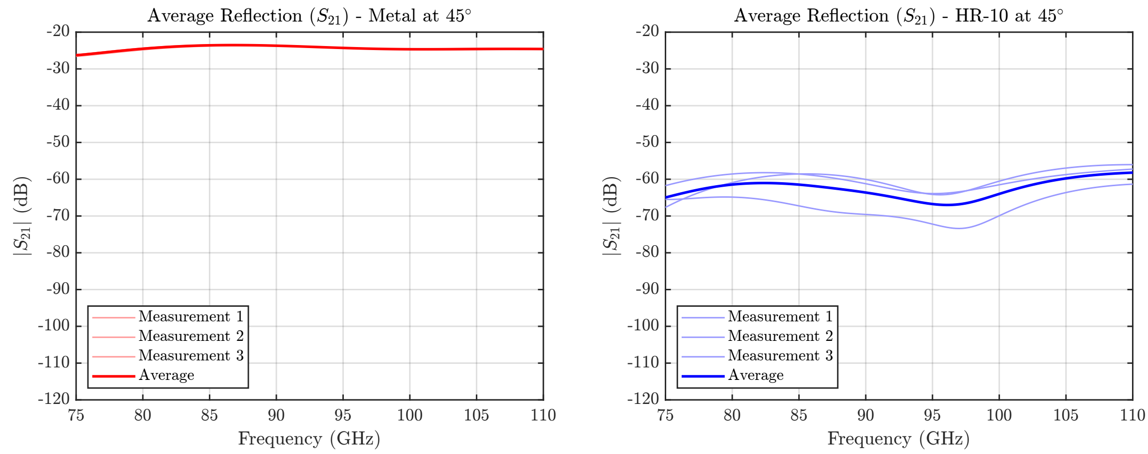

(a) Average reflection - Metal (45°) (b) Average reflection - HR-10 (45°)

Figure 4.17: Average reflection $|S_{21}|$ of metal and HR-10 materials at 45°.

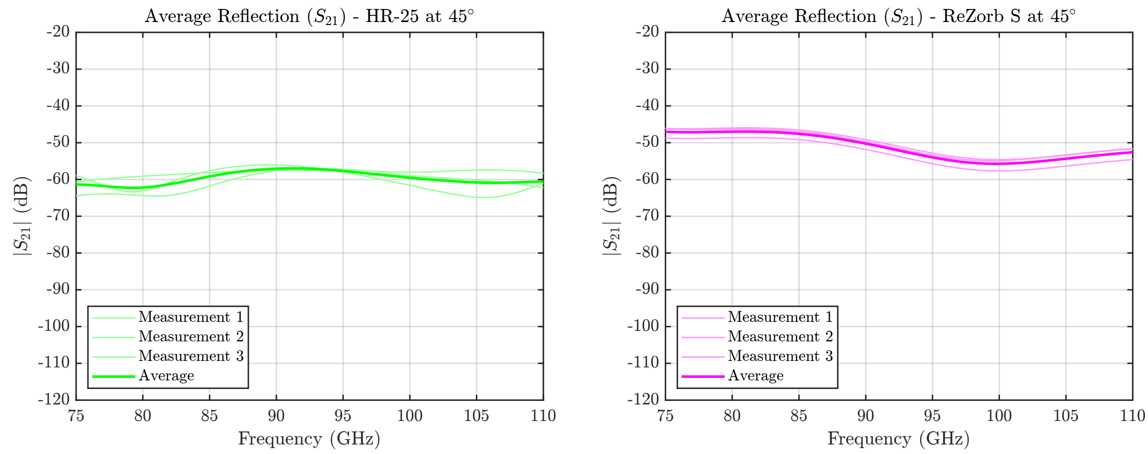

(c) Average reflection - HR-25 (45°) (d) Average reflection - ReZorb S (45°)

Figure 4.18: Average reflection $|S_{21}|$ of the HR-25 and ReZorb S materials at 45°.

The impact of variability between measurements (Figure 4.17 Figure 4.18) is once again noticeable, especially in the HR-10 and HR-25 materials. Interestingly, this variability was also slightly visible in ReZorb S, although to a lesser extent. This behavior reinforces the importance of preforming multiple tests to guarantee the statistical robustness of the results, especially in materials with physical properties that are not completely uniform.

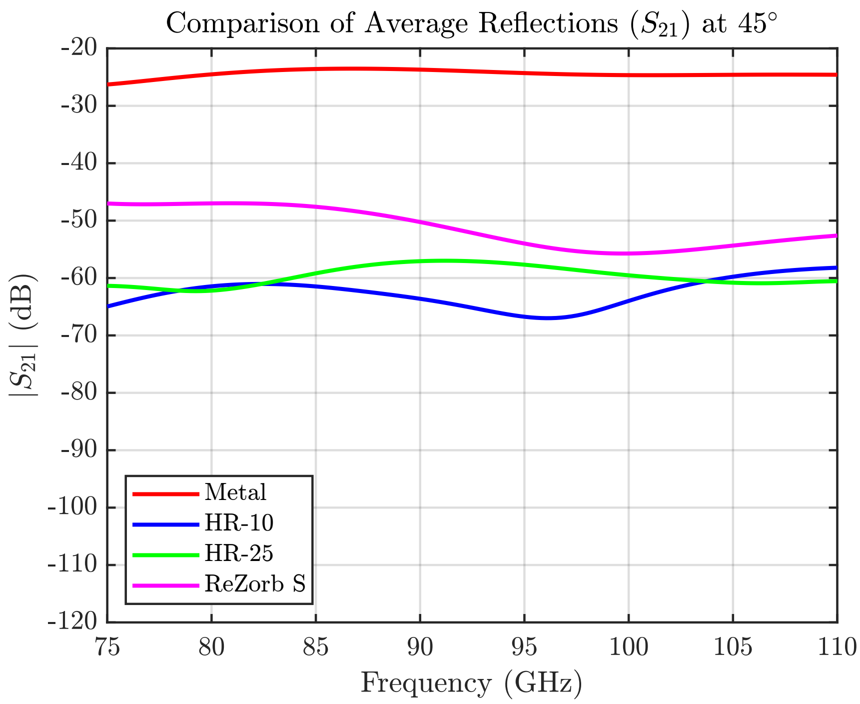

Figure 4.19: Comparison of the average reflection $|S_{21}|$ for the materials tested at 45° incidence.

It can be seen from Figure 4.19 that the results obtained for ReZorb S and HR-25 are very similar to those recorded at 30°, maintaining stable and effective performances in attenuating the reflected signal. In the case of the ReZorb S, there is a slight improvement in the higher frequencies of the analyzed band.

However, the most significant improvement in this range goes to HR-10, which shows a significant improvement compared to the lower angles. Its curve shows superior performance over a large part of the band, especially in the central area, where it reaches the lowest reflection values. This behavior suggests that, for incidents at 45°, HR-10 becomes the best absorber among the four materials evaluated, surpassing the other options in electromagnetic absorption efficiency.

4.5 Overall comparison and partial conclusions

This section aims to integrate the different sets of results obtained, perpendicular reflection (S_{11}), transmittance (S_{21}) and reflection with angular variation (S_{21}), in order to establish a comprehensive view of the electromagnetic performance of the materials tested. The comparison will consider both the spectral behavior (in the 76-110 GHz band) and the variation with the angle of incidence.

4.5.1 Summary of the results of S_{11}

The metallic material showed the highest values of $|S_{11}|$, as expected, reflecting a large part of the incident energy. Among absorbers, HR-25 stood out with the lowest levels of perpendicular reflection in the 76 to 81 GHz range, precisely the frequency band of interest for automotive radar applications, and was therefore the best in this metric within the relevant range.

4.5.2 Summary of transmittance results (S_{21} perpendicular)

Transmittance was practically zero in the case of metal, confirming total wave blocking. HR-10 showed the highest transmittance among the absorbers, consistent with its semi-transparent nature and translucent visual appearance. ReZorb S showed very low transmittance and outperformed HR-25 in this metric.

4.5.3 Summary of results with angular variation

At 15°, none of the materials performed exceptionally well, but HR-25 was the most effective absorber. At 30°, there was a general improvement, with HR-25 maintaining the best performance by a significant margin. At 45°, there was a remarkable reversal: the HR-10 stood out with significant improvements, outperforming the other materials in this configuration, especially at the higher frequencies. Even so, the HR-25 maintained a very solid performance, falling only slightly behind the HR-10 at this angle in the relevant frequency range.

4.5.4 Partial conclusions

- HR-25 proved to be the absorber with the best performance in reflection measurements, standing out particularly in the 76-81 GHz range at S_{11} and maintaining consistent results in measurements with angular variation.

- ReZorb S showed the best performance in perpendicular transmittance (S_{21}), being the most effective in attenuating direct signal transmission of the signal.

- HR-10, although with poor transmittance performance, showed a clear evolution as the angle of incidence increased, proving to be the best absorber at 45°, which can be advantageous in scenarios with predominant oblique incidence.

- The metal, used as a reference, met expectations: high reflection and no transmission. However, small losses observed in the traces may be associated with irregularities in its surface.

Based on the quantitative analysis of the parameters S_{11} and S_{21} in the frequency range of interest (76–81 GHz), it was possible to extract the average values for transmittance and reflection. Table 4.1 summarizes the average values obtained for each case.

Table 4.1: Average values of S_{11} and S_{21} parameters between 76–81 GHz, organized by angle.

Material	**Angle (°)**	**Parameter**	**Average (dB)**
HR-10	15	S_{21} (Reflection)	-33.92
HR-25	15	S_{21} (Reflection)	-40.71
ReZorb S	15	S_{21} (Reflection)	-32.03
HR-10	30	S_{21} (Reflection)	-55.04
HR-25	30	S_{21} (Reflection)	-66.18
ReZorb S	30	S_{21} (Reflection)	-47.77
HR-10	45	S_{21} (Reflection)	-62.30
HR-25	45	S_{21} (Reflection)	-62.01
ReZorb S	45	S_{21} (Reflection)	-47.07
HR-10	90	S_{21} (Transmittance)	-39.70
HR-25	90	S_{21} (Transmittance)	-47.15
ReZorb S	90	S_{21} (Transmittance)	-51.20
HR-10	90	S_{11}	-45.02
HR-25	90	S_{11}	-58.35
ReZorb S	90	S_{11}	-49.86

4.6 Characterization of absorbers

This chapter presents a more in-depth physical characterization of the materials tested, complementing the analyses based on the parameters S_{11} and S_{21}. The aim is to quantify the intensity of the incident field on the sample during the tests and, from the results obtained, to infer the energy absorption efficiency of the materials under realistic conditions. This type of analysis makes it possible to put the results obtained in the laboratory into context with practical situations, such as exposure to radar signals in real environments.

4.6.1 Estimating the incident electric field

In order to assess the compatibility between laboratory conditions and real operating scenarios, it is useful to estimate the intensity of the electric field incident on the materials during the tests. This estimate makes it possible to relate the S-parameters, usually expressed in dB, to real physical quantities such as the electric field E (in V/m) or the power density S (in W/m^2), making it possible to check whether the excitation levels used are representative of real applications, such as automotive radars.

Assuming propagation in free space, the value of the incident electric field can be estimated by the equation [79]:

$$E = \sqrt{30 \cdot G \cdot P_t} \cdot \frac{1}{r} \tag{4.1}$$

where:

- E is the incident electric field (V/m),
- G is the antenna gain (dimensionless),
- P_t is the transmitted power (W),
- r is the distance from the antenna to the material (m).

Alternatively, the power density [80] can be used:

$$S = \frac{P_t \cdot G}{4\pi r^2} \tag{4.2}$$

The (4.1) and (4.2) equations are widely used in modeling radiopropagation systems and evaluating electromagnetic compatibility [27].

During the measurements, the VNA, with the VNAX WR10+ extenders, was configured with an output power of 10 dBm on both ports, as shown in Figure 4.20. This value corresponds to:

$$P_t = 10^{\frac{10}{10}} \cdot 10^{-3} = 0.01 \text{ W} = 10 \text{ mW} \tag{4.3}$$

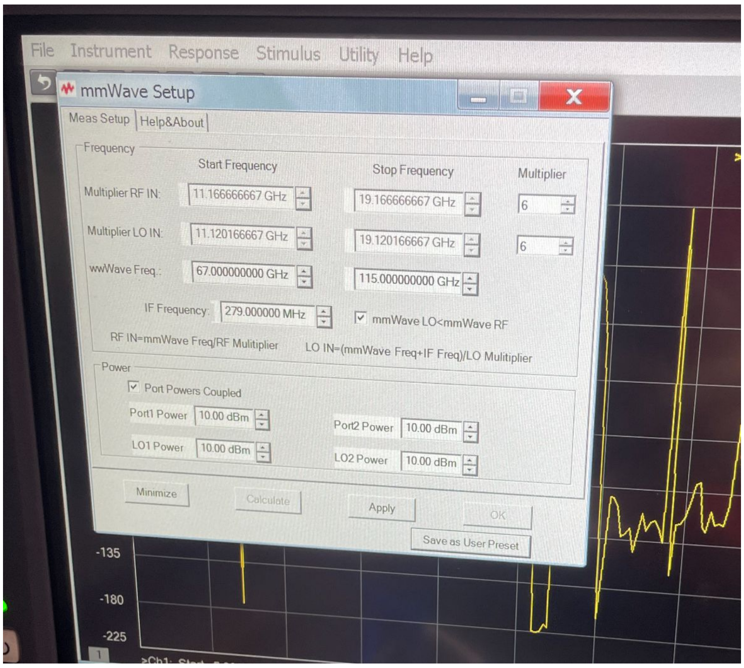

Figure 4.20: VNA configuration with VNAX extenders, indicating 10 dBm power at the measurement ports.

The gain of the antennas used (SAR-2507-10-S2) is approximately 20 dBi, which corresponds to $G \approx 100$ (on a linear scale). The distance between the transmitting antenna and the material varied between the reflection and transmission tests, so both estimates are presented.

The gain of the antennas used is approximately 25 dBi, which corresponds to G≈ 316.23 (on a linear scale). The distance between the transmitting antenna and the material varied between the reflection and transmission tests, so both estimates are shown.

4.6.1.1 Reflection - Case of parameter S_{11}

In this case, the material is approximately r = 0.20 m from the transmitting antenna. Substituting the values into the equation (4.1):

$$\begin{aligned} E &= \sqrt{30 \cdot 316.23 \cdot 0.01} \cdot \frac{1}{0.20} \\ &= \sqrt{94.87} \cdot 5 \\ &\approx 9.74 \cdot 5 = \boxed{48.7 \text{ V/m}} \end{aligned}$$

This value represents the average intensity of the electric field affecting the materials during the S_{11} measurements.

4.6.1.2 Transmission - Case of parameter S_{21}

In the S_{21} measurements, the material is halfway between two antennas, and a distance of approximately $r = 0.50$ m is estimated from the transmitting antenna to the material. Replacing:

$$\begin{aligned} E &= \sqrt{30 \cdot 316.23 \cdot 0.01} \cdot \frac{1}{0.50} \\ &= \sqrt{94.87} \cdot 2 \\ &\approx 9.74 \cdot 2 = \boxed{19.5 \text{ V/m}} \end{aligned}$$

This field is lower than in the S_{11} case, which is consistent with the increased distance and dispersion of the wave in free space.

The conclusion is that the tests were carried out under electric field intensities of around 20-50 V/m, compatible with the intensities observed in short-range radar applications, validating the practical applicability of the results obtained [81].

4.6.2 Reflection, transmission and absorption analysis

The S-parameters measured in the laboratory represent normalized transmission (S_{21}) and reflection (S_{11}) coefficients, which can be directly related to the amount of energy reflected, transmitted or absorbed by the material under test. To do this, it is necessary to convert the measured complex values into scalar quantities by squaring the modulus, resulting in the following expressions [82]:

$$R(f) = |S_{11}(f)|^2 \tag{4.4}$$

$$T(f) = |S_{21}(f)|^2 \tag{4.5}$$

$$A(f) = 1 - R(f) - T(f) \tag{4.6}$$

where:

- R(f) represents the fraction of reflected power;
- T(f) represents the fraction of transmitted power;
- A(f) represents the fraction of absorbed power.

These expressions assume that there are no other losses in the system (e.g. lateral radiation, diffraction, leakage), and that energy is conserved for each frequency analyzed. This approach is widely used in the analysis of absorbers [80, 83].

4.6.2.1 Performance criteria

The effective absorption criteria defined by:

$$A(f) > 0.9 \tag{4.7}$$

In other words, when more than 90% of the incident energy is dissipated by the material, effective electromagnetic absorption is considered to exist. This threshold is often used in literature to classify high-performance materials [84].

4.6.2.2 Practical application

Equations (4.4)–(4.6) are only applicable to tests carried out at normal incidence (angle of 90°), where:

- S_{11} was measured with the material placed directly in front of the transmitting antenna;
- S_{21} was measured with the material positioned between the two antennas (direct transmission);
- Thus, R(f) and T(f) correspond respectively to the frontal reflection and transmittance of the material.

In the tests carried out with angular variation (15°, 30°, 45°), the S_{21} parameter was used to measure the power reflected from a second receiver placed at an angle. In these cases, S_{21} does not represent transmission, but rather reflection at an angle, so absorption should be re-evaluated with:

$$A(f) = 1 - |S_{21}(f)|^2 \tag{4.8}$$

This distinction is essential to ensure that the calculations correctly reflect the physics of the measured phenomenon. Thus, the expressions (4.4)–(4.6) will be applied exclusively to data at normal incidence, as described, with cases of angular reflection being treated separately.

Based on this analysis, it will be possible:

- Identify the frequency bands with the best absorption;
- Compare the behavior of different materials at normal incidence;
- Evaluate the consistency of the response with the angle of incidence in other tests;
- Classify materials based on their absorption efficiency.

The quantitative results for the normal incidence cases are presented in the next section, including the conversion of S_{11} and S_{21} to percentages of reflection, transmission and absorption.

4.6.2.3 Absorption calculation with transmittance reference

Assuming that at normal incidence, in the absence of material, the transmission coefficient is $S_{21,\text{ref}} \approx -22$ dB, as we see in Figure 4.7, we can calculate the fraction of transmitted energy T and reflected energy R for each material using (Values taken from Table 4.1):

$$T = \frac{|S_{21}|^2}{|S_{21,\text{ref}}|^2} = \frac{10^{S_{21}/10}}{10^{-22/10}} \tag{4.9}$$

Applying these equations (4.4), (4.6), (4.9):

- **HR-10**

$$T = \frac{10^{-39.70/10}}{10^{-22/10}} = \frac{1.07 \times 10^{-4}}{6.31 \times 10^{-3}} = 0.0169$$
$$R = 10^{-49.86/10} = 1.03 \times 10^{-5}$$
$$A = 1 - 0.0169 - 0.0000103 = \mathbf{0.983}$$

- **HR-25**

$$T = \frac{10^{-47.15/10}}{10^{-22/10}} = \frac{1.93 \times 10^{-5}}{6.31 \times 10^{-3}} = 0.00305$$
$$R = 10^{-58.35/10} = 1.47 \times 10^{-6}$$
$$A = 1 - 0.00305 - 0.00000147 = \mathbf{0.996}$$

- **Rezorb S**

$$T = \frac{10^{-51.20/10}}{10^{-22/10}} = \frac{7.59 \times 10^{-6}}{6.31 \times 10^{-3}} = 0.00120$$
$$R = 10^{-49.86/10} = 1.03 \times 10^{-5}$$
$$A = 1 - 0.00120 - 0.0000103 = \mathbf{0.9988}$$

It can be concluded that the tested materials have very high absorption, especially Rezorb S, with absorption close to 99.9%. HR-10 has the lowest absorption, which is in line with its more transparent nature and lower material density.

To analyze the absorption of the materials at different angles of incidence (15°, 30° and 45°), the transmittance T obtained for each material at normal incidence (90°) was assumed to be valid, since it was not possible to calculate the transmittance for other angles. The reference $S_{21,\text{ref}}$, on the other hand, was measured with a metal plate and, for uniformity, was taken as the average reference value:

$$S_{21,\text{ref}} = -25 \text{ dB}$$

On this basis, the corrected transmittance was determined using the formula:

$$T = \frac{|S_{21}^{90^\circ}|^2}{|S_{21,\text{ref}}|^2} = \frac{10^{S_{21}^{90^\circ}/10}}{10^{-25/10}} \tag{4.10}$$

where $S_{21}^{90^\circ}$ corresponds to the average value of S_{21} measured at normal incidence for each material.

The reflection R was determined based on the values of S_{21} measured for each angle of incidence, assuming that in these measurements the reflected signal was the main component detected.

The results obtained for each material and angle of incidence are summarized in Table 4.2. It should be noted that the T values are constant for each material, and the R values vary with the angle of incidence.

Table 4.2: Absorption of materials for different angles of incidence (reference: $S_{21,\text{ref}} = -25$ dB).

Material	**Angle (°)**	S_{21} (dB)	R	T	A
HR-10	15	-33.92	0.000406	0.03388	0.96571
HR-25	15	-40.71	0.0000851	0.00609	0.99382
ReZorb S	15	-32.03	0.000628	0.00240	0.99697
HR-10	30	-55.04	0.00000313	0.03388	0.96612
HR-25	30	-66.18	0.00000024	0.00609	0.99391
ReZorb S	30	-36.25	0.000237	0.00240	0.99736
HR-10	45	-62.30	0.00000059	0.03388	0.96612
HR-25	45	-62.01	0.00000063	0.00609	0.99391
ReZorb S	45	-47.07	0.00196	0.00240	0.99564

4.6.2.4 General analysis of absorption results

All the materials tested showed excellent absorption levels, both for normal incidence (90°) and oblique incidence (15°, 30°, 45°). These results confirm the effectiveness of the three materials as millimeter wave absorbers, even under variations in the angle of incidence.

Only HR-10 showed a slight decrease in absorption for the 15° angle, while maintaining values well above 90%, which still meets the criteria required to be classified as an effective absorber. This slight variation may be due to the internal structure or thickness of the material, but does not significantly compromise its overall performance.

Overall, the results indicate that all the absorbers tested are suitable for applications in which the direction of incidence of the waves is not fixed, while maintaining high efficiency in reducing reflected and transmitted energy.

4.6.3 Normalized attenuation coefficient

To allow a fair comparison between absorbers with different thicknesses, it is common to calculate the normalized attenuation coefficient, defined as [85]:

$$\alpha = \frac{-20\log_{10}\left(\frac{|S_{21}|}{|S_{21,\text{ref}}|}\right)}{d} \tag{4.11}$$

where $|S_{21}|$ represents the modulus of the transmission coefficient measured with the material, $|S_{21,\text{ref}}|$ is the modulus of the reference transmission coefficient (without material), and d is the thickness of the material in centimeters. The value obtained expresses the attenuation rate per centimeter of material, in dB/cm.

4.6.3.1 Applicability

It should be noted that this expression is only valid when S_{21} corresponds to the transmittance of the material, measured with the material positioned between the antennas, at normal incidence. In these cases, the signal passes directly through the material along its thickness, making it possible to infer the volumetric attenuation. For measurements at oblique incidence, where the value of S_{21} essentially represents the reflected (rather than transmitted) component, this equation no longer has any physical meaning.

4.6.3.2 Calculation for the materials tested

Assuming $S_{21,\text{ref}} = -22$ dB (i.e. $|S_{21,\text{ref}}| = 10^{-22/20} \approx 0.0794$) (Figure 4.7), the following values are obtained:

- **HR-10** (10 mm = 1.0 cm)

$$\alpha = \frac{-20\log_{10}\left(\frac{10^{-39.70/20}}{10^{-22/20}}\right)}{1.0} = \frac{-20\log_{10}(0.0103/0.0794)}{1.0} = 17.75\ dB/cm$$

- **HR-25** (25 mm = 2.5 cm)

$$\alpha = \frac{-20\log_{10}\left(\frac{10^{-47.15/20}}{10^{-22/20}}\right)}{2.5} = \frac{-20\log_{10}(0.0044/0.0794)}{2.5} = 15.10\ dB/cm$$

- **Rezorb S** (4.7 mm = 0.47 cm)

$$\alpha = \frac{-20\log_{10}\left(\frac{10^{-51.20/20}}{10^{-22/20}}\right)}{0.47} = \frac{-20\log_{10}(0.00275/0.0794)}{0.47} = 28.27\ dB/cm$$

4.6.3.3 Comparative results

Table 4.3: Normalized attenuation coefficient of materials at normal incidence.

Material	S_{21} (dB)	Thickness (cm)	α (dB/cm)
HR-10	-39.70	1.0	17.75
HR-25	-47.15	2.5	15.10
Rezorb S	-51.20	0.47	28.27

4.6.3.4 Discussion

The results show that, even with very different thicknesses, the Rezorb HRs have similar levels of attenuation per centimeter of material. Rezorb S stands out as the most effective in terms of attenuation relative to thickness, reaching more than 28 dB/cm. This value is especially relevant when physical space is a limiting factor. The HR-10 performs slightly better per centimeter than the HR-25, although the latter may be more effective in total absorption due to its greater thickness.

Chapter 5

Conclusion

Throughout this work, a detailed characterization of absorbers in the 76-81 GHz range was carried out, with the aim of evaluating their performance in automotive radar scenarios. Using repeated and controlled measurements on WR10 rectangular waveguides, supported by a measurement system with VNAX extenders and a high-precision vector network analyzer, it was possible to obtain a precise quantification of the transmittance and reflectance of the materials tested: HR-10, HR-25 and ReZorb S.

The experimental results showed that the HR-25 material had the highest average attenuation of the transmitted signal, followed by the ReZorb S and HR-10 materials. The angular variation proved to be a determining factor in absorption efficiency, with significant increases in absorption values for incidence angles of 30 and 45. These data show the effectiveness of the materials, especially in situations where electromagnetic waves are incident at oblique angles, a relevant scenario in automotive applications.

The intensity of the electric field incident on the sample was also calculated based on the antenna gain and the measurement distance, making it possible to assess the relationship between laboratory measurements and real operating conditions. The conversion of the S parameters into energy quantities (transmission, reflection and absorption) provided a robust quantitative analysis of the electromagnetic behavior of the materials tested.

Based on the materials analyzed, it can be concluded that although HR-10 showed reasonable performance in angular absorption measurements, it showed limitations in transmittance tests (S_{21}), especially when compared to the results of HR-25 and ReZorb S materials. Its lower thickness and density may explain the lower effective attenuation capacity of the transmitted signal, which somewhat contradicts the results provided by the brand.

On the other hand, ReZorb S stood out as the most suitable material for direct application in a robotic arm with automotive radar. Its samples are small, easily manipulated and can be combined modularly, making it easy to coat curved or articulated surfaces. In addition, it has significant absorption in both normal and oblique incidence, making it a practical and effective choice.

The thicker HR-25, on the other hand, showed excellent absorption performance, particularly in angular measurements, making it a strong candidate for coating anechoic chambers, where electromagnetic performance is a priority. It should be noted, however, that traditional absorbers with pyramidal geometry will most likely remain the best choice in these applications, due to their proven effectiveness in minimizing reflections over a wide angular and frequency range. Even so, in situations where the thickness available for coating is limited due to space or mounting restrictions, HR-25 could prove to be a viable alternative, offering a balance between performance and size.

In short, the methodology implemented has made it possible to rigorously assess the performance of absorbers and support their practical application in real contexts. The energy, angular and spectral analysis carried out provides a solid basis for material selection in automotive radar systems and test environments.

5.1 Future work

As a continuation of this work, the following approaches are suggested:

- Test a wider range of absorbers, including composites with different geometries, textures or conductive additives;
- Integrate free-field measurements (free-space), with antennas and reflectors at greater distances, to validate consistency with waveguide results;
- Study the thermal behavior of materials, evaluating the stability of absorption in different temperature ranges;
- Analyzing the durability of materials in adverse environments (humidity, dust, vibration), especially with a view to their application in vehicles;
- Exploring the application of meta-material structures or hybrid layers that combine absorption and selective transparency at specific frequencies;
- Developing a computer simulation model to predict the performance of materials based on their physical and geometric properties.

These lines of research will allow for a better understanding and optimization of the behaviour of absorbers in real scenarios, contributing to the development of more effective solutions that can be integrated into next-generation automotive radar systems.

References

[1] S. M. Patole et al. "Automotive radars: A review of signal processing techniques". In: *IEEE Signal Processing Magazine* 34.2 (2017), pp. 22–35. DOI: 10.1109/MSP.2016.2628914.

[2] Organização Mundial da Saúde. "Relatório Mundial sobre a Situação da Segurança Viária 2023". In: (2023). URL: https://www.paho.org/pt/noticias/13-12-2023-apesar-do-progresso-notavel-seguranca-viaria-continua-sendo-um-problema-mundial.

[3] Jürgen Hasch et al. "Millimeter-Wave Technology for Automotive Radar Sensors in the 77 GHz Frequency Band". In: *IEEE Transactions on Microwave Theory and Techniques* 60.3 (2012), pp. 845–860. DOI: 10.1109/TMTT.2011.2178427. URL: https://ieeexplore.ieee.org/document/6151878.

[4] J. Gavan. "Challenges in anechoic chamber testing of automotive radar sensors". In: *Microwave Journal* 62.12 (2019), pp. 30–37.

[5] Hermann Rohling, Jan Mende, and Sven Heuel. "A Novel Automotive Radar System for Urban Environment". In: *Advances in Radio Science* 16 (2018), pp. 131–137. DOI: 10.5194/ars-16-131-2018.

[6] Christian Hülsmeyer. "Improvement in Hertzian-wave Projecting and Receiving Apparatus for Locating the Position of Distant Metal Objects". In: *British Patent Specification* 13170 (1904). URL: https://www.daidalos.blog/en/innovations/milestones/artikel/the-telemobiloscope/.

[7] Robert Watson-Watt. "The Pulse Technique in Location by Radio Methods". In: *Proceedings of the IRE* 33.6 (1945), pp. 377–384. DOI: 10.1109/JRPROC.1945.234762.

[8] Merrill I. Skolnik. *Introduction to Radar Systems*. 3rd. McGraw-Hill, 2001. ISBN: 978-0071181897.

[9] R. D. Kellogg and W. D. Jones. *Automotive Radar Sensor: An Experimental System*. Tech. rep. GMR-1719. Technical Report. Warren, Michigan: General Motors Research Laboratories, 1972.

[10] Hermann Rohling, Sven Heuel, and Henning Ritter. "Pedestrian Detection Procedure Integrated into an ACC System". In: *IEEE Transactions on Intelligent Transportation Systems* 10.4 (2009), pp. 723–732. DOI: 10.1109/TITS.2009.2026670.

[11] ResearchGate. *Automotive radar applications*. https://www.researchgate.net/figure/Automotive-radar-applications-This-work-will-focus-on-the-long-range-adaptive-cruise_fig1_330691252. Accessed: 28-09-2025.

[12] J. C. Costa, P. Almeida, and M. A. Silva. "Advances in radar absorbing materials for automotive applications". In: *Journal of Electromagnetic Engineering and Science* 20.4 (2020), pp. 254–266. DOI: 10.1109/JEES.2020.3034567.

[13] Mark A. Richards. “Fundamentals of Radar Signal Processing”. In: (2014).

[14] Wevolver. *Steering Towards Safer Rides: The Role of Radar and ToF Sensors in In-Cabin Monitoring Systems (ICMS)*. https://www.wevolver.com/article/steering-towards-safer-rides-the-role-of-radar-and-tof-sensors-in-in-cabin-monitoring-systems-icms. Accessed: 28-09-2025.

[15] Christian Doppler. *Über das farbige Licht der Doppelsterne und einiger anderer Gestirne des Himmels*. Original work proposing the Doppler Effect. Prague: Borrosch & Andr., 1842.

[16] Wenbin Hao et al. “Pedestrian and Animal Recognition Using Doppler Radar Signature and Deep Learning”. In: *Sensors* 22.9 (2022), p. 3387. DOI: 10.3390/s22093387. URL: https://www.mdpi.com/1424-8220/22/9/3387.

[17] Code 3 Garage. *How Police Radar Works*. https://code3garage.com/equipment/how-police-radar-works/. Accessed: 28-09-2025.

[18] David M. Pozar. *Microwave Engineering*. 4th ed. Wiley, 2011.

[19] T. Iguchi R. Meneghini and L. Tian. “Effects of Rain on Millimeter-Wave Propagation: Experimental and Theoretical Considerations”. In: *IEEE Transactions on Geoscience and Remote Sensing* 56.6 (2018), pp. 3305–3315. DOI: 10.1109/TGRS.2018.2806168.

[20] F. Richter and S. P. van der Laan. “Dust and Smoke Effects on Automotive Radar Performance: A Study on Scattering and Absorption Mechanisms”. In: *IEEE Sensors Journal* 20.8 (2020), pp. 4312–4320. DOI: 10.1109/JSEN.2020.2966657.

[21] Electronics Notes. *Antenna Near Field and Far Field Regions*. Accessed: 2025-03-24. https://www.electronics-notes.com/articles/antennas-propagation/antenna-theory/antenna-near-field-far-field.php. n.d.

[22] Antenna Theory. *Antenna Field Regions*. Accessed: 2025-03-24. https://www.antenna-theory.com/basics/fieldRegions.php. n.d.

[23] Wikipedia. *Fraunhofer Distance*. Accessed: 2025-03-24. https://en.wikipedia.org/wiki/Fraunhofer_distance. n.d.

[24] Wikipedia contributors. *Near and far field — Wikipedia, The Free Encyclopedia*. https://en.wikipedia.org/wiki/Near_and_far_field. Accessed: 28-09-2025. 2025.

[25] Wikipedia contributors. *Fraunhofer distance — Wikipedia, The Free Encyclopedia*. [Online; accessed 26-Mar-2025]. 2025. URL: https://en.wikipedia.org/wiki/Fraunhofer_distance.

[26] Mehdi Monemi, Mehdi Rasti, and Matti Latva-aho. “Revisiting the Fraunhofer and Fresnel Boundaries for Phased Array Antennas”. In: *arXiv preprint arXiv:2411.02417* (2024). URL: https://arxiv.org/abs/2411.02417.

[27] Constantine A. Balanis. *Antenna Theory: Analysis and Design*. 4th. John Wiley & Sons, 2016. ISBN: 9781118642061.

[28] Warren L. Stutzman and Gary A. Thiele. *Antenna Theory and Design*. 3rd. John Wiley & Sons, 2012. ISBN: 9780470576649.

[29] M. D. Foegelle and D. D. Hill. “Establishing far-field conditions in compact ranges for EMC measurements”. In: *IEEE Transactions on Electromagnetic Compatibility* 42.4 (2000), pp. 420–427. DOI: 10.1109/15.887122.

[30] C. Lindsey and C. Long. “Accurate Far-Field Distance Determination Using Antenna Beamwidths”. In: *IEEE Antennas and Propagation Magazine* 47.2 (2005), pp. 96–100. DOI: 10.1109/MAP.2005.1465172.

[31] National Instruments. *Far-Field and Near-Field Measurement Considerations*. Disponível em: https://www.nsi-mi.com/system-solutions/far-field-systems. 2020.

[32] K. J. Vinoy and R. M. Jha. *Radar Absorbing Materials: From Theory to Design and Characterization*. Boston: Kluwer Academic Publishers, 1996. ISBN: 978-0792397533.

[33] H. Xu et al. "Design of a broadband metamaterial absorber based on hollow pyramidal structure". In: *Materials Today Communications* 25 (2020), p. 101603.

[34] Wikipédia. *Câmara anecoica*. Acessado em: 24 mar. 2025. 2025. URL: https://pt.wikipedia.org/wiki/C%C3%A2mara_anecoica.

[35] A. M. Folgueiras and M. T. de Rezende. "Materiais absorvedores de radiação eletromagnética: princípios, síntese e caracterização". In: *Revista Brasileira de Ensino de Física* 27.4 (2005), pp. 505–513. DOI: 10.1590/S1806-11172005000400011.

[36] E. P. dos Santos and R. L. S. Adriano. "Desenvolvimento de técnicas numéricas aplicadas à modelagem de problemas de irradiação e espalhamento eletromagnético". In: *Revista Brasileira de Ensino de Física* 41.1 (2019), e1301. DOI: 10.1590/1806-9126-RBEF-2019-0013.

[37] Electrónica Embajadores. *Holland Shielding Systems 3640-96 Absorvedor EMI piramidal à base de espuma PU H=96 mm (20 unidades)*. https://www.electronicaembajadores.com/pt/Productos/Detalle/MIMA364096/materiais-de-engenharia/materiais-absorcao-rf-emi/holland-shielding-systems-3640-96-absorvedor-emi-piramidal-a-base-de-espuma-pu-h-96-mm-20-unidades/. Accessed: 28-09-2025.

[38] Y. Ma et al. "Electromagnetic wave absorbing properties of pyramidal absorbing mortar in 2–18 GHz". In: *Journal of Building Engineering* 45 (2022), p. 103599.

[39] Carlos Rocha. "Test and Validate Radar Units". Master's thesis. Porto, Portugal: Faculdade de Engenharia da Universidade do Porto, 2023.

[40] X. Chen et al. "Robotic testing system for automotive radar sensors". In: *IEEE Transactions on Instrumentation and Measurement* 67.5 (2018), pp. 1122–1130.

[41] J. Lin et al. "Target simulation for automotive radar hardware-in-the-loop testing". In: *IEEE Transactions on Vehicular Technology* 66.10 (2017), pp. 8657–8665.

[42] J. C. C. Freitas and M. A. S. Oliveira. "Caracterização experimental da permissividade dielétrica complexa de materiais sólidos". In: *Revista Brasileira de Ensino de Física* 31.3 (2009), p. 3503. DOI: 10.1590/S1806-11172009000300003.

[43] Christian Wolff. *Vector Network Analyzer (VNA)*. Accessed: 2025-03-24. 2023. URL: https://www.radartutorial.eu/17.bauteile/bt51.en.html.

[44] David Hotte et al. "Radar cross-section measurement in millimetre-wave for passive millimetre-wave identification tags". In: – *(unspecified in figure source)* (2015). Figure configuration of bi-static and mono-static measurement benches (Fig. 2) – adapted. URL: https://www.researchgate.net/figure/Con-fi-gurations-of-the-two-possible-measurement-benches-a-Bi-static-measurement-of-the_fig2_281458827.

[45] David M. Pozar. *Microwave Engineering, 4th Edition*. Capítulo 4: Parâmetros de dispersão. 2011.

[46] Keysight Technologies. *Vector Network Analyzer (VNA) Fundamentals*. Acedido em Maio 2025. 2018. URL: https://www.keysight.com/us/en/assets/7018-02657/brochures/5990-3269.pdf.

[47] Agilent Technologies. *Time-Domain Reflectometry Using a Network Analyzer*. Application Note 1287-11. 2005. URL: https://www.keysight.com/us/en/assets/7018-03173/application-notes/5989-5723.pdf.

[48] Keysight Technologies. *Time Domain Analysis with a Vector Network Analyzer*. Acesso em maio de 2025. 2024. URL: https://helpfiles.keysight.com/csg/N52xxB/Time/TimeDomain.htm#How.

[49] Rohde & Schwarz. *Time Domain Analysis with Vector Network Analyzers*. 2018. URL: https://scdn.rohde-schwarz.com/ur/pws/dl_downloads/dl_common_library/dl_brochures_and_datasheets/pdf_1/VNA-Time-Domain_Application_Note_en_3606-7824-92_v0100.pdf.

[50] David M. Pozar. *Microwave Engineering*. 4th. John Wiley & Sons, 2011.

[51] Keysight Technologies. *Time Domain Analysis*. https://helpfiles.keysight.com/csg/pxivna/Time/TimeDomain.htm. Accessed: 28-09-2025.

[52] Jerzy Krupka. "Frequency domain complex permittivity measurements at microwave frequencies". In: *Measurement Science and Technology* 17.6 (2006), R55–R70.

[53] William B Weir. "Automatic measurement of complex dielectric constant and permeability at microwave frequencies". In: *Proceedings of the IEEE* 62.1 (1974), pp. 33–36.

[54] James Baker-Jarvis, Michael D Janezic, and Edward J Vanzura. "A nonlinear least-squares solution for extracting complex permittivity from transmission/reflection measurements". In: *IEEE Transactions on Instrumentation and Measurement* 39.3 (1990), pp. 436–441.

[55] Natalia K. Nikolova. *Rectangular waveguide measurement setup*. https://www.researchgate.net/figure/Rectangular-waveguide-measurement-setup_fig6_272353049. Acesso em junho de 2025.

[56] A. Basir et al. "Measurement and Characterization of 3D-Printed Microwave Absorbers in the W-Band". In: *IEEE Access* 10 (2022), pp. 123456–123467. DOI: 10.1109/ACCESS.2022.3188464. URL: https://www.researchgate.net/figure/Schematic-of-a-VNA-based-measurement-setup-with-frequency-extenders-employed-for_fig6_362695494.

[57] Eravant. *STO User Manual*. Acesso em maio de 2025. 2022. URL: https://sftp.eravant.com/content/resources/Eravant-STO-User-Manual-and-setup.pdf.

[58] Amtechs Corporation. *Using VNA Frequency Extenders*. Acesso em maio de 2025. 2023. URL: https://www.amtechs.co.jp/product/d57f46c3f80dd5d9f9cf6798cadbb1df653d3 pdf.

[59] ResearchGate. *Rectangular waveguide measurement setup*. https://www.researchgate.net/figure/Rectangular-waveguide-measurement-setup_fig6_272353049. Accessed: 28-09-2025.

[60] Dong-Youp Lee, Jong-Han Park, and Byung-Seo Kim. "Development of active frequency extender for 220 GHz band with an active probe". In: *Journal of Semiconductor Technology and Science* 14.2 (2014), pp. 259–265. URL: https://www.researchgate.net/figure/A-schematic-diagram-of-an-active-probe-frequency-extender_fig3_264578943.

[61] Copper Mountain Technologies. *An Introduction to VNA Calibration Theory*. Acesso em junho de 2025. 2020. URL: https://coppermountaintech.com/an-introduction-to-vna-calibration-theory/.

[62] Keysight Technologies. *VNA Calibration Basics*. Acesso em junho de 2025. URL: https://www.keysight.com/zz/en/assets/7018-06888/brochures/5990-3265EN.pdf.

[63] I. Rolfes and B. Schiek. "Calibration methods for microwave free space measurements". In: *Advances in Radio Science* 2 (2004), pp. 19–25.

[64] All About Circuits. *Understanding the 12-Term Error Model and SOLT Calibration Method for VNA Measurements*. https://www.allaboutcircuits.com/technical-articles/understanding-the-12-term-error-model-and-solt-calibration-method-for-vna-measurements/. Accessed: 28-09-2025.

[65] Rohde & Schwarz GmbH & Co. KG. "Medindo as propriedades eletromagnéticas de materiais — A influência de plásticos e compostos no desempenho de sensores automotivos". In: *Rohde & Schwarz Application Notes* (2021). Acessado em 24 de março de 2025. URL: https://www.rohde-schwarz.com/br/aplicacoes/medindo-as-propriedades-eletromagneticas-de-materiais-aplicacao_56279-1004017.html.

[66] Laird Technologies. *ReZorb™ S Datasheet*. Acesso em: abril 2025. Nov. 2023. URL: https://www.laird.com/products/absorbers/textured-elastomer-absorbers/rezorb-s.

[67] Laird Technologies. *Eccosorb™ HR - Microwave Absorbing Foam*. Acesso em: abril 2025. 2021. URL: https://www.laird.com/products/absorbers/microwave-absorbing-foams/single-layer-foams/eccosorb-hr.

[68] Soliani EMC. *Conical RADAR ABSORBENT MATERIAL (RAM) of 6mm: 95.00344-00*. https://www.solianiemc.com/wp-content/uploads/2025/03/95.00344-00-1-1.pdf. Acesso em maio de 2025. 2025.

[69] EMC Elektronik. *Absorber for Anechoic Chambers and EMC Test Sites*. https://www.emcelectronic.com/uploads/dosya/absorber1.pdf. Acesso em maio de 2025. 2024.

[70] Keysight Technologies. *PNA Network Analyzer N5224B Datasheet*. https://www.keysight.com/pt/en/assets/7018-06897/data-sheets/5990-4593.pdf. Accessed: 2025-07-14. 2024.

[71] Virginia Diodes, Inc. *WR10 VNAX Frequency Extension Module*. https://www.vadiodes.com/index.php/en/products/vector-network-analyzer?id=850. Accessed: 2025-07-14. 2024.

[72] Virginia Diodes, Inc. *VNAX Product Manual*. Document code: VDI-707.1, Accessed: 2025-07-14. 2024.

[73] Eravant. *SAR-2507-10-S2 Standard Gain Horn Antenna Datasheet*. https://sftp.eravant.com/content/datasheets/SAR-2507-10-S2.pdf. Accessed: 2025-07-14. 2024.

[74] Bosch Professional. *GLL 3-80 Line Laser Datasheet and Manual*. https://www.bosch-professional.com/sa/en/products/gll-3-80-0601063S00. Accessed: 2025-07-14. 2024.

[75] Constantine A. Balanis. *Antenna Theory: Analysis and Design*. 4th. John Wiley & Sons, 2016. ISBN: 978-1-118-64006-6.

[76] everythingRF. *What is Half Power Beam Width (HPBW)?* https://www.everythingrf.com/community/what-is-half-power-beam-width. Accessed: 28-09-2025.

[77] Ulrich Halbritter. *Time-of-Flight System for Distance Measurement and Object Detection*. Analog Devices Technical Article. "The distance can be estimated as the depth $d = (c \times \Delta t)/2$, where c is the speed of light." 2020. URL: https://www.analog.com/en/resources/technical-articles/tof-system-for-distance-measurement-and-object-detection.html.

[78] Natalia Nikolova. *Horn Antennas*. https://www.ece.mcmaster.ca/faculty/nikolova/antenna_dload/current_lectures/L18_Horns.pdf. Lecture notes, McMaster University. 2023. URL: https://www.ece.mcmaster.ca/faculty/nikolova/antenna_dload/current_lectures/L18_Horns.pdf.

[79] National Instruments. *Power Density and Electric Field Strength*. https://www.ni.com/en-us/innovations/power-density-and-electric-field-strength.html. Acesso em: 22 jul. 2025. 2024.

[80] Microwaves101. *Friis Transmission Equation*. https://www.microwaves101.com/encyclopedias/friis-transmission-equation. Acesso em: 22 jul. 2025. 2024.

[81] ETS-Lindgren. *Automotive Radar Testing Overview*. https://www.ets-lindgren.com/news/automotive-radar-testing-overview. Acesso em: 22 jul. 2025. 2024.

[82] C. S. Daw, C. E. A. Finney, and E. R. Tracy. "A review of symbolic analysis of experimental data". In: *Review of Scientific Instruments* 74.2 (2003), pp. 915–930. DOI: 10.1063/1.1531823.

[83] A.M. Nicolson and G.F. Ross. "Measurement of the intrinsic properties of materials by time-domain techniques". In: *IEEE Transactions on Instrumentation and Measurement* 19.4 (1970), pp. 377–382. DOI: 10.1109/TIM.1970.4313932.

[84] I. Poole. *Electromagnetic Absorbers*. https://www.electronics-notes.com/articles/antennas-propagation/emc-emi/electromagnetic-absorbers.php. Acesso em: 22 jul. 2025. 2024.

[85] Teledyne LeCroy (Signal Integrity Blog). *Reading S-Parameters: S_{21} as a Measure of Signal Attenuation*. Online. 2020. URL: https://blog.teledynelecroy.com/2020/05/reading-s-parameters-monotonic-drop-offs.html (visited on 07/31/2025).